ERDC/EL TR-00-18

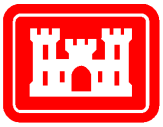

US Army Corps
of Engineers®
Engineer Research and
Development Center

Strategic Environmental Research and Development Program

SEAM3D: A Numerical Model for Three-Dimensional Solute Transport and Sequential Electron Acceptor-Based Bioremediation in Groundwater

Dan W. Waddill and Mark A. Widdowson

November 2000

Environmental Laboratory

The contents of this report are not to be used for advertising, publication, or promotional purposes. Citation of trade names does not constitute an official endorsement or approval of the use of such commercial products.

The findings of this report are not to be construed as an official Department of the Army position, unless so designated by other authorized documents.

COPYRIGHT NOTICE AND DISCLAIMER

For technical information and to report program errors, please contact:

Mark A. Widdowson, Ph.D., P.E.
Associate Professor of Civil Engineering
The Charles E. Via, Jr., Department of Civil and Environmental Engineering
Virginia Polytechnic Institute and State University
Blacksburg, VA 24061-0105
Email: *mwiddows@vt.edu*

Strategic Environmental Research and Development Program

ERDC/EL TR- 00-18
November 2000

SEAM3D: A Numerical Model for Three-Dimensional Solute Transport and Sequential Electron Acceptor-Based Bioremediation in Groundwater

by Dan W. Waddill and Mark A. Widdowson

Virginia Polytechnic Institute and State University
The Charles E. Via, Jr., Department of Civil
and Environmental Engineering
Blacksburg, VA 24061-0105

Final Report

Approved for public release; distribution is unlimited

Prepared for Strategic Environmental Research and Development Program
Arlington, VA 22203

Under Work Unit CU-1062

Monitored by U.S. Army Engineer Research and Development Center
Environmental Laboratory
3909 Halls Ferry Road, Vicksburg, MS 39180-6199

Contents

List of Figures

List of Tables

Preface

This report provides documentation of the computer code SEAM3D, including mathematical model development, model and code verification exercises, application of the code to a field problem, and guidance for users of the code. Portions of this model development and this report preparation were conducted under the Cleanup Pillar of the Strategic Environmental Research and Development Program (SERDP), as part of Work Unit CU-1062, "Development of Simulators for In-Situ Remediation Evaluation, Design, and Operation." SERDP is sponsored by the U.S. Department of Defense, U.S. Environmental Protection Agency, and U.S. Department of Energy. Work Unit CU-1062 was conducted by the U.S. Army Engineer Research and Development Center (ERDC) under the purview of the Environmental Laboratory (EL). EL involvement in SERDP was coordinated by Dr. John Cullinane, Program Manager for the EL Installation Restoration Research Program (IRRP). Mr. Charles Miller was Assistant Manager for the IRRP. Ms. Catherine Vogel was the Cleanup Program Manager for SERDP.

The Principal Investigator of Work Unit CU-1062 was Dr. Mark S. Dortch, Chief, Water Quality and Contaminant Modeling Branch (WQCMB), Environmental Processes and Effects Division (EPED), EL. The work documented in this report was conducted by Virginia Polytechnic Institute and State University (Virginia Tech) through a research contract (DACA39-95-K-0054) monitored by ERDC. The ERDC Contracting Officer's Representative and contract monitor was Dr. Carlos E. Ruiz of the WQCMB.

The principal investigator for this study was Dr. Mark A. Widdowson of the Charles E. Via, Jr., Department of Civil and Environmental Engineering, Virginia Tech. Model development was performed by Drs. Widdowson and Dan W. Waddill, also of Virginia Tech. Code development, user's guide preparation, and model applications were performed by Drs. Waddill and Widdowson. Drs. Ruiz and Dortch provided guidance during model and code development. Dr. Francis H. Chapelle of the U.S. Geological Survey (USGS) was instrumental in development of the conceptual and mathematical models. This report was prepared by Drs. Waddill and Widdowson. Drs. Ruiz and Dortch reviewed this report.

Field and laboratory measurements made by the USGS were essential to the verification of SEAM3D. Chapter 4 describes the application of a site model developed using SEAM3D to the intrinsic bioremediation of gasoline-derived

contaminants in groundwater at a leaking underground storage tank site (Laurel Bay, SC). This part of the research was made possible by the efforts of Dr. Chapelle, Dr. James F. Landmeyer, and Dr. Paul M. Bradley of the USGS, Columbia, SC. This work resulted from a cooperative research agreement between the USGS and Virginia Tech.

Drs. Richard E. Price and John W. Keeley were Chief of EPED and Acting Director of EL, respectively, during the conduct of this study.

At the time of publication of this report, Dr. James R. Houston was Director of ERDC, and COL Robin R. Cababa, EN, was Commander.

This report should be cited as follows:

> Waddill, D. W., and Widdowson, M. A. (2000). "SEAM3D: A numerical model for three-dimensional solute transport and sequential electron acceptor-based bioremediation in groundwater," ERDC/EL TR-00-18, U.S. Army Engineer Research and Development Center, Vicksburg, MS.

1 Introduction

Biodegradation Modeling

During recent decades, leaking storage tanks and pipelines have allowed petroleum-derived hydrocarbons to contaminate soil and groundwater at thousands of sites. Microbes degrade many hydrocarbons in aerobic groundwater with molecular oxygen serving as a terminal electron acceptor (EA). Generally, oxygen is rapidly depleted, but hydrocarbons may continue to degrade under anaerobic conditions if alternate EAs are available. Research has shown that a variety of hydrocarbons will degrade using the following EAs: nitrate (Arcangeli and Arvin 1994), oxidized manganese (Baedecker et al. 1993; Lovley 1991), ferric iron (Lovley and Lonergan 1990), sulfate (Reuter et al. 1994), and carbon dioxide under methanogenic conditions (Grbic-Galic and Vogel 1987).

In certain cases, natural (or intrinsic) in situ bioremediation may provide a low-cost alternative to other methods of site restoration. However, the effectiveness of intrinsic bioremediation depends on the relationship between the contaminant biodecay rate and the groundwater velocity (Chapelle and Bradley 1998). Biodecay rate is affected by many factors, including the geochemical environment, contaminant type and concentration, EA availability, and the dominant terminal EA process (TEAP). Since these factors are often site dependent and vary with time and space, prediction of the biodecay rate is difficult. Nevertheless, to design successful and cost-effective strategies to clean up a site, the potential for bioremediation should be assessed. Due to variability in the biological processes, evidence suggests that bioremediation potential must be evaluated on a site-by-site basis (Atlas and Cerniglia 1995), and mathematical solute transport models can assist in such evaluations. Field evidence suggests that up to five EAs may be active in bioremediation at a single site (Baedecker et al. 1993; Borden, Gomez, and Becker 1995; Ludvigsen et al. 1995); thus accurate predictions of biodegradation may require simulation of multiple alternate EAs.

In unconfined aquifers, biodegradation rates may vary over the vertical dimension as redox conditions near the water table differ from conditions at lower depths. For example, Vroblesky and Chapelle (1994) found that variable recharge caused the predominant TEAP at the water table to shift among ferric iron (Fe(III)) reduction, sulfate reduction, and methanogenesis, while the

dominant TEAP at the aquifer bottom remained methanogenesis. Moreover, recharge brings oxygenated water to the upper boundary of a plume, and field evidence indicates that the elevation of the center of mass of a plume may decrease with time (Borden, Gomez, and Becker 1995). Due to the lack of adequate data, modeling in three dimensions is not always justified; however, the three-dimensional approach may be beneficial for sites where sampling is rigorous.

Overview of SEAM3D

This report describes the development, verification, and application of SEAM3D (Sequential Electron Acceptor Model, 3 Dimensional), a numerical model for subsurface solute transport with aerobic and sequential anaerobic biodegradation. The model can depict multiple constituents in a three-dimensional, anisotropic, heterogeneous domain. Hydrocarbon contaminants are simulated as electron donors (i.e., substrates) for microbial growth, with available EAs used in the following sequence: oxygen (O_2), nitrate (NO_3^-), oxidized manganese (Mn(IV)), ferric iron (Fe(III)), sulfate (SO_4^{2-}), and carbon dioxide (CO_2). SEAM3D can account for reduced manganese (Mn(II)), ferrous iron (Fe(II)), hydrogen sulfide (H_2S), methane (CH_4), and a user-defined nitrogenous compound as products of biodegradation. In addition, each hydrocarbon substrate can produce a single daughter product. Biodegradation of each substrate follows Monod kinetics, modified to include the effects of EA and nutrient availability. Inhibition functions allow any EA to inhibit utilization of all other EAs that provide less energy to the microbes. Microbial biomass is simulated as scattered microcolonies attached to the porous medium. The model assumes that interphase diffusional limitations to microbial growth are negligible, and no geometrical parameters are assigned to the colonies.

Purpose of This Report

The purpose of this report is (a) to describe SEAM3D, a three-dimensional numerical model for calculation of subsurface transport and biodegradation of multiple aqueous phase solutes using multiple EAs and nutrients in a fully saturated porous medium; (b) to present scenarios for verification of the SEAM3D computer code; (c) to present results of a field scale application of SEAM3D to an unconfined aquifer contaminated by gasoline; and (d) to provide detailed information on model input, output, and execution.

2 Model Development

Conceptual Model

SEAM3D is capable of depicting subsurface transport of multiple solutes in a three-dimensional, anisotropic, heterogeneous domain as influenced by advection, dispersion, adsorption, and biodegradation. The solutes may be biodegradable substrates, nutrients, and EAs for microbial growth; products of biodegradation; daughter products of the substrates; or nonreactive tracers. Typically, the substrates are hydrocarbons that act as electron donors, and the nutrients are inorganic compounds such as phosphate or ammonia. Biodegradation of each substrate is assumed to follow Monod kinetics, although other kinetic models have been proposed (de Blanc, McKinney, and Speitel 1995). The Monod equations are modified to include effects of EA and nutrient availability (Bailey and Ollis 1977), inhibition (Widdowson, Molz, and Benefield 1988), and threshold concentrations (Button 1985). Microbial growth occurs only when substrate concentrations are sufficient to permit the population to double (Simkins and Alexander 1984).

The Monod equation is empirically derived, and is often written in terms of the maximum specific growth rate[1] μ^{max} ($M_b\ M_b^{-1}\ T^{-1}$ where M_b is the microbial biomass and T is time) rather than the maximum specific rate of substrate utilization ν^{max} ($M_s\ M_b^{-1}\ T^{-1}$ where M_s is the substrate mass). Nevertheless, SEAM3D uses the latter formulation to allow values of the use coefficients (see "NAPL dissolution" section) for EAs and nutrients to be estimated from stoichiometric relationships (Borden, Gomez, and Becker 1995). The model assumes that biomass yield (see "NAPL dissolution" section) and ν^{max} are constant with respect to time, even though environmental factors may affect their value (Button 1985). In part, this assumption may be justified since yield often remains constant when carbon sources are the limiting substrate (Simkins and Alexander 1984).

When multiple EAs are available, microbes tend to use them in sequence, starting with the one that provides the highest Gibbs free energy (Table 1). SEAM3D simulates a sequence of six EAs, which are used in the following order (Jørgensen 1989): O_2, NO_3^-, Mn(IV), Fe(III), SO_4^{2-}, and CO_2. Due to the

[1] For convenience, symbols, EAs, and products of biodegradation are listed and defined in the Notation (Appendix B).

Table 1
Electron Acceptors (EAs) Used by the Six Heterotrophic Microbial Populations for Biodegradation of Hydrocarbon Substrates

x[1]	Microbial Population	Ie[2]	EA	Use Possibly Inhibited by	End Products[3]
1	Strict aerobes	1	O_2	--	H_2O, CO_2 [3]
2	Facultative NO_3^- reducers	1	O_2	--	H_2O, CO_2 [3]
		2	NO_3^-	O_2	NO_2
3	Anaerobic Mn(IV) reducers	3	Mn(IV)	O_2, NO_3	Mn(II)
4	Anaerobic Fe(III) reducers	4	Fe(III)	O_2, NO_3, Mn(IV)	Fe(II)
5	Anaerobic SO_4^{2-} reducers	5	SO_4^{2-}	O_2, NO_3, Mn(IV), Fe(III)	H_2O, H_2S
6	Anaerobic methanogens	6	CO_2[3]	O_2, NO_3, Mn(IV), Fe(III), SO_4	H_2O, CH_4

Note: The EAs are listed in order of highest to lowest Gibbs free energy provided. Use of each EA is inhibited by the presence of an EA that provides higher energy.
[1] Subscript for microcolony.
[2] Subscript for valid EA within a microcolony.
[3] H_2O and CO_2 are not simulated in SEAM3D.

low solubility of most Fe(III) and Mn(IV) compounds, these constituents are assumed to occur as solid-phase ions, while the other EAs are dissolved in the aqueous phase. Substrate utilization includes a Monod term for the aqueous phase EAs (see "NAPL dissolution" section); however, utilization is zero order with respect to solid phase Mn(IV) and Fe(III), based on the assumption that these ions are readily available over a range of concentrations. If the concentration of Mn(IV) or Fe(III) falls below a minimum value, then utilization ceases.

SEAM3D can simulate a user-specified nitrogenous compound (N_{user}), Mn(II), Fe(II), H_2S, and CH_4 as products of biodegradation, with each hydrocarbon substrate potentially serving as a source of CH_4. Nitrate serves as the source of N_{user}, Mn(IV) is the source of Mn(II), Fe(III) is the source of Fe(II), and SO_4^{2-} is the source of H_2S. The model handles only a single product of NO_3^- reduction to avoid the complexities of the denitrification process. While products may not be of regulatory concern, these geochemical parameters are easily measured at petroleum-contaminated sites and are viewed as indicators of biodegradation (Landmeyer, Chapelle, and Bradley 1996). Thus, their inclusion in a simulation may assist in the calibration of biodegradation parameters and interpretation of site conditions. In addition, SEAM3D allows each substrate to produce a single daughter product that cannot undergo further biodegradation, but can undergo first-order decay.

The microbial phase is conceptualized as six independent heterotrophic groups (Table 1) that exist as scattered microcolonies attached to the porous

medium. Although transport of microbes within the pore water has been reported (Kim and Corapcioglu 1996), these organisms are assumed to have a negligible effect on biodegradation. The microcolonies and diffusional layer thickness are assumed to be small enough that solute diffusion from the aqueous phase occurs on a much smaller time scale than biodegradation. Thus microbial growth depends directly on the aqueous phase concentrations. Since Mn(IV) and Fe(III) are part of the aquifer solids, they are assumed to be in sufficient contact with the microbes that diffusional limitations do not restrict their use (Brauner and Widdowson 1997). SEAM3D does not explicitly simulate an acclimation period (Chapelle 1993) in which microbes prepare to utilize new subtrates. Thus the time scale for acclimation to substrate is assumed to be much smaller than the overall time scale (often many years) for biodegradation.

Nonaqueous phase liquid (NAPL) mass can be placed at any block in the model domain to simulate dissolution of contaminants from the NAPL into the aqueous phase. The NAPL is conceptualized as being entirely residual, or trapped, within the porous medium, and NAPL flow is not simulated. This simplifying requirement is based on the assumption that the time scale for aqueous phase transport is much greater than the time duration of NAPL mobility. This assumption is likely to be valid for relatively small NAPL spills. For the initial condition, the user specifies the initial mass of NAPL for each dissolution block, and additional mass can be added to the NAPL according to user-defined schedules as the simulation progresses. SEAM3D allows the NAPL to be composed of a maximum of eight biodegradable substrates and five nonbiodegradable tracers, each of which can dissolve into the aqueous phase. The user defines the composition of the NAPL by specifying the mass fraction of each soluble substrate and tracer in the NAPL. If the sum of the mass fractions is less than 1.0, SEAM3D assigns the remaining NAPL mass as a relatively insoluble, or inert, fraction.

Transport and reaction equations

Aqueous phase transport is described by the advection-dispersion equation, which may be written for each hydrocarbon substrate as

$$-\frac{\partial}{\partial x_i}\left(\bar{v}_i S_{ls}\right)+\frac{\partial}{\partial x_i}\left(D_{ij}\frac{\partial S_{ls}}{\partial x_j}\right)+\frac{q_s}{\theta}S_{ls}^{*}-R_{sink,ls}^{bio}+R_{source,ls}^{NAPL}=R_{ls}\frac{\partial S_{ls}}{\partial t} \qquad (1)$$

where

x_i, x_j = distance (L)

$\bar{v}_i$ = average pore-water velocity (L T^{-1})

S_{ls} = aqueous phase substrate concentration (M_{ls} L^{-3}) for ls=1,2,...,NS (number of substrates)

M_{ls} = total mass of the aqueous phase

D_{ij} = tensor for the hydrodynamic dispersion coefficient (L^2 T^{-1})

q_s = volumetric flux of water per unit volume of aquifer (T^{-1}) with $q_s > 0$ for sources and $q_s < 0$ for sinks.

θ = effective transport porosity (L^o)

S_{ls}^* = substrate point source concentration ($M_{ls}\, L^{-3}$)

$R_{sink,ls}^{bio}$ = substrate biodegradation sink term ($M_{ls}\, L^{-3}\, T^{-1}$)

$R_{source,ls}^{NAPL}$ = substrate source term due to NAPL dissolution ($M_{ls}\, L^{-3}\, T^{-1}$)

R_{ls} = retardation factor for substrate *ls* (L^o)

t = time (T)

and *M, L,* and *T* denote mass, length, and time scales. In the case of a point sink, the concentration is generally not specified, and the model uses $S_{ls}^* = S_{ls}$. Non-biodegradable tracers are simulated with a first-order decay term replacing the biodegradation sink term in Equation 1.

For each aqueous phase EA, transport follows

$$-\frac{\partial}{\partial x_i}\left(\bar{v}_i E_{le}\right)+\frac{\partial}{\partial x_i}\left(D_{ij}\frac{\partial E_{le}}{\partial x_j}\right)+\frac{q_s}{\theta}E_{le}^* - R_{sink,le}^{bio} = \frac{\partial E_{le}}{\partial t} \qquad (2)$$

where

E_{le} = EA concentration ($M_{le}\, L^{-3}$) for *le* = 1, 2, and 5

E_{le}^* = EA point source concentration ($M_{le}\, L^{-3}$)

$R_{sink,le}^{bio}$ = EA biodegradation sink term ($M_{le}\, L^{-3}\, T^{-1}$)

A retardation factor does not appear in Equation 2 since O_2, NO_3^-, and SO_4^{2-} are not typically adsorbed to aquifer solids. Equation 2 does not apply when *le* = 3 or 4, since Mn(IV) and Fe(III) are bound to the solid phase (the change in Mn(IV) and Fe(III) concentrations over time will be described in the next section). For each nutrient, transport follows

$$-\frac{\partial}{\partial x_i}\left(\bar{v}_i N_{ln}\right)+\frac{\partial}{\partial x_i}\left(D_{ij}\frac{\partial N_{ln}}{\partial x_j}\right)+\frac{q_s}{\theta}N_{ln}^* - R_{sink,ln}^{bio} = R_{ln}\frac{\partial N_{ln}}{\partial t} \qquad (3)$$

where

N_{ln} = aqueous phase nutrient concentration [$M_{ln}\, L^{-3}$] for *ln* = 1,2,...,NN (number of nutrients)

N_{ln}^* = nutrient point source concentration [$M_{ln}\, L^{-3}$]

$R_{sink,ln}^{bio}$ = nutrient biodegradation sink term [$M_{ln}\, L^{-3}\, T^{-1}$]

R_{ln} = retardation factor for nutrient ln [L^o]

For each biodegradation product (including daughter products), transport follows

$$-\frac{\partial}{\partial x_i}\left(\bar{v}_i P_{lp}\right)+\frac{\partial}{\partial x_i}\left(D_{ij}\frac{\partial P_{lp}}{\partial x_j}\right)+\frac{q_s}{\theta}P_{lp}^{*}-\lambda_{lp}P_{lp}+R_{source}^{bio}=R_{lp}\frac{\partial P_{lp}}{\partial t} \qquad (4)$$

where

P_{lp} = aqueous phase product concentration [$M_{lp}\ L^{-3}$] for lp = 1,2,...,NP (number of products)

P_{lp}^{*} = product point source concentration [$M_{lp}\ L^{-3}$]

λ_{lp} = product first-order decay coefficient [T^{-1}]

R_{source}^{bio} = a biodegradation source term [$M_{lp}\ L^{-3}\ T^{-1}$]

R_{lp} = retardation factor for product lp [L^o]

The biodegradation source/sink term is evaluated by summing the effect of each microcolony on the substrates, EAs, nutrients, and products of biodegradation. The x subscripts for the six microcolonies and the le subscripts for the valid EAs within a microcolony are given in Table 1. Currently, SEAM3D allows microcolony 2 to utilize both O_2 and NO_3^-, while the other microcolonies utilize only one EA. For each substrate degraded by microcolony x, the sink term is

$$R_{sink,ls}^{bio}=\sum_x \frac{M_x}{\theta}r_{x,ls} \qquad (5)$$

where

M_x = microbial biomass concentration [$M_b\ L_{pm}^{-3}$] for x = 1,2,...,NM (number of microcolonies)

$r_{x,ls}$ = utilization rate of substrate ls in microcolony x [$M_{ls}\ M_b^{-1}\ T^{-1}$]

For each EA, the sink term is

$$R_{sink,le}^{bio}=\sum_x \frac{M_x}{\theta}r_{x,le} \qquad (6)$$

where $r_{x,le}$ is the utilization rate of EA le in microcolony x [$M_{le}\ M_b^{-1}\ T^{-1}$]. For each nutrient, the sink term is

$$R_{sink,\mathrm{ln}}^{bio}=\sum_x \frac{M_x}{\theta}r_{x,\mathrm{ln}} \qquad (7)$$

where $r_{x,ln}$ is the utilization rate of nutrient *ln* in microcolony *x* [$M_{ln}\ M_b^{-1}\ T^{-1}$]. For the product CH_4, the source term is

$$R^{bio}_{source,CH_4} = \sum_{ls} \zeta_{x,ls} \frac{M_x}{\theta} r_{x,ls} \tag{8}$$

where $\zeta_{x,ls}$ is the product generation coefficient [$M_{lp}\ M_{ls}^{-1}$], with $x = 6$ for CH_4 production. For the daughter products of the substrates, the source term is

$$R^{bio}_{source,ls} = \zeta^{dau}_{x,ls} \frac{M_x}{\theta} r_{x,ls} \tag{9}$$

where $\zeta^{dau}_{x,ls}$ is the daughter product generation coefficient [$M_{ld}\ M_{ls}^{-1}$]. For the EA products, the source term is

$$R^{bio}_{source,le} = \zeta_{x,le} \frac{M_x}{\theta} r_{x,le} \tag{10}$$

with $\zeta_{x,le}$ the EA product generation coefficient and $x = le = 2$ for N_{user}, $x = le = 3$ for Mn(II), $x = le = 4$ for Fe(II), and $x = le = 5$ for H_2S.

NAPL dissolution

When groundwater contacts a NAPL, components of the NAPL will dissolve into the aqueous phase until equilibrium is reached or NAPL mass is depleted. Since model handling of the dissolution of nonbiodegradable tracers is identical to that of biodegradable substrates, the following description will focus on substrates only. For each substrate *ls*, the driving force for dissolution is the difference between the actual aqueous phase concentration S_{ls} and the equilibrium concentration S^{eq}_{ls}. In general, the rate of dissolution of S_{ls} into groundwater depends on the interfacial area between the NAPL and water (Imhoff, Jaffe, and Pinder 1993), aquifer heterogeneity (Mayer and Miller 1996), the size and shape of the NAPL blobs (Powers, Abriola, and Weber 1994), and the groundwater velocity (Pfannkuch 1984). Thus, if transport processes occur more quickly than NAPL dissolution, S_{ls} may remain lower than S^{eq}_{ls}. This effect can be described mathematically (Imhoff, Jaffe, and Pinder 1993; Parker et al. 1991) by a mass transfer rate coefficient k^{NAPL}, such that the NAPL dissolution term (Equation 1) for substrate *ls* becomes

$$R^{NAPL}_{source,ls} = \max\left[0, k^{NAPL}\left(S^{eq}_{ls} - S_{ls}\right)\right] \tag{11}$$

Using Raoult's Law, S^{eq}_{ls} can be calculated (Corapcioglu and Baehr 1987; Parker et al. 1991) as

$$S^{eq}_{ls} = f_{ls} S^{sol}_{ls} \tag{12}$$

where f_{ls} is the mole fraction of substrate *ls* in the NAPL [$mol_{ls}\ mol_{NAPL}^{-1}$]; and S_{ls}^{sol} is the solubility of pure substrate *ls* in water. During each time-step, f_{ls} is computed as

$$f_{ls} = \frac{S_{ls}^{NAPL} / \omega_{ls}}{I^{NAPL} / \omega_I + \sum_{ls=1}^{NS} S_{ls}^{NAPL} / \omega_{ls} + \sum_{lt=1}^{NT} T_{lt}^{NAPL} / \omega_{lt}} \tag{13}$$

where

S_{ls}^{NAPL} = NAPL mass of substrate *ls* per unit mass dry soil [$M_{ls}\ M_{solid}^{-1}$]

I^{NAPL} = NAPL concentration of inert (i.e., relatively insoluble) constituents [$M_I\ M_{solid}^{-1}$]

T_{lt}^{NAPL} = NAPL concentration of nonbiodegradable tracer *lt* [$M_{ls}\ M_{solid}^{-1}$]

ω_j = molecular weight of NAPL constituent *j*

Equations 12 and 13 represent the concept that the effective solubility of any NAPL constituent is reduced when other constituents are simultaneously dissolving into the aqueous phase. With each time-step, S_{ls}^{NAPL} is updated as

$$\frac{dS_{ls}^{NAPL}}{dt} = -\frac{\theta}{\rho_b} R_{source,ls}^{NAPL} \tag{14}$$

where ρ_b is the bulk density of the porous medium [$M_{solid}\ L_{pm}^{-3}$]. Thus, dissolution causes the NAPL concentration of substrate *ls* to decrease as the aqueous phase concentration increases.

Utilization equations

Utilization of each substrate within microcolony *x* follows

$$r_{x,ls} = \sum_{le} \nu_{x,ls,le} \tag{15}$$

where $\nu_{x,ls,le}$ is the specific rate of substrate utilization (see Equation 19) for microcolony *x* growing on substrate *ls* and EA *le* [$M_{ls}\ M_b^{-1}\ T^{-1}$], and the summation over *le* includes only the valid EAs for microcolony *x* (Table 1). Utilization of each EA follows

$$r_{x,le} = \sum_{ls} \gamma_{x,ls,le} \nu_{x,ls,le} \tag{16}$$

where $\gamma_{x,ls,le}$ is the EA use coefficient [$M_{le}\ M_{ls}^{-1}$], representing the mass of EA *le* used per unit mass of substrate *ls*. Since Mn(IV) and Fe(III) are assumed to be attached to the solid phase, transport is not considered and utilization follows

$$-\frac{M_x}{\rho_b} r_{x,le} = \frac{dE_{le}}{dt} \tag{17}$$

where $x = le = 3$ for Mn(IV) and $x = le = 4$ for Fe(III); and E_{le} is the solid phase concentration [$M_{le}\ M_{solid}^{-1}$]. Utilization of each nutrient follows

$$r_{x,\ln} = \sum_{le} \sum_{ls} \psi_{x,ls,le} \nu_{x,ls,le} \tag{18}$$

where $\psi_{x,ls,le}$ is the nutrient use coefficient [$M_{ln}\ M_{ls}^{-1}$] representing the mass of nutrient *ln* used per unit mass of substrate *ls*.

Using Monod kinetics modified for nutrient and EA availability, $\nu_{x,ls,le}$ may be written

$$\nu_{x,ls,le} = \nu_{x,ls,le}^{\max} \left[\frac{\overline{S}_{ls}}{\overline{K}^{s}_{x,ls,le} + \overline{S}_{ls}} \right] \left[\frac{\overline{E}_{le}}{\overline{K}^{e}_{x,le} + \overline{E}_{le}} \right] N_x I_{le,li} \tag{19}$$

where

$v_{x,ls,le}^{\max}$ = maximum specific rate of substrate utilization

$\overline{S}_{ls}$ = effective concentration of substrate *ls* [$M_{ls}\ L^{-3}$]

$\overline{K}^{s}_{x,ls,le}$ = effective half-saturation constant for substrate *ls* utilizing EA *le* [$M_{ls}\ L^{-3}$]

$\overline{E}_{le}$ = effective concentration of EA *le* [$M_{le}\ L^{-3}$]

$\overline{K}^{e}_{x,le}$ = effective half-saturation constant for EA *le* [$M_{le}\ L^{-3}$];

N_x = Monod function describing nutrient limitations

$I_{le,li}$ is an inhibition function (Widdowson, Molz, and Benefield 1988) defined by

$$I_{le,li} = 1 \qquad \text{for } le = 1 \tag{20}$$

and

$$I_{le,li} = \prod_{li=1}^{le-1} \left[\frac{\kappa_{le,li}}{\kappa_{le,li} + \overline{E}_{li}} \right] \qquad \text{for } le = 2, 3, 4, 5 \text{ or } 6 \tag{21}$$

where $\kappa_{le,li}$ is the EA inhibition coefficient [$M_{le}\ L^{-3}$] representing inhibition of the use of EA *le* by EA *li* and $\overline{E}_{li}$ is the effective concentration of inhibiting EA *le* by EA *li*. If an EA is not specified in a particular simulation, then it is not included in Equation 21. The inhibition function represents the concept that the availability of any EA may inhibit utilization of other EAs that provide less Gibbs free energy to the microbes. As $\kappa_{le,li}$ is assigned a larger value or $\overline{E}_{li}$

decreases, then the inhibitory effect decreases. In analogous fashion, the presence of CH_4 is allowed to inhibit methanogenesis. In this case, the inhibition coefficient κ represents the CH_4 concentration that causes the rate of methanogenesis to be reduced by one half.

N_x may be defined (Widdowson, Molz, and Benefield 1988) as

$$N_x = \prod_{ln} \left[\frac{\overline{N}_{ln}}{\overline{K}^n_{x,ln} + \overline{N}_{ln}} \right] \tag{22}$$

where $\overline{N}_{ln}$ is the effective concentration of nutrient *ln* [$M_{ln}\, L^{-3}$]; and $\overline{K}^n_{x,ln}$ is the effective half-saturation constant for nutrient *ln* ($M_{ln}\, L^{-3}$). Since Equation 22 uses the product of each nutrient Monod term, all nutrients are allowed to limit microbial growth simultaneously. Alternatively, a user option permits only the minimum nutrient to limit growth as follows:

$$N_x = \min_{ln} \left[\frac{\overline{N}_{ln}}{\overline{K}^n_{x,ln} + \overline{N}_{ln}} \right] \tag{23}$$

where the minimum is taken over the range of specified nutrients.

Effective concentrations are used in Equations 19-23 to account for threshold concentrations below which the cells cannot grow (Button 1985; Bosma et al. 1996). $\overline{S}_{ls}$ is defined as

$$\overline{S}_{ls} = \max(S_{ls} - S^t_{ls}, 0) \tag{24}$$

where S^t_{ls} is the threshold concentration of substrate *ls*. Likewise, $\overline{K}^s_{x,ls,le}$ is defined as

$$\overline{K}^s_{x,ls,le} = \max(K^s_{x,ls,le} - S^t_{ls}, 0) \tag{25}$$

where $K^s_{x,ls,le}$ is the half-saturation constant for substrate *ls* utilizing EA *le* [M_{ls} L^{-3}]. In analogous fashion, $\overline{E}_{le}$, $\overline{N}_{ln}$, $\overline{K}^e_{x,le}$, and $\overline{K}^n_{x,ln}$ are defined using E^t_{le} and $N^t_{\ln}$ as the threshold concentrations. When actual concentrations are below threshold, lack of growth is generally attributed to endogenous requirements for cell maintenance (Button 1985). Another explanation is that low concentrations of substrate, EAs, or nutrients may fail to induce enzymes for carrier proteins that transport these components into the cell (Bosma et al. 1996).

For the Mn(IV) and Fe(III) reducing populations, the substrate utilization rate is assumed to be independent of the EA concentration (E_{le}) over a range of

values. Therefore, when E_{le} exceeds E_{le}^{t}, the expression is zero order with respect to the EA, and Equation 19 becomes

$$\nu_{x,ls,le} = \nu_{x,ls,le}^{\max} \left(\frac{\overline{S}_{ls}}{\overline{K}^{s}_{x,ls,le} + \overline{S}_{ls}} \right) N_x I_{le,li} \tag{26}$$

Conversely, when E_{le} falls below E_{le}^{t}, $\nu_{x,ls,le}^{\max}$ is set to zero in Equation 26 and substrate utilization due to that population ceases. This approach, suggested by Chapelle[1] is designed to simulate bioavailability of solid-phase constituents; i.e., when $E_{le} < E_{le}^{t}$ the microbes no longer have direct access to EA on the solid phase.

SEAM3D also assumes that methanogenesis is not limited by EA availability, since CO_2 is typically produced during oxidation of substrates under all other TEAPs modeled. These TEAPs precede methanogenesis and tend to occur at higher rates. Thus, CO_2 is assumed to be abundant, and the rate of substrate utilization follows Equation 26 under methanogenesis. This simplification allows SEAM3D to avoid simulating the complexities of the carbon cycle in the subsurface environment. To fully describe the fate and transport of CO_2, an existing geochemical model could be coupled with the biodegradation model.

Microbial growth equations

Derivation of the microbial growth equations distinguishes between background substrates, which are not modeled explicitly, and the hydrocarbon substrates being modeled. Background substrates are the carbon sources that microbes utilize prior to aquifer contamination by hydrocarbon substrates. When the aquifer is uncontaminated, the background substrate, EA, nutrient, and biomass concentrations are assumed to be at steady state. Thus the background death rate $k_{d_x}^{bk}$ is equal to the growth rate at time zero $G_x^{bk,0}$, just prior to hydrocarbon contamination. SEAM3D calculates $G_x^{bk,0}$ as

$$G_x^{bk,0} = Y_x^{bk} \nu_x^{\max,bk} \left(\frac{\overline{E}_{le}}{\overline{K}^{e}_{x,le} + \overline{E}_{le}} \right) N_x \tag{27}$$

where

$$Y_x^{bk} = \frac{1}{NS} \sum_{ls} Y_{x,ls,le} \tag{28}$$

[1] F. H. Chapelle, Personal Communication, 1996, U.S. Geological Survey, Columbus, SC.

where $Y_{x,ls,le}$ is the biomass yield coefficient [$M_b\ M_{ls}^{-1}$], representing the mass of microcolony x produced per unit mass of substrate ls while utilizing EA le

and

$$\nu_x^{\max,bk} = \frac{1}{NS}\sum_{ls} \nu_{x,ls,le}^{\max} \tag{29}$$

for le representing the final EA utilized by population x. The use of averaged values for Y_x^{bk} and $\nu_x^{\max,bk}$ ensures that $k_{d_x}^{bk}$ will be of the same order of magnitude as the growth rates $G_{x,ls,le}$ due to hydrocarbon substrates (see Equation 31). Initial values for $\overline{E}_{le}$ and N_x are obtained as the spatial average of the initial concentrations, thus requiring the user to input initial concentrations that represent pristine conditions. In Equation 27, the substrate Monod term has been set to one, under the assumption that the half-saturation constant for background substrate is quite small, as is often the case in oligotrophic systems. The inhibition term does not appear in Equation 27 since it is assumed that each population has reached steady state in the presence of inhibitory EAs.

When contamination occurs, steady state no longer applies, as hydrocarbon substrates cause biomass growth accompanied by depletion of EAs and nutrients. As a result, periods of rapid microbial growth may be followed by rapid death. The mass balance equation for growth and death of microbial population x is written

$$\frac{1}{M_x}\frac{dM_x}{dt} = -k_{d_x} + G_{x,ls,le} \tag{30}$$

where k_{d_x} is the "effective" death rate [T^{-1}], and $G_{x,ls,le}$ is the growth rate due to the hydrocarbon substrates, defined as

$$G_{x,ls,le} = \sum_{le}\ \sum_{ls} Y_{x,ls,le}\nu_{x,ls,le} \tag{31}$$

The effective death rate k_{d_x} is computed as the difference between $k_{d_x}^{bk}$ (assumed constant over time) and the current growth rate as follows:

$$k_{d_x} = \max\left[0,\ k_{d_x}^{bk} - \left(G_x^{bk} + G_{x,ls,le}\right)\right] \tag{32}$$

where G_x^{bk} is given by Equation 27 with $\overline{E}_{le}$ and N_x computed from current concentrations at each block in the model domain. In regions having no hydrocarbon substrate, EAs and nutrients remain at background levels; thus $k_{d_x} = 0$, and biomass concentrations also remain at background levels. When hydrocarbon substrates cause sufficient microbial utilization of EA and nutrient, G_x^{bk} and $G_{x,ls,le}$ decrease such that $k_{d_x} > 0$. The value of k_{d_x} will return to zero if

hydrocarbon subtrates are transported out of a zone, and EA and nutrient concentrations return to backgound levels.

If necessary, biomass size is limited by switching to Monod, no-growth kinetics (Simkins and Alexander 1984) when substrate concentrations are insufficient to allow the microbes to double. Thus, G_x^{bk} and $G_{x,ls,le}$ are set to zero when

$$M_x \geq \sum_{ls} \left(Y_{x,ls,le} \, S_{ls} \right) \tag{33}$$

where *le* is the index of the predominant TEAP for population *x*. Overall, Equations 27 to 33 link biomass concentrations to the available substrates, EAs, and nutrients, thereby preventing excessive growth or death. Simulation of biomass may not be desirable in all situations, perhaps due to lack of data. Thus, microbial death and growth can be eliminated from the model by setting the input values of $k_{d_x}^{bk}$ and $Y_{x,ls,le}$ to zero.

Model Implementation

The sequential EA model is implemented as a numerical, block-centered, finite difference computer algorithm (SEAM3D). SEAM3D, version 2.0, is based on the code MT3DMS (Zheng and Wang 1999) whereas SEAM3D, version 1.0 (Waddill and Widdowson 1997) is based on the code MT3D (Zheng 1990; Zheng 1993). MT3D is capable of simulating a single solute in groundwater under the influence of advection, dispersion, source/sink mixing, adsorption, and first-order decay. SEAM3D extends the modular structure of MT3D such that computer memory is not reserved for unused options. For example, if the user chooses to model aerobic biodecay only, then memory is not reserved for the anaerobic processes. SEAM3D interfaces with the groundwater flow model MODFLOW (McDonald and Harbaugh 1988); thus it supports a variety of aquifer configurations and boundary conditions, including confined or unconfined aquifer layers; inclined and/or variable thickness layers; specified concentration or mass flux boundaries; and sources/sinks due to wells, drains, rivers, recharge, and evapotranspiration.

In solving the advection term in the transport equations, SEAM3D supports only the explicit finite difference algorithm. In contrast to the particle tracking algorithms, the finite difference option ensures that mass will be conserved as constituents are utilized or produced during biodegradation. Numerical dispersion error can be minimized by setting the grid spacing on the order of the dispersivity values (Zheng and Bennett 1995). During each transport time-step, SEAM3D calculates concentration changes due to advection, dispersion, and source/sink mixing. The resulting values for $\overline{S}_{ls}$, $\overline{E}_{le}$, and $\overline{N}_{\ln}$ are used in Equation 18 or 25 to obtain $\nu_{x,ls,le}$, from which the utilization rates are calculated in Equations 15, 16, and 18, and biomass concentrations are calculated in Equation 30. The code allows the transport time-step to be subdivided into smaller increments for the biodegradation calculations.

3 SEAM3D Code Verification and Demonstration

When transport parameters were identical and biodegradation was ignored, transport of any type of solute in SEAM3D duplicated the MT3D solute in all verification problems described by Zheng (1990). Since these problems involved code comparison to one-, two-, and three-dimensional analytical transport solutions, the following discussion will focus on the verification of the biodegradation algorithm in SEAM3D. Test cases were devised in which advection, dispersion, and source/sink terms were negligible, so concentration changes depended solely on biodegradation. In each case, the model domain represented a 16- by 16- by 1-m confined aquifer, divided into 16 blocks using 4- by 4- by 1-m spacing. In the generation of the groundwater flow field, the piezometric surface was maintained horizontal, so $\overline{v}_i$ and q_s were zero in the transport simulations. Transport and biodegradation parameters were identical at all nodes, forcing the concentration gradients to be zero.

In general, analytical solutions for the biodegradation equations (5-10) do not exist because the source/sink terms are coupled to biomass growth, and $\nu_{x,ls,le}$ shows a nonlinear dependence on $\overline{S}_{ls}$, $\overline{E}_{le}$, and $\overline{N}_{\ln}$ through the Monod terms in Equation 19 or 26. However, analytical solutions may be obtained if parameters are chosen to prevent biomass growth and to avoid the nonlinear regions of the Monod curve. When the concentration of a limiting factor C is much less than its half-saturation constant K^c, the utilization rate ν can be described by a first order approximation. If C is much greater than K^c, then the Monod curve asymptotically approaches $\nu^{\max}$, and ν becomes zero order with respect to C (Simkins and Alexander 1984).

For verification of SEAM3D, parameters were chosen to produce an analytical solution for comparison. Thus, the purpose of each test case was to check the accuracy of the computer code, not to demonstrate realistic growth and utilization behavior. In all cases, the threshold concentrations S_{ls}^t, E_{le}^t, and N_{ln}^t were zero, allowing the actual concentrations and half-saturation constants to be used in place of the effective values. In each case, two nutrients were simulated using the multiplication option (Equation 22), with N_{ln} = 9.0 g m^{-3} initially, and the half-saturation constant for nutrient ln $K_{x,ln}^n$ = 1.0 g m^{-3}. The nutrient utilization term $\psi_{x,ln}$ was zero, so N_{ln} remained constant, and the value of N_x was constant at 0.81. The inhibition coefficient $\kappa_{le,li}$ was 81 g m^{-3} (μg g^{-1} for Mn(IV)

and Fe(III)), and concentration of the inhibiting EAs E_{li} was 9.0 g m^{-3} (μg g^{-1} for Mn(IV) and Fe(III)). Use coefficients for each E_{li} were always zero, so the value of each inhibition term $\kappa_{le,li}/(\kappa_{le,li} + E_{li})$ in Equation 21 was constant at 0.9. Retardation factors were calculated using a linear adsorption isotherm. Additional parameters that were identical in all cases included effective porosity ($\theta = 0.25$), initial biomass concentration ($M_x = 0.01$ g m^{-3}), and EA product generation coefficient ($\zeta_{x,le} = 0.5$).

SEAM3D Code Verification

Substrate test case

The substrate test case involved degradation of three substrates (S_{ls}) by methanogens ($x = 6$) utilizing two nutrients. The purpose of this test was to verify proper utilization of multiple substrates having different sorptive properties. Methanogens were chosen to allow the inhibition function (Equation 21) to be tested for all EA inhibitors. The governing equation for this test was derived by combining Equations 5, 15, and 26 in the $R^{bio}_{\sin k,ls}$ term of Equation 1 as follows:

$$\frac{\partial S_{ls}}{\partial t} = -\frac{M_6 \nu^{\max}_{6,ls,6}}{\theta R_{ls}} \left(\frac{S_{ls}}{K^{s}_{6,ls,6} + S_{ls}} \right) N_6 I_{6,li} \tag{34}$$

As described previously, N_6 and $I_{6,li}$ were forced to be constant over time, with $N_6 = 0.81$. Methanogens were inhibited by O_2, NO_3^-, Mn(IV), Fe(III), and SO_4^{2-}, so $I_{6,li} = 0.5905$. The substrate retardation factors were $R_1 = 1$, $R_2 = 2$, and $R_3 = 3$. Since the biomass yield $Y_{x,ls,le}$ and background death rate $k^{bk}_{d_x}$ were zero (Table 2), M_6 was constant, and only S_{ls} varied with time. Because S_{ls} was much less than $K^{s}_{6,ls,6}$ (Table 2), Equation 34 simplified to

$$\frac{dS_{ls}}{dt} \cong -k_1 S_{ls} \tag{35}$$

where the first-order decay k_1

$$k_1 = \frac{M_6 \nu^{\max}_{6,ls,6}}{K^{s}_{6,ls,6} \theta R_{ls}} N_6 I_{6,li} \tag{36}$$

Predicted concentrations showed close agreement with the analytical solutions (Figure 1) for the three values of k_1 (0.00191, 0.00383, and 0.00765 day^{-1}). Since each k_1 incorporated all aspects of the model relevant to substrate utilization, this case provided an adequate test of the handling of the process by the code. It is emphasized that parameters were selected to impose first-order

Table 2
Parameters for Substrate Test Case

Test Case	*x*	*ls*	$K^{s}_{x,ls,le}$ g m^{-3}	$K^{e}_{x,le}$ g m^{-3}	$\nu^{\max}_{x,ls,le}$ day^{-1}	$k^{bk}_{d_x}$ day^{-1}	$Y_{x,ls,le}$ g m^{-3}	S_{ls} g m^{-3}	$\gamma_{x,ls,le}$ g g^{-1}
Substrate	6	1	800	--	8	0	0	10	0
	6	2	800	--	32	0	0	10	0
	6	3	800	--	96	0	0	10	0
Sulfate	5	1-3	0.001	800	3	0	0	9999	4
Fe(III)	4	1-3	0.001	--	0.212	0	0	9999	40
Microbial growth	6	1-3	0.001	--	0.0279	0	0.5	9999	0
Growth limitation	6	1-3	10	--	0.05	0	0.5	20	0
Growth versus death	5	1-3	5	5	0.1	--	0.5	5	4

Note: Parameters for substrate half-saturation coefficient $K^{s}_{x,ls,le}$, electron acceptor half-saturation coefficient $K^{e}_{x,le}$, maximum specific rate of substrate utilization $\nu^{\max}_{x,ls,le}$, background microbial death rate $k^{bk}_{d_x}$, yield coefficient $Y_{x,ls,le}$, initial substrate concentration S_{ls}, and electron acceptor use coefficient $\gamma_{x,ls,le}$. Values of the EA index le were identical to the microbial population index x.

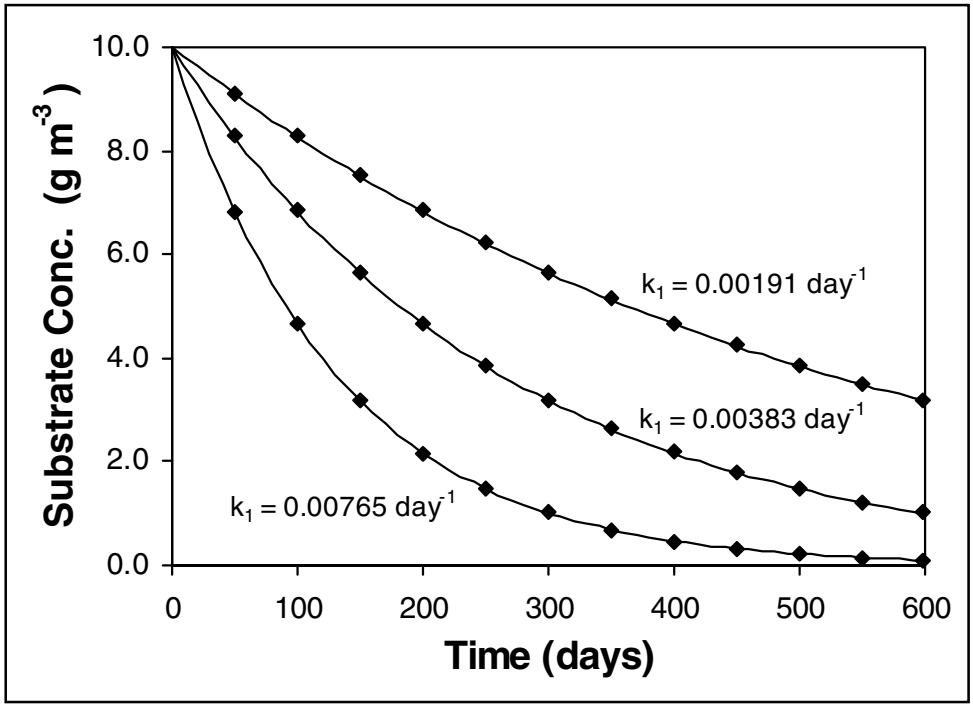

Figure 1. SEAM3D-predicted substrate concentrations (diamonds) versus analytical solutions (lines) with parameters chosen to impose three rates of first-order decay

decay for model verification, and they do not represent field or laboratory measurements. In a field situation, microbial growth and limited EA availability can cause actual decay of hydrocarbon substrates to deviate significantly from a first-order approximation.

Sulfate test case

To verify utilization of aqueous-phase EAs and the creation of products, model parameters were chosen to allow EA utilization by three substrates to follow first-order kinetics. All EAs were tested successfully, but only the results for SO_4^{2-} ($x = le = 5$) will be presented here. Equations 6, 16, and 19, were combined in the $R_{sink,le}^{bio}$ term of Equation 2 to derive a governing equation, which simplified to

$$\frac{dE_5}{dt} \cong -k_1 E_5 \tag{37}$$

where

$$k_1 = \sum_{ls=1}^{3} \frac{M_5 \gamma_{5,ls,5} \nu_{5,ls,5}^{\max}}{K_{5,5}^{e} \theta} N_5 I_{5,li} \tag{38}$$

The substrate Monod term does not appear in Equation 38 because S_{ls} was much greater than $K_{5,ls,5}^{s}$ (Table 2), so the term was approximately equal to one. As before, N_5, M_5, and $I_{5,li}$ were forced to be constant over time, with $N_5 = 0.81$. Sulfate reducers were inhibited by O_2, NO_3^-, Mn(IV), and Fe(III), so $I_{5,li} = 0.6561$. The sulfate concentration (E_5) was 9.0 g m^{-3} initially, so E_5 was always much less than $K_{5,5}^{e}$ (Table 2), and the EA Monod term simplified to ($E_5 / K_{5,5}^{e}$).

For generation of the product H_2S ($lp = 5$), Equations 2, 6, 9, and 37 were combined in the R_{source}^{bio} term of Equation 4 to derive a governing equation, which simplified to

$$\frac{dP_5}{dt} \cong k_1 \frac{\zeta_{5,5}}{R_5} E_5 \tag{39}$$

where k_1 is defined by Equation 38, and R_5 is the H_2S retardation factor. Integration of Equation 34 gives $E_5 = E_5^o \exp(-k_1 t)$, where E_5^o is the initial concentration of SO_4^{2-}. After substitution for E_5, Equation 38 can be integrated to obtain

$$P_5 \cong -\frac{\zeta_{5,5}}{R_5} E_5^o \left[\exp(-k_1 t) - 1\right] + P_5^o \tag{40}$$

where P_5^o is the initial concentration of H_2S. For this test case, R_5 was 1 and P_5^o was 0. Predicted concentrations of SO_4^{2-} and H_2S show close agreement with the analytical solutions (Figure 2), with the generation coefficient $\zeta_{5,5} = 0.5$ causing 9.0 g m^{-3} SO_4^{2-} to produce 4.5 g m^{-3} H_2S.

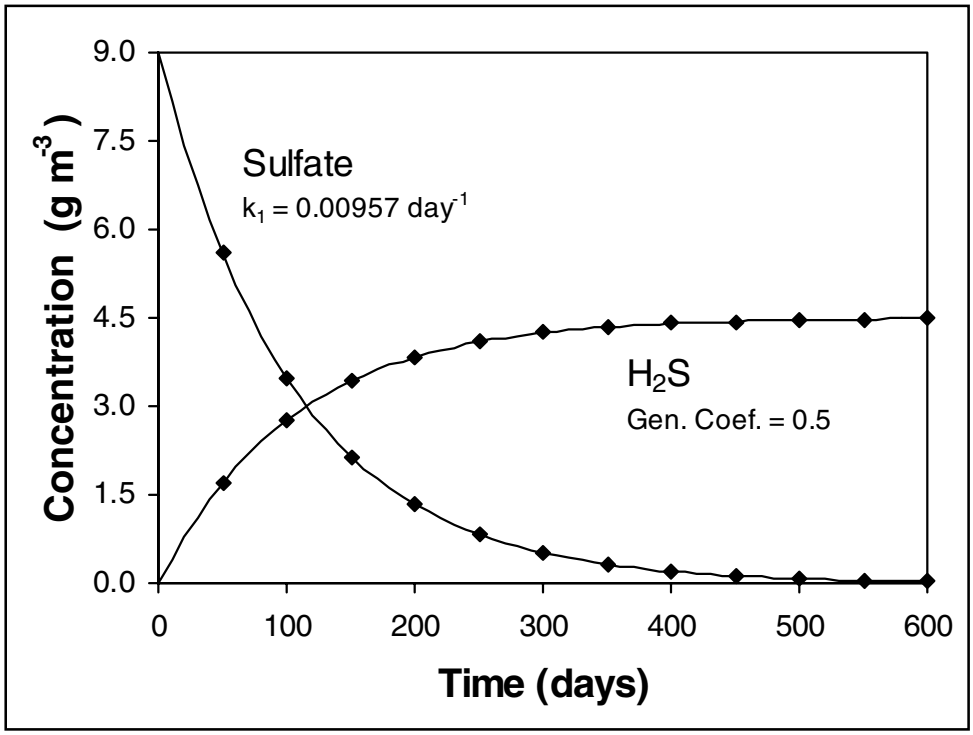

Figure 2. SEAM3D-predicted SO_4^{2-} and H_2S concentrations (diamonds) versus analytical solutions (lines)

Fe(III) test case

To verify model handling of solid-phase EAs and their products, parameters were chosen to allow EA utilization by three substrates to follow zero-order kinetics. Both Fe(III) and Mn(IV) were tested successfully, but only the results for Fe(III) ($x = le = 4$) will be presented here. Equations 16 and 26 were combined in Equation 17 to derive a governing equation, which simplified to

$$\frac{dE_4}{dt} \cong -k_0 \tag{41}$$

where

$$k_0 = (1\times10^6)\sum_{ls=1}^{3}\frac{M_4\gamma_{4,ls,4}\nu_{4,ls,4}^{\max}}{\rho_b}N_4 I_{4,li} \tag{42}$$

and the factor of (1×10^6) converts micrograms to grams. As before, N_4, M_4, and $I_{4,li}$ were forced to be constant over time, with $N_4 = 0.81$. Fe(III) reducers were inhibited by O_2, NO_3^-, and Mn(IV), so $I_{4,li} = 0.729$. The initial concentration of Fe(III) was 210 μg g^{-1}, the threshold concentration was 10 μg g^{-1}, and ρ_b was 1.5 g cm^{-3}. As before, the substrate Monod term does not appear in Equation 42, because S_{ls} was much greater than $K^s_{4,ls,4}$ (Table 2). For generation of the product Fe(II) ($lp = 4$), Equations 9, 17, and 41, were combined in the R^{bio}_{source} term of Equation 4 to derive a governing equation, which simplified to

$$\frac{dP_4}{dt} \cong \frac{k_0}{(1\times10^6)} \frac{\zeta_{4,4}\rho_b}{R_4\theta} \tag{43}$$

where k_0 is defined by Equation 42 and R_4 is the Fe(II) retardation factor. In this test case, R_4 was 5.0, and initial P_4 was 0. Predicted concentrations of Fe(III) and Fe(II) show close agreement with the analytical solutions (Figure 3).

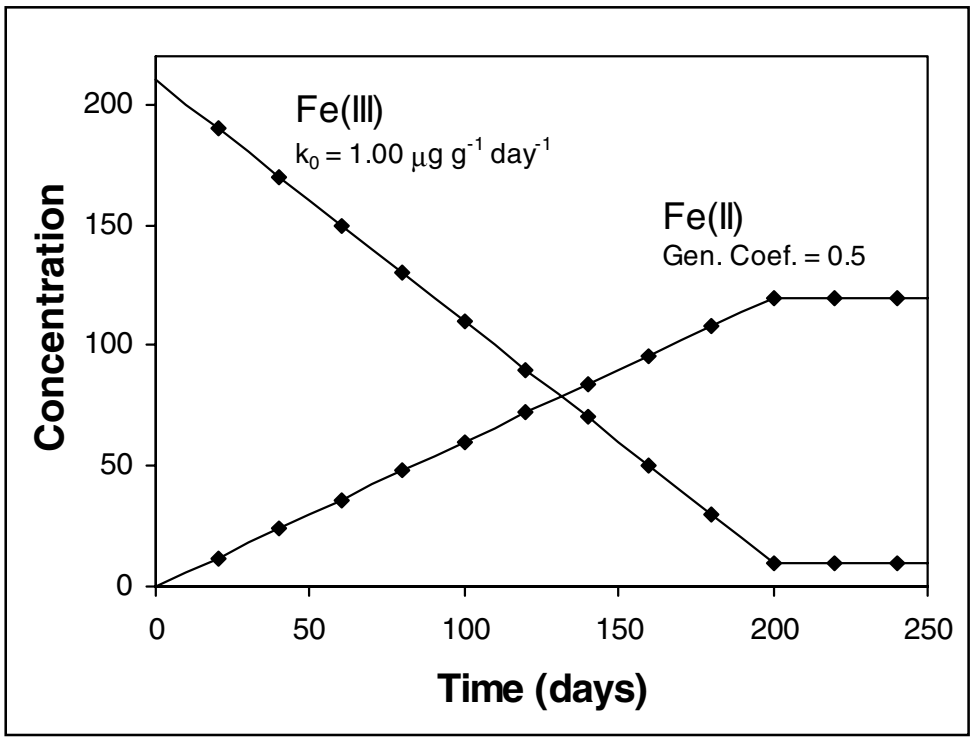

Figure 3. SEAM3D-predicted Fe(III) and Fe(II) concentrations (diamonds) versus analytical solutions (lines). Units are μg g^{-1} for Fe(III) and g m^{-3} for Fe(II)

Microbial growth test case

Model implementation of microbial growth was verified by choosing parameters to allow methanogens ($x = le = 6$) to grow exponentially on three

substrates. Equations 26, 31, and 32 were combined in Equation 30 to derive a governing equation, which simplified to

$$\frac{dM_6}{dt} \cong k_1 M_6 \tag{44}$$

where

$$k_1 = -k_{d_6} + \sum_{ls=1}^{3} Y_{6,ls,6} \nu_{6,ls,6}^{\max} N_6 I_{6,li} \tag{45}$$

As in the substrate test case, N_6 and $I_{6,li}$ were forced to be constant over time, with $N_6 = 0.81$ and $I_{6,li} = 0.6561$. Values for each S_{ls} were much greater than $K^s_{6,ls,6}$ (Table 2), so the substrate Monod term dropped out of Equation 45. Predicted values of biomass concentration M_x show close agreement with the analytical solution (Figure 4).

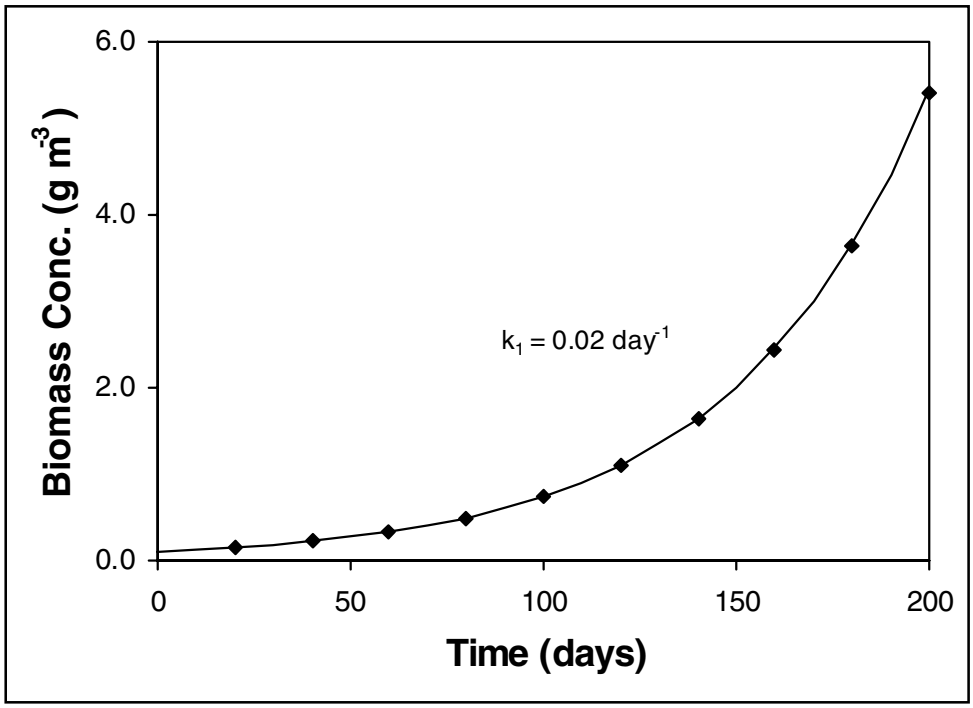

Figure 4. SEAM3D-predicted biomass concentrations (diamonds) versus analytical solutions (lines) for the microbial growth test case

NAPL dissolution test case

In order to verify the NAPL dissolution algorithm, model parameters were chosen to allow dissolution of a single substrate to follow first-order kinetics. The model domain was 100 by 20 by 20 m, divided into 20 columns, 4 rows, and 4 layers using 5- by 5- by 5-m blocks. Velocity was 0.32 m day^{-1}, and longitudinal dispersivity was 0.5 m. The 16 blocks in the first column ($j = 1$)

contained NAPL source. For each block where NAPL mass existed, the initial NAPL concentration of the substrate $S_{ls}^{NAPL,0}$ was 9.9×10^{-6} g g^{-1}, so the initial NAPL mass of substrate *ls* ($M_{ls}^{NAPL,0}$) was 29.7 kg. The initial NAPL concentration of the tracer $T_{lt}^{NAPL,0}$ was zero, so the NAPL concentration of inert constituents I^{NAPL} was 9.99×10^{-3} g g^{-1}. In addition, k^{NAPL} was 0.03 day^{-1}, R_{ls} was 1001, S_{ls}^{sol} was 20,000 g m^{-3}, ω_{ls} and ω_I were 150 g mole^{-1}, ρ_b was 1.5 x 10^6 g m^{-3}, and θ was 0.25.

Since $T_{lt}^{NAPL,0}$ was zero and $S_{ls}^{NAPL,0}$ was always much less than I^{NAPL}, Equation 13 simplified to

$$f_{ls} = \frac{S_{ls}^{NAPL} / \omega_{ls}}{I^{NAPL} / \omega_I} \tag{46}$$

The large values for R_{ls} and S_{ls}^{sol} allowed S_{ls}^{eq} to be much greater than S_{ls}, so S_{ls} could be omitted from Equation 11. Equations 12 and 13 were substituted in Equation 11 to obtain

$$R_{source,ls}^{NAPL} = k^{NAPL}\left(\frac{S_{ls}^{NAPL} / \omega_{ls}}{I^{NAPL} / \omega_I}\right) S_{ls}^{sol} \tag{47}$$

Since transport affected the concentrations at individual blocks, the analytical solution was derived for the total mass of substrate throughout the domain. This allowed changes in NAPL and aqueous phase masses to depend solely on the dissolution rate. For the NAPL, the total mass of substrate M_{ls}^{NAPL} was obtained as

$$M_{ls}^{NAPL} = \sum_{j,i,k} \rho_b S_{ls}^{NAPL} \tag{48}$$

where *j*, *i*, and *k* are indices for the columns, rows, and layers of the domain. For the aqueous phase, the total mass M_{ls} was calculated as

$$M_{ls} = \sum_{j,i,k} \theta S_{ls} \tag{49}$$

Equations 47 and 48 were combined in Equation 14 to derive a governing equation for the NAPL, which simplified to

$$\frac{dM_{ls}^{NAPL}}{dt} \cong -k_1 M_{ls}^{NAPL} \tag{50}$$

where

$$k_1 = \frac{\theta}{\rho_b} k^{NAPL} \left(\frac{\omega_I}{I^{NAPL} \omega_{ls}} \right) S_{ls}^{sol} \tag{51}$$

For generation of aqueous phase substrate, Equations 47 and 49 were combined in the $R_{source,ls}^{NAPL}$ term of Equation 1 to derive a governing equation, which simplified to

$$\frac{dM_{ls}}{dt} \cong \frac{k_1}{R_{ls}} M_{ls}^{NAPL} \tag{52}$$

where k_1 is defined by Equation 51. Integration of Equation 50 gives $M_{ls}^{NAPL} = M_{ls}^{NAPL,0} \exp(-k_1 t)$. After this expression is substituted for M_{ls}^{NAPL}, Equation 52 can be integrated to obtain

$$M_{ls} \cong -\frac{1}{R_{ls}} M_{ls}^{NAPL,0} \left[\exp(-k_1 t) - 1 \right] + M_{ls}^{o} \tag{53}$$

where M_{ls}^{o} is the initial aqueous phase mass of substrate, set to zero for this test case. Predicted concentrations of NAPL and aqueous phase masses show close agreement with the analytical solutions (Figure 5).

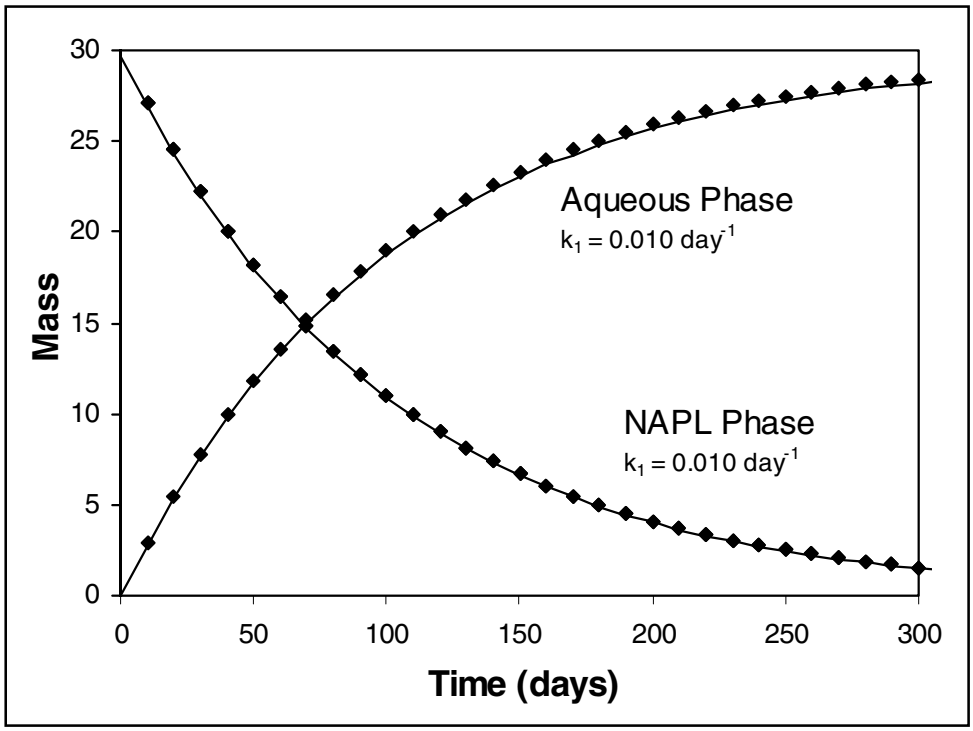

Figure 5. SEAM3D-predicted NAPL and aqueous phase substrate concentrations (diamonds) versus analytical solutions (lines) for the NAPL dissolution test case. Units are kg for the NAPL and g for the aqueous phase

SEAM3D Code Demonstrations

Demonstration of growth limitation

The no-flow domain from the previous sections was used to demonstrate the method for microbial growth limitation in the section "Microbial growth equations" in Chapter 2. Three hydrocarbon substrates were utilized by methanogens, with relevant parameters shown in Table 2. The boundary condition for each substrate was constant concentration, which is commonly used to represent a contaminant source zone. When the growth limitation method was not employed, M_x grew exponentially (Figure 6) without bound.

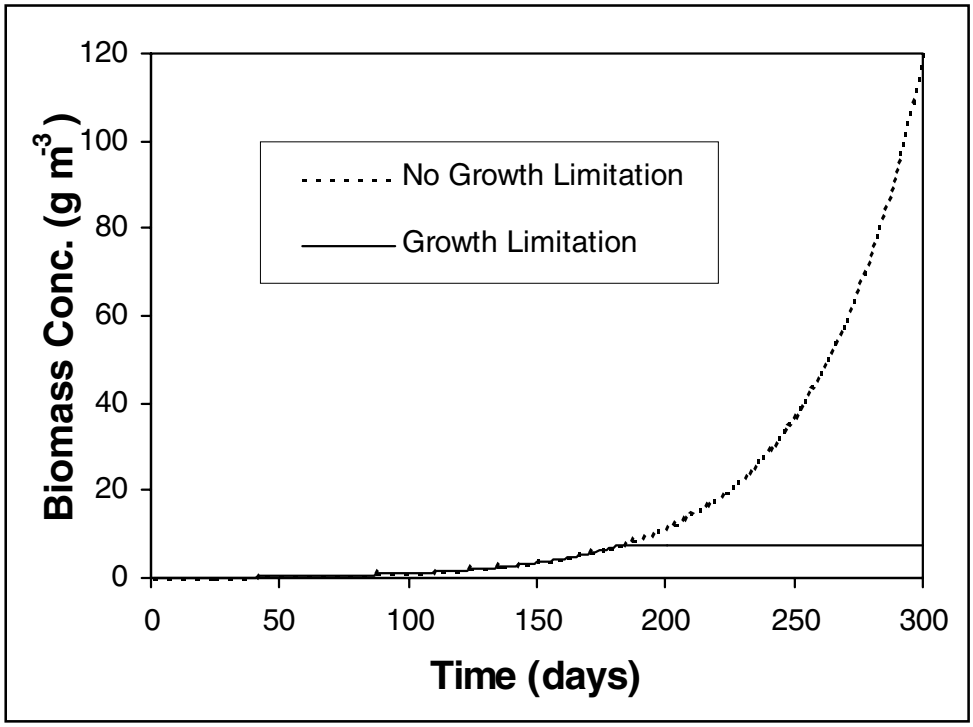

Figure 6. SEAM3D-predicted biomass concentrations versus time, showing the effect of the growth limitation algorithm

The growth limitation method did not affect biomass at early times (Figure 6) when ample substrate was available for the microbes. However, by 180 days, M_x had increased to 7.5 g m^{-3}, which is the critical value obtained from Equation 33. Thus the total substrate concentration did not allow another doubling of the microbes, and the population quit growing. In field-scale simulations, substrate, EA, and nutrient availability generally prevent biomass from reaching the critical concentration. However, the critical concentration may be reached at the upgradient edge of a contaminant source zone, where substrate, EA, and nutrients may be abundant for many years. Also, restrictions on microbial growth may be needed to simulate sites where engineered systems provide nutrients and EAs to an aquifer for enhanced bioremediation.

Demonstration of microbial growth versus death

The no-flow domain from the previous sections was used to demonstrate microbial growth as influenced by the effective death term discussed in the "Microbial growth equations" section in Chapter 2. Three substrates and two nutrients were utilized by SO_4^{2-} reducers, with relevant parameters shown in Table 2. Initial concentrations were 9.0 g m^{-1} for SO_4^{2-}, and 0.01 g m^{-1} for biomass. Nutrient initial concentrations were 9.0 g m^{-1}, with $K^n_{x,ln}$ = 5.0 g m^{-3} and $\psi_{x,ln}$ = 4.0. All blocks in the model domain were active for all components. When the effective death term was used, the value for $k^{bk}_{d_x}$ was 0.0133 day^{-1}, and the value of k_{d_x} varied according to Equation 32. For comparison, additional simulations were performed with k_{d_x} forced to be constant at 0.0, 0.005, and 0.02 day^{-1}.

In the absence of microbial death (k_{d_x} = 0), biomass increased monotonically until EA and nutrients became depleted (Figure 7), with 2.09 g m^{-3} substrate utilized. When k_{d_x} varied, biomass peaked at 230 days, and a total of 1.81 g m^{-3} substrate was utilized. A similar amount of substrate (1.82 g m^{-3}) was utilized when k_{d_x} = 0.005 day^{-1}; however, for k_{d_x} = 0.02 day^{-1}, only 0.349 g m^{-3} was utilized because the growth rate never exceeded the death rate. Thus, biomass concentration simply decreased from its initial value (Figure 7).

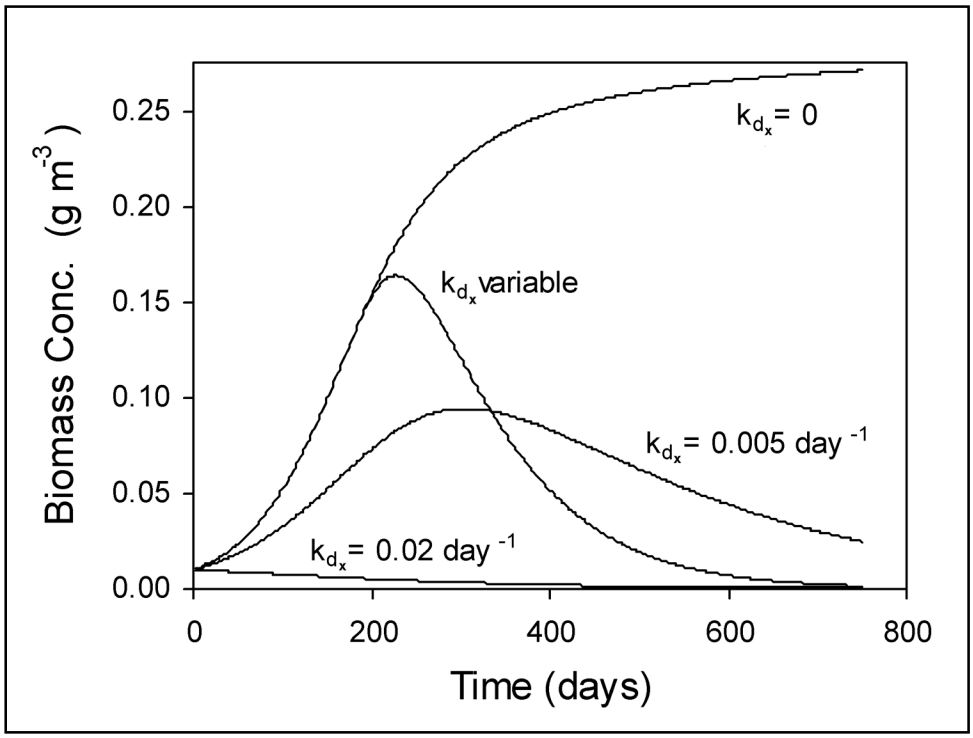

Figure 7. SEAM3D-predicted biomass concentrations versus time for various values of the death rate k_{d_x}

Biodegradation of five hydrocarbons

The no-flow domain from the previous sections was used to demonstrate utilization of five hydrocarbons (HCs) by O_2, NO_3^-, Fe(III), SO_4^{2-}, and methanogens at various values for ν^{max}. For all EAs and microbial populations, the following initial values were used:

Variable	Value
M_x	0.001 g m^{-3}
$\kappa_{le,li}$	0.1 g m^{-3} (μg g^{-1} for Fe(III)
$K^s_{x,ls,le}$	0.01 g m^{-3}
$K^e_{x,le}$	1.0 g m^{-3}
$Y_{x,ls,le}$	0.5 g g^{-1}

The small value for $K^s_{x,ls,le}$ caused utilization to be zero order with respect to hydrocarbon concentration; thus the relative rates of utilization of the five hydrocarbons remained constant, even as their concentrations changed. Initial aqueous concentrations were 12 g m^{-3} for all hydrocarbons, 8 g m^{-3} for O_2, 40 g m^{-3} for NO_3^-, 90 μg g^{-1} for Fe(III), and 60 g m^{-3} for SO_4^{2-}. EA use coefficients $\gamma_{x,ls,le}$ were 3.0, 4.0, 40.0, and 4.0 g g^{-1} for O_2, NO_3^-, Fe(III), and SO_4^{2-}, respectively. For the first hydrocarbon (HC1), $\nu^{max}_{x,ls,le}$ was 1.0 day^{-1} for O_2 and 0.5 day^{-1} for all anaerobic processes. These rates were divided in half for each successive hydrocarbon, HC2 to HC5. All hydrocarbons were retarded with R_{ls} = 2, and effective porosity was 0.3.

As expected, each hydrocarbon was utilized twice as fast as its successor; e.g., all 12 g m^{-3} HC1 were used by 61 days, while 6 g m^{-3} HC2 remained (Figure 8). The low values for $\kappa_{le,li}$ caused a high degree of inhibition; thus each EA was depleted (Figure 9) before utilization of the next EA began. Analysis of the data showed that each EA was utilized correctly according to its use coefficient. Initially, there were sufficient O_2, NO_3^-, Fe(III), and SO_4^{2-} to degrade 37.6 g m^{-3} hydrocarbon, and 37.7 g m^{-3} were degraded by the time (about 44 days) all four EAs were consumed. Note that due to retardation, the aqueous concentrations in Figure 8 reflect only half of the 37.7 g m^{-3} that were degraded. Following the depletion of each EA (shown by the arrows in Figure 8), there was a period of slow utilization as the next microbial population grew to a significant level. If the $\kappa_{le,li}$ and initial M_x had been larger, then these periods would have been less pronounced. Nevertheless, an initially small M_x may cause a lag in substrate utilization as the microbes acclimate to the changing availability of EAs.

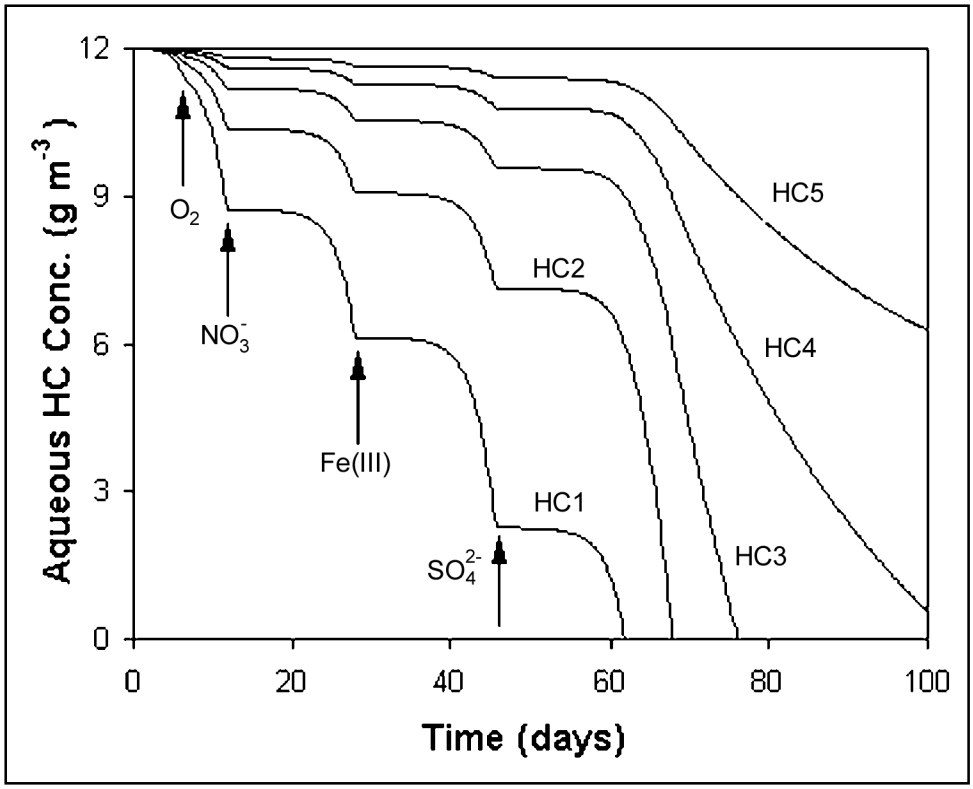

Figure 8. SEAM3D predictions of the five hydrocarbon (HC) substrate concentrations, showing the effect of varying the maximum specific rate of substrate utilization $v^{\max}_{x,ls,le}$. Arrows indicate the termination of each EA process

Three-dimensional example problem

Selected capabilities of SEAM3D were demonstrated in a hypothetical fully three-dimensional domain. SEAM3D was applied to a hypothetical, three-dimensional domain (Figures 10 and 11), whose dimensions were selected as 1,000 m in the longitudinal x-direction, by 400 m in the transverse y-direction, and by 15 m in the vertical z-direction. The domain was divided into 40 rows, 100 columns, and 5 layers using 10- by 10- by 3-m blocks. The analysis focuses on biodegradation of a single hydrocarbon using O_2, NO_3^-, Fe^{3+}, SO_4^{2-}, and CO_2 (for methanogenesis) as EAs. For comparison, additional simulations are made using oxygen as the sole EA.

Flow parameters. MODFLOW was used to generate the steady-state flow field for contaminant transport. The uppermost aquifer was unconfined with a hydraulic conductivity of 6 m^2 day^{-1} (Figure 11). The lower layers were given a transmissivity (TR) of 18 m^2 day^{-1}, and the vertical leakage between layers was 6 m^2 day^{-1}. Thus, the aquifer was basically homogeneous, even though it was divided into five layers. Boundary conditions were no flow along y = 0 and y = 400, and a constant head of 53 m at x = 0 and 48 m at x = 1000. Thus without recharge, the hydraulic gradient was a uniform 0.005. The bottom of the

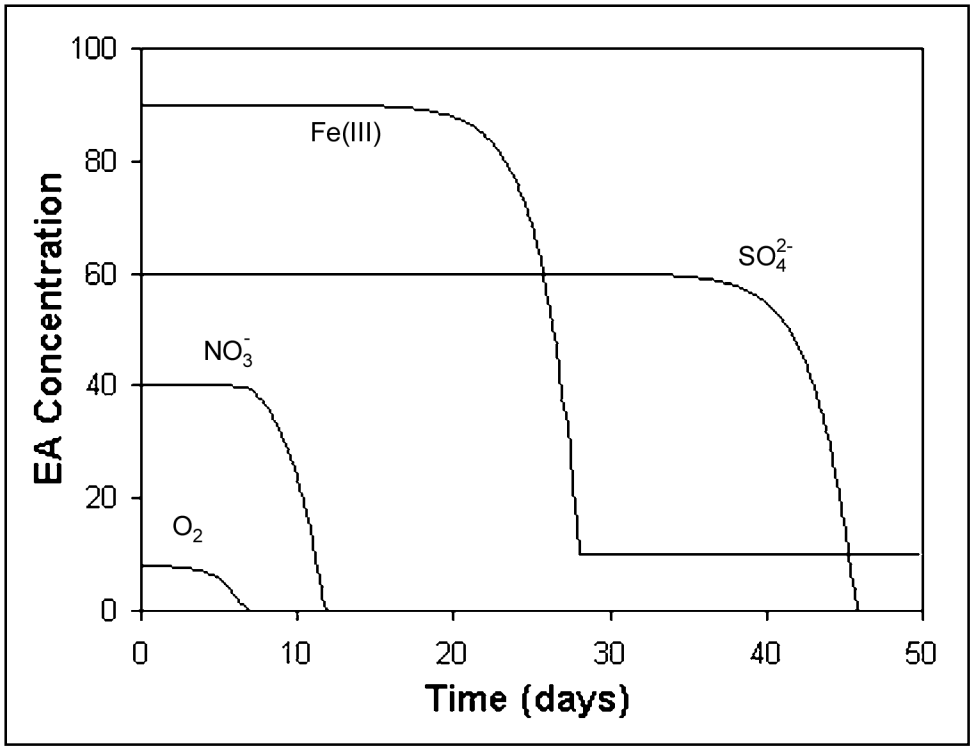

Figure 9. SEAM3D predictions of EA concentrations, showing that utilization of each EA is inhibited until the preceding EA has been depleted

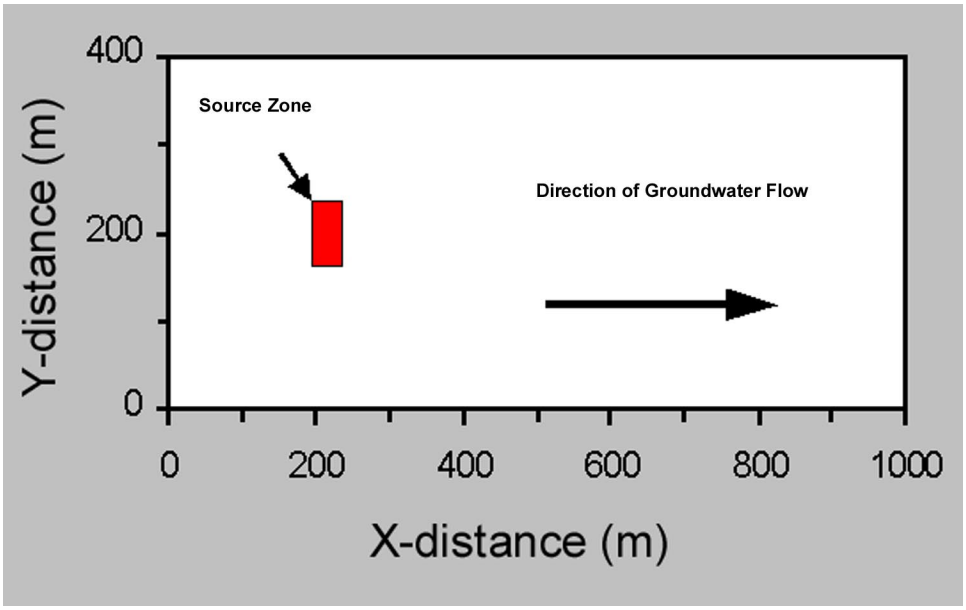

Figure 10. Areal view of the three-dimensional model domain

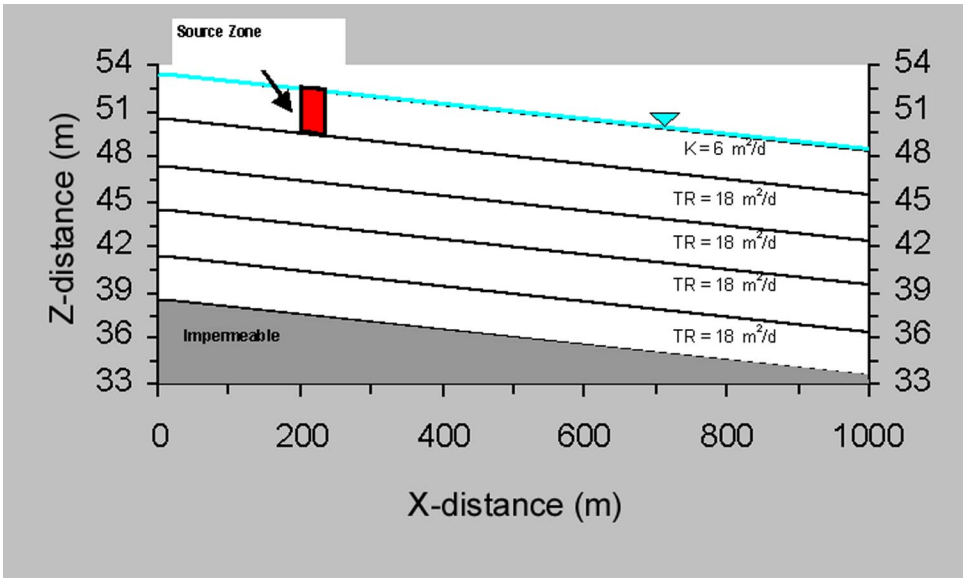

Figure 11. Vertical cross section through the model domain, showing the water table, model layers, and aquifer bottom elevations

unconfined aquifer was given the same slope as the water table, so its thickness was uniform.

Transport parameters. A single biodegradable hydrocarbon (properties similar to toluene) and a nonbiodegradable tracer were simulated. Biodegradation involving O_2 as the sole EA was compared with sequential biodegradation involving O_2, NO_3^-, solid Fe(III), SO_4^{2-}, and methanogenesis. In both cases, a single dissolved nutrient for microbial growth was also simulated. Longitudinal dispersivity α_x was chosen as 15 m, transverse dispersivity α_y was 4.5 m, and vertical dispersivity α_z was 0.12 m. The effective porosity for transport was 0.25. The retardation factor for the end product Fe(II) was chosen to be 4.5, while all other solutes were not retarded.

A constant source of contaminant was located near x = 200 and y = 200 (Figure 10). Biodegradable hydrocarbon and nonbiodegradable tracer were introduced only in the uppermost layer of the domain (Figure 11). Initial concentrations at all nodes were 4.1 g m^{-3} for dissolved oxygen (DO), 8.1 g m^{-3} for NO_3^-, 10.1 g m^{-3} for SO_4^{2-}, 50 g m^{-3} for nutrient, 0.02 g m^{-3} for dissolved Fe(II), 0.01 g m^{-3} for H_2S, 0.001 g m^{-3} for CH_4, and 100 µg g^{-1} for solid-phase Fe(III). Initial concentrations for the hydrocarbon and tracer were 45 g m^{-3} in the source area and zero elsewhere. Minimum concentrations (below which biodegradation will not occur) were set at 10 µg g^{-1} for Fe(III) and 0.3 g m^{-3} for aqueous EAs.

Boundary conditions were specified as constant concentration equal to the initial condition at x = 0 for all aqueous-phase EAs, end products, and the nutrient. Hydrocarbon and tracer boundary conditions were specified as constant concentration in the source area. For all species, nodes not specified as constant concentration were allowed to be active, and solute flowed out of the domain under zero dispersion if necessary. All simulations ran for 4,000 days.

Results and discussion. The final areal distributions of the nonbiodegradable tracer, the hydrocarbon with aerobic decay, and the hydrocarbon with sequential decay are shown in Figure 12. For each species, concentrations diminish with increasing depth, since contaminant mass must disperse from the source area to the lower layers. This effect is most pronounced when all EAs are used. Biodegradation also limits lateral spreading, so both hydrocarbon plumes are narrower than the tracer in the y-direction. The downgradient edge of the tracer plume travels approximately 100 m further than the hydrocarbon plume with aerobic decay, and 200 m further than the hydrocarbon with sequential decay. Thus, even though the initial concentrations of NO_3^-, SO_4^{2-}, and Fe(III) are relatively low, they do contribute to the containment of the plume.

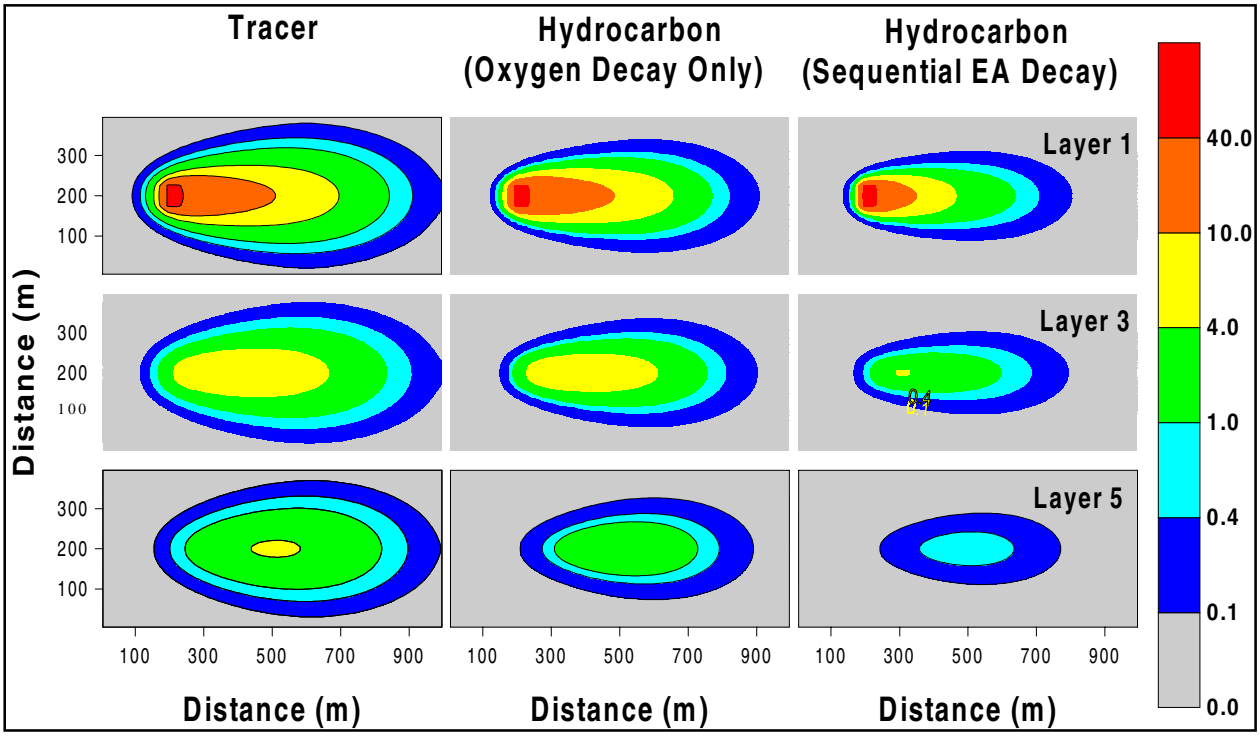

Figure 12. Concentrations, g/m^3, of nonbiodegradable tracer (left) versus hydrocarbon in layers 1, 3, and 5 at 4,000 days. Hydrocarbon was simulated with O_2 decay only (middle) and with DO, NO_3^-, Fe(III), SO_4^{2-}, and CO_2 as sequential EA (right)

Figures 13 and 14 show the final areal distributions of the EAs O_2, NO_3^-, solid Fe(III), and SO_4^{2-}. As expected, EA depletion decreases with depth, reflecting the hydrocarbon distribution. No Fe(III) was used in the bottom layer, indicating that O_2 and NO_3^- are inhibiting Fe(III) reduction. Since O_2, NO_3^-, and Fe(III) would all inhibit SO_4^{2-} use, the SO_4^{2-} depletion in the bottom layer must be caused by dispersion to the upper layers, and not to SO_4^{2-} reduction in the bottom layer.

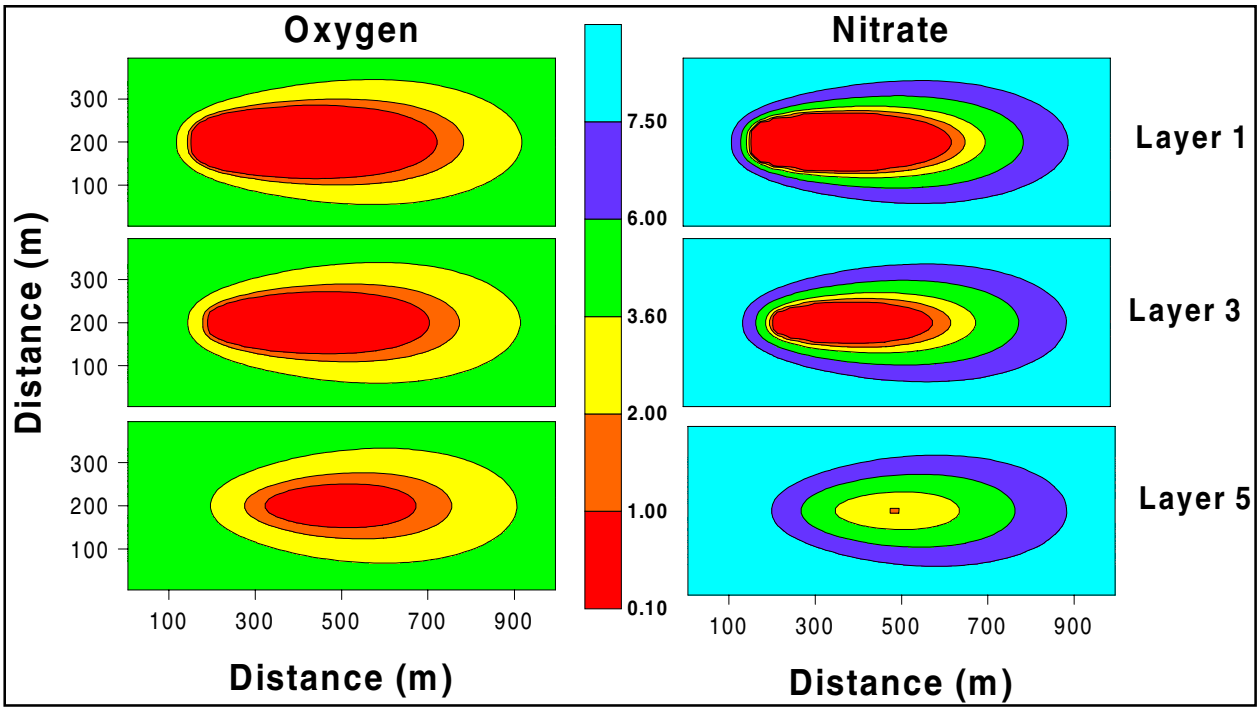

Figure 13. Concentrations of EAs O_2 and NO_3^- in layers 1, 3, and 5 at 4,000 days

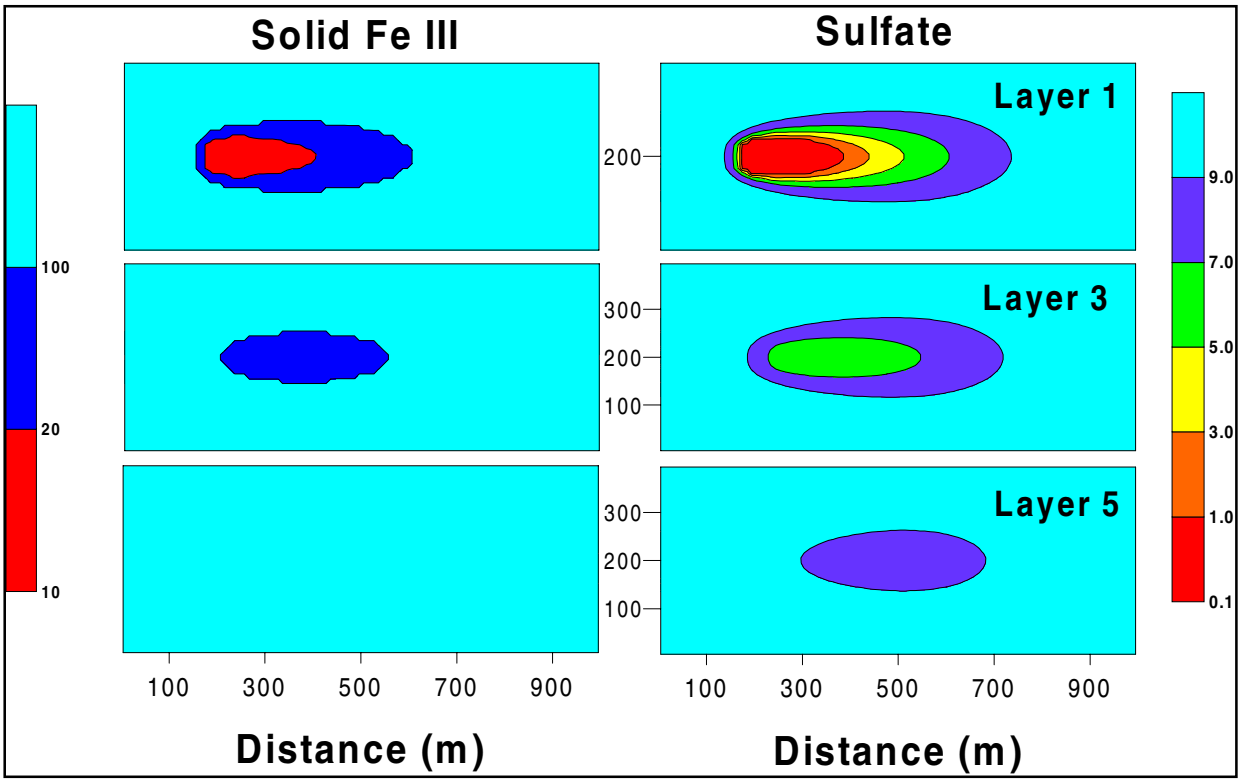

Figure 14. Concentrations of EAs Fe(III) and SO_4^{2-} in layers 1, 3, and 5 at 4,000 days

The end products of biodegradation (Figure 15) show the same trends as the hydrocarbon and the EAs. In the two upper layers, CH_4 concentrations are higher than H_2S, even though the maximum specific rate of substrate utilization ν^{max} is lowest for methanogenesis. This occurs because SO_4^{2-} depletion limits H_2S production, while hydrocarbon is still available for methane production. In addition, the model assumes that the EA CO_2 for methanogenesis is abundant due to the other biodecay processes that produce CO_2. Since SO_4^{2-} reduction inhibits methanogenesis, H_2S production begins prior to methanogenesis; thus H_2S is transported further than methane (Figure 15). Due to its retardation factor of 4.5, Fe(II) moves more slowly than H_2S or methane, even though Fe(II) production begins prior to the other end products. Still, all three end products have been transported beyond their zones of production, demonstrating that the presence of an end product does not necessarily indicate the EA process.

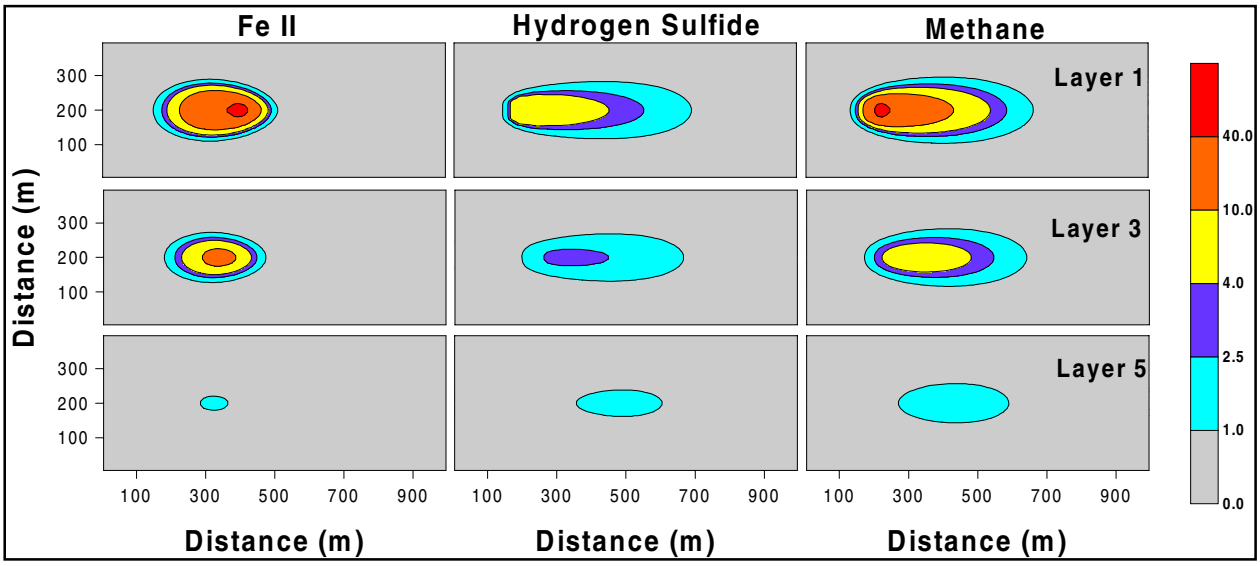

Figure 15. Concentrations of end products in layers 1, 3, and 5 at 4,000 days

Conclusions

The computer code SEAM3D demonstrated close agreement with analytical solutions for biodegradation of multiple solutes utilizing the entire range of EAs. Test cases were chosen to verify the major aspects of the biodegradation algorithm, and the results suggest that the computer code correctly implements the model. Demonstration scenarios indicated that the method of linking growth and death rates to concentrations of available substrates, EAs, and nutrients placed reasonable limits on microbial biomass. Although an acclimation period to new substrates is not included in the conceptual model, the effect of microbial acclimation to changing EA availability was shown to cause a lag in utilization.

4 Application of SEAM3D to a Field Site

Introduction

SEAM3D was applied to a subsurface spill of gasoline from underground storage tanks at the Laurel Bay Exchange, Marine Corps Air Station, Beaufort, SC. Site records indicate that the spill probably began in late 1990. Site measurements indicated that gasoline had spread along the water table as a NAPL and created a continuing source of groundwater contamination. EAs available at the site included O_2, Fe(III), SO_4^{2-}, and CO_2. Concentrations of NO_3^- were measured at the site and found to be too low to degrade significant amounts of hydrocarbon. Groundwater samples taken in 1994 indicated that biodegradation of benzene, toluene, ethylbenzene, and xylenes (BTEX) was occurring with O_2 and Fe(III) acting as EAs (Landmeyer, Chapelle, and Bradley 1996). Production of Fe(II) was observed only in locations where O_2 was depleted, suggesting O_2 inhibition of Fe(III)-based biodegradation. No H_2S or CH_4 production was measured in 1994, but additional data collected in 1996 and 1997 showed significant concentrations of H_2S and CH_4 and elevated levels of molecular hydrogen (H_2). This indicated that SO_4^{2-} reduction and methanogenesis had begun at least 4 years after the contamination occurred.

Gasoline is a complex mixture of dozens of organic compounds, and the composition of gasoline varies with time of year, manufacturer, and octane level (Sigsby et al. 1987). Therefore, gasoline contains numerous substrates that can utilize EAs. To model EA depletion accurately, it is important to account for all biodegradable substrates. Otherwise, the model will overpredict the amount of EA available to react with the compounds of interest such as BTEX. For example, if a gasoline spill occurs and benzene only is simulated, then the model allows all available EA mass to react with the benzene. In reality, other hydrocarbons from the gasoline are utilized and prevent a certain percentage of the EAs from biodegrading with benzene. For modeling purposes, it is impractical to simulate all components of gasoline individually. Therefore, it is common practice (Baehr and Corapcioglu 1987; Rixey et al. 1991; Rixey and Dortch 1992) to lump certain compounds together and create a simplified NAPL representative of gasoline (Table 3). For example, it may be reasonable to lump all aliphatics together since they generally have low solubility and are utilized only under aerobic conditions. For these simulations, the BTEX compounds were treated individually because toluene tends to biodegrade preferentially

Table 3
Mass Fraction of Various Components of Gasoline, g g^{-1}, as Measured or Used in Simulations by the Researchers Listed

Component	Sigsby et al. 1987		Baehr and Corapcioglu 1987	Rixey et al. 1991	Parr, Walters, and Hoffman 1991	Rixey and Dortch 1992
	No-lead Regular	No-lead Premium				
Benzene	1.76	1.96	1.14	1.0	1.94	1.0
Toluene	5.54	20.25	6.07	7.0	4.73	5.0
Ethylbenzene	1.17	0.94	--	9.0[1]	2.00	10.0
Xylene	7.04	4.21	--	--	9.65	--
Total aromatics	31.23	44.2	27.52	39.0	--	36.0
Total aliphatics	68.77	55.8	52.26	61.0	--	64.0
Heavy ends	--	--	20.21	--	--	--

[1] Total of ethylbenzene and xylene.

relative to the others; not all BTEX biodegrade using all of the EAs simulated; and the predicted benzene concentration is typically the basis for regulatory decisions on intrinsic bioremediation.

Site Description

The contaminated site is located at the Laurel Bay Exchange, Marine Corps Air Station, Beaufort, SC. A continuing source of groundwater contamination resulted when gasoline leaked from storage tanks at the Marine Corps Exchange (MCEX) Service Station. Details of the site history and hydrogeology are given in ABB Environmental Services (ABB-ES) (1993) and Landmeyer, Chapelle, and Bradley (1996), so this section will serve to summarize information relevant to the modeling effort.

NAPL source history

Three underground gasoline storage tanks (Figure 16) were installed at the MCEX site in 1973. The tanks were first tested for tightness by the overfill method in December 1989, but the results were inconclusive for all three tanks. Tanks 1537 and 1538 failed a test for tightness by the underfill method in December 1990, and in September 1991, 51 mm (2 in.) of NAPL was observed in monitoring well LB-EX-1. In November 1991, tanks 1536 and 1537 were determined to be tight, but tank 1538 was still leaking, so it was emptied and taken out of service. A total of approximately 0.095 m^3 (25 gal) of NAPL was

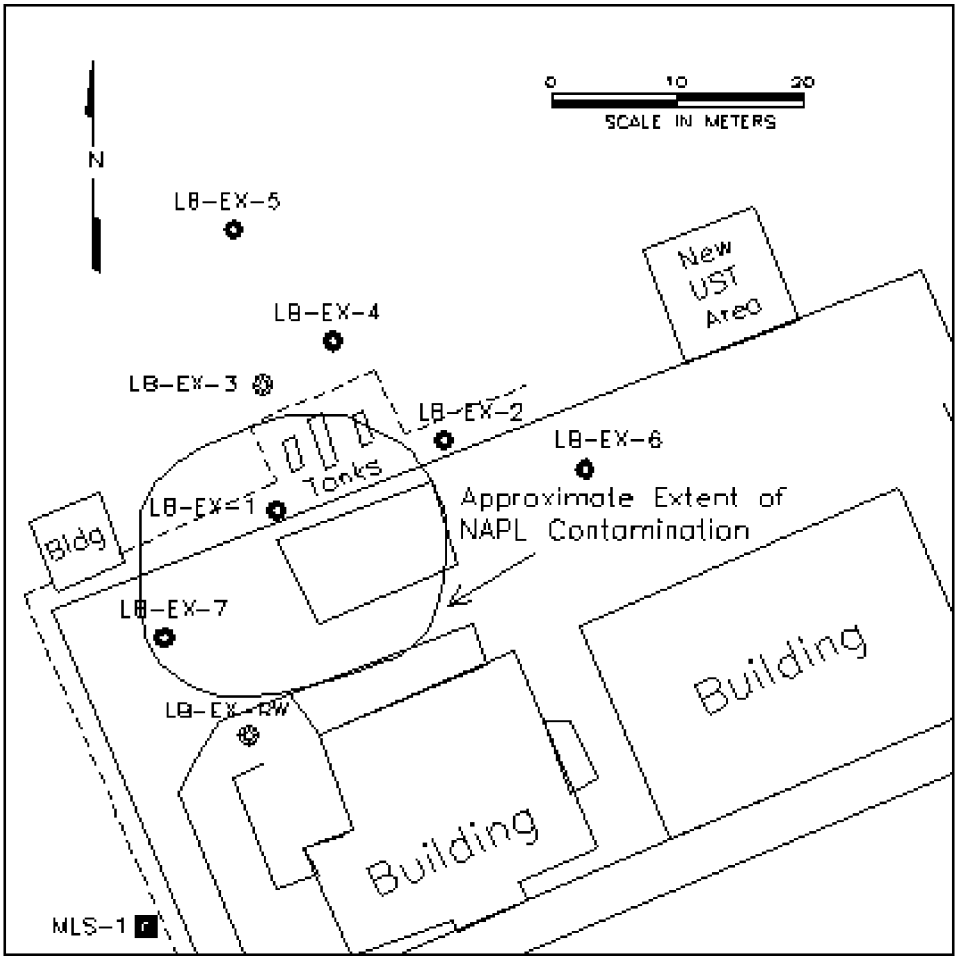

Figure 16. Site map of the Laurel Bay Exchange, Marine Corps Air Station, Beaufort, SC, showing locations of the leaking gasoline storage tanks and the estimated extent of nonaqueous phase contamination in 1993

bailed out of LB-EX-1 from October 1991 until March 1993, with NAPL thickness in the well ranging from 100 to 900 mm. In April 1993, ABB-ES investigated the area to determine the horizontal and vertical extent of contamination. Based on observation of visible NAPL sheen and analysis of soil cores, ABB-ES estimated that NAPL occupied a circular area approximately 22 m in diameter (Figure 16). Thus, NAPL had migrated in the direction of the water table gradient from the immediate vicinity of the tanks. In late 1993, the tanks and surrounding sediments were removed (Landmeyer, Chapelle, and Bradley 1996).

Field monitoring

During their site investigation, ABB-ES drilled 27 soil borings to the water table and installed 12 shallow groundwater monitoring wells (LB-EX-5 through -16) screened over the water table. The screened interval below the water table varied from 2.52 to 3.79 m, depending on the water table elevation and the well

location. In addition to the shallow wells, a deep well (LB-EX-17) was installed in the base of the aquifer next to LB-EX-8 (Figure 17) to provide an estimate of the vertical gradient in piezometric head and the vertical extent of contaminant migration. ABB-ES measured concentrations of BTEX and methyl-tert-butyl-ether (MTBE) in the soil vapor, water, and solids. In March 1994, the United States Geological Survey (USGS) continued the site investigation and installed monitoring wells LB-EX-18 to LB-EX-22 (Figure 17). The USGS tested the groundwater for BTEX and MTBE, and also measured concentrations of

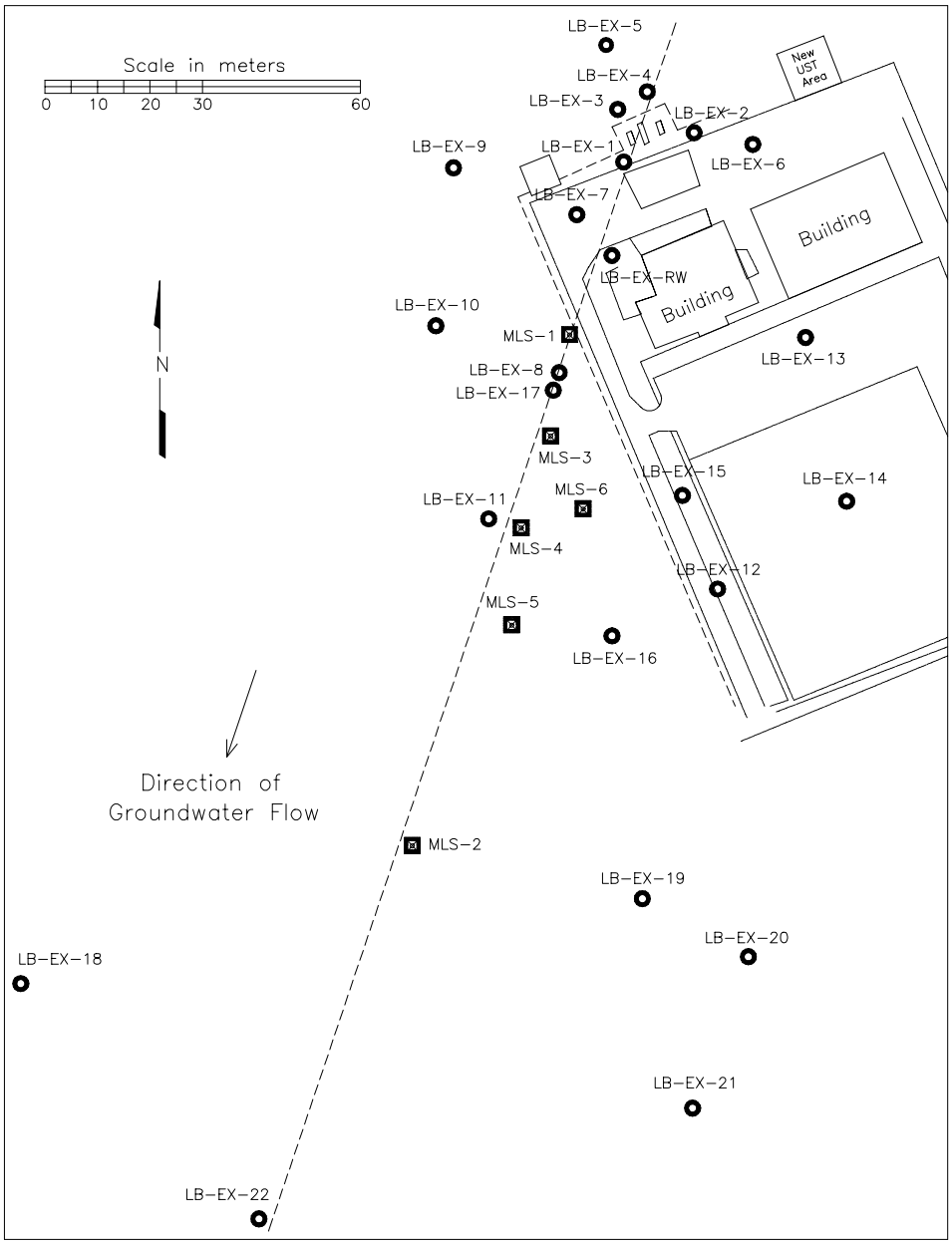

Figure 17. Locations of the monitoring wells and multilevel samplers installed at the gasoline spill site. The dashed line marks the transect through the center of the plume

potential EAs (O_2, NO_3^-, SO_4^{2-}) and products of biodegradation (Fe(II), H_2S, CH_4, H_2, and dissolved inorganic carbon). To obtain additional data on the vertical distribution of contamination, two multilevel sampling (MLS) wells were installed at the site in October 1995, and four additional multilevel samplers (Figures 17 and 18) were installed in June 1996. The USGS measured concentrations of BTEX, EAs, and products again in June 1996 and January 1997. Due to the relatively low elevation of the water table in June 1996, only the lower ports of the multilevel samplers (Table 4) could be sampled. In January 1997, MLS-1 was the only multilivel sampler from which measurements were obtained.

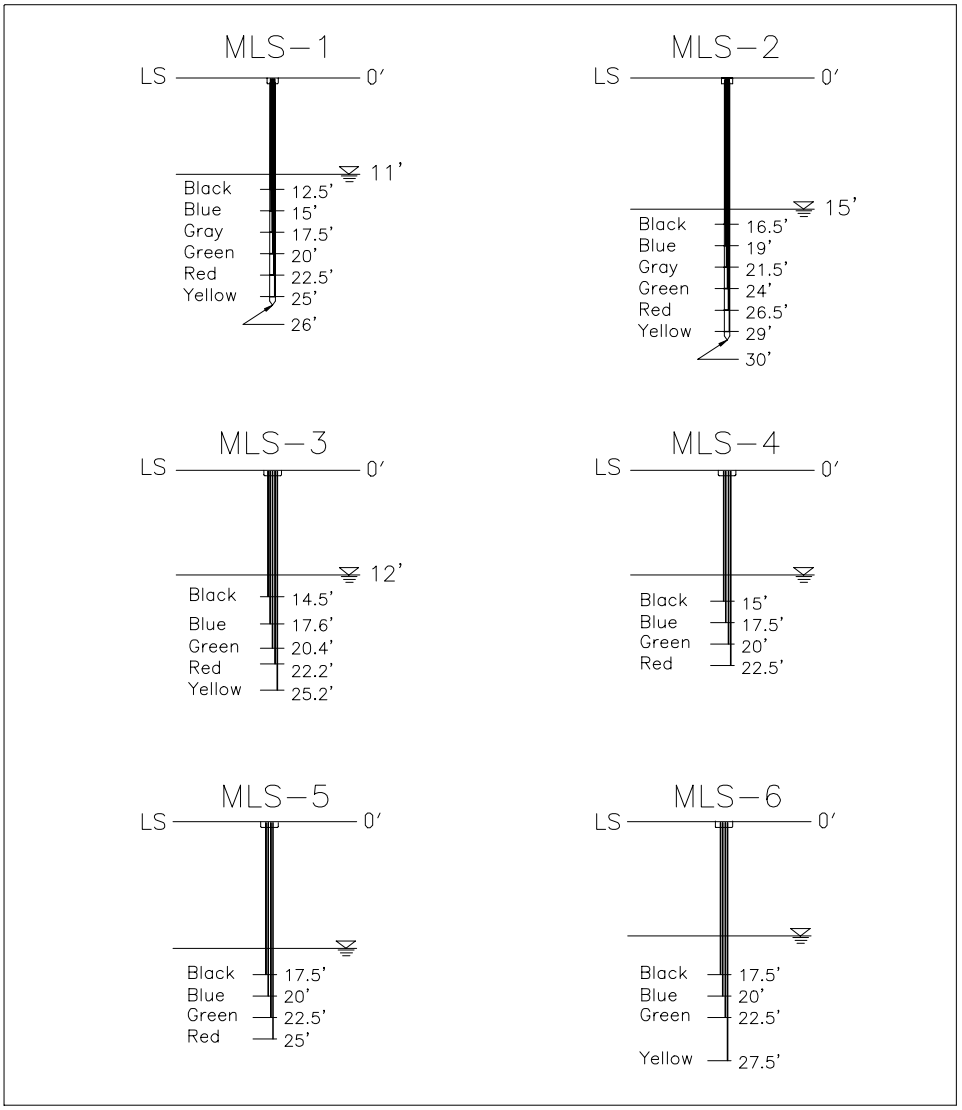

Figure 18. Detail of the multilevel samplers used to monitor the vertical distribution of contamination. The color code for the sampling tubes is indicated, and the depth below land surface (LS) in feet is given (to convert depths to meters, multiple by 0.3048)

Table 4
Concentrations of BTEX, MTBE, EAs, and Products of Biodegradation Measured in the MLS Wells on June 25, 1996

Well	Port Depth[1] m	Concentration, g m^{-3}									
							EA		Product		
		Benzene	Toluene	Ethyl Benzene	Total Xylene	MTBE	O_2	SO_4^{2-}	Fe(II)	H_2S	CH_4
MLS-1	2.0	--	--	--	--	--	--	1.58	4.94	13.6	--
	2.7	5.80	22.7	3.06	9.45	0.69	0.00	0.07	4.67	1.10	0.20
	3.5	7.09	21.4	3.33	9.69	22.9	0.00	0.13	4.90	4.30	0.40
MLS-3	2.5	--	--	--	--	--	--	18.6	10.3	0.20	0.60
	3.4	0.73	0.30	0.41	0.57	2.20	0.00	3.49	2.31	30.0	--
MLS-4	0.6	--	--	--	--	--	--	39.8	4.86	0.40	0.20
	1.3	--	--	--	--	--	0.00	2.5	4.65	0.10	0.20
	2.1	9.40	0.02	1.13	2.43	102.0	0.00	4.09	4.26	10.8	0.20
MLS-5	1.1	--	--	--	--	--	0.91	9.45	0.29	0.00	--
	1.9	0.06	0.28	0.01	0.04	2.18	1.04	10.9	2.06	0.00	--
	2.6	0.10	0.13	0.02	0.06	2.34	1.25	10.4	1.68	0.00	--
MLS-6	2.7	--	--	--	--	--	0.00	25.5	4.64	0.0	0.20
	4.2	1.34	2.00	0.22	0.59	19.2	0.00	7.52	4.15	0.0	0.10

[1] Port depth refers to depth below the 1996 water table.

Hydrogeology

The unconfined Atlantic Coastal Plain aquifer at the MCEX site is composed mostly of fine-grained silty sand (ABB-ES 1993). The depth from the ground surface to the regional confining unit is approximately 12 m, while the depth to the water table averages 3 m. Thus the saturated thickness of the aquifer is approximately 9 m. Measurements of the water table elevations at the site have revealed water table fluctuations of less than 1 m, although fluctuations of 2 m have been reported in the general area (ABB-ES 1993). ABB-ES performed slug tests on LB-EX-6, -13, -14, and -16 and calculated a geometric mean hydraulic conductivity of 3.383 m day^{-1} for the aquifer. The horizontal water table gradient was estimated as 0.0059 in 1993, 0.0046 in 1994, and 0.0059 in 1996. The vertical gradient in piezometric head was estimated as 0.023 in 1993 and 0.017 in

1996, based on measured water levels in shallow well LB-EX-08 and deep well LB-EX-17.

Laboratory investigations

Landmeyer, Chapelle, and Bradley (1996) measured adsorption of benzene and toluene onto aquifer solids, and used a linear model to estimate the distribution coefficient K_D. Values of K_D ranged from 0.057 to 0.14 $cm^3\ g^{-1}$ for toluene and 0.057 to 0.28 $cm^3\ g^{-1}$ for benzene. Laboratory measurements of toluene biodegradation were obtained from microcosms containing sediments and groundwater collected near LB-EX-RW and LB-EX-8. Microbial degradation rates under aerobic and anaerobic conditions were estimated from the measured rate of $^{14}CO_2$ production from radiolabeled toluene. The aerobic biodecay rate was estimated as 0.64 day^{-1}, while the anaerobic rate was 0.003 day^{-1}. The anaerobic biodegradation rate for benzene was estimated as 0.00025 day^{-1} (Landmeyer, Chapelle, and Bradley 1996) using trial and error matching of measured benzene concentrations versus concentrations predicted by the solute transport model SUTRA (Voss 1984), using first-order decay to simulate benzene biodegradation.

SEAM3D Parameter Estimation

All parameters for SEAM3D were initially chosen based on site data or literature values. Subsequently, the model was calibrated to the 1993, 1994, and 1996 data by adjusting a limited number of parameters to create a match between predicted and observed concentrations of hydrocarbons, EAs, and products. In general, parameters were not adjusted if an accurate measurement was available. Parameters that were allowed to be adjusted included dispersivities, maximum specific rates of substrate utilization $\nu^{\max}_{x,ls,le}$, inhibition coefficients $\kappa_{le,li}$, and mass fractions of BTEX and other constituents in the NAPL. Only the inhibition coefficients were adjusted using the 1996 data.

Model domain and control parameters

The three-dimensional model domain for flow and transport (Figure 19 and 20) was 400 m in the longitudinal x-direction, 98 m in the transverse y-direction, and 9 m in the vertical z-direction. The domain was divided into 49 rows, 200 columns, and 9 layers using 2- by 2- by 1-m blocks. The uppermost aquifer layer was specified as unconfined, and the bottom elevation of this layer was given the same slope as the water table. Thus the vertical thickness of the aquifer was uniform. The flow solution was steady state, while the transport simulations were transient, with both the transport time-step and the biodegradation time-step set to 1.5 days. Time zero for the simulations was chosen as December 15, 1990, when the tanks first failed a test for tightness. For model calibration, simulations ran for 2,025 days, to encompass the 1993, 1994, and 1996 data. Predictive simulations ran for 6,000 days, although data for comparison were available only for the 1997 data at 2,230 days.

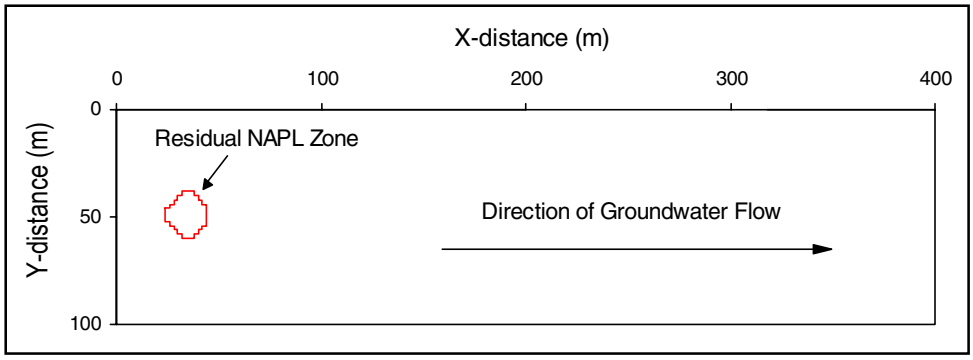

Figure 19. Areal view of the SEAM3D model domain used to simulate the Laurel Bay site

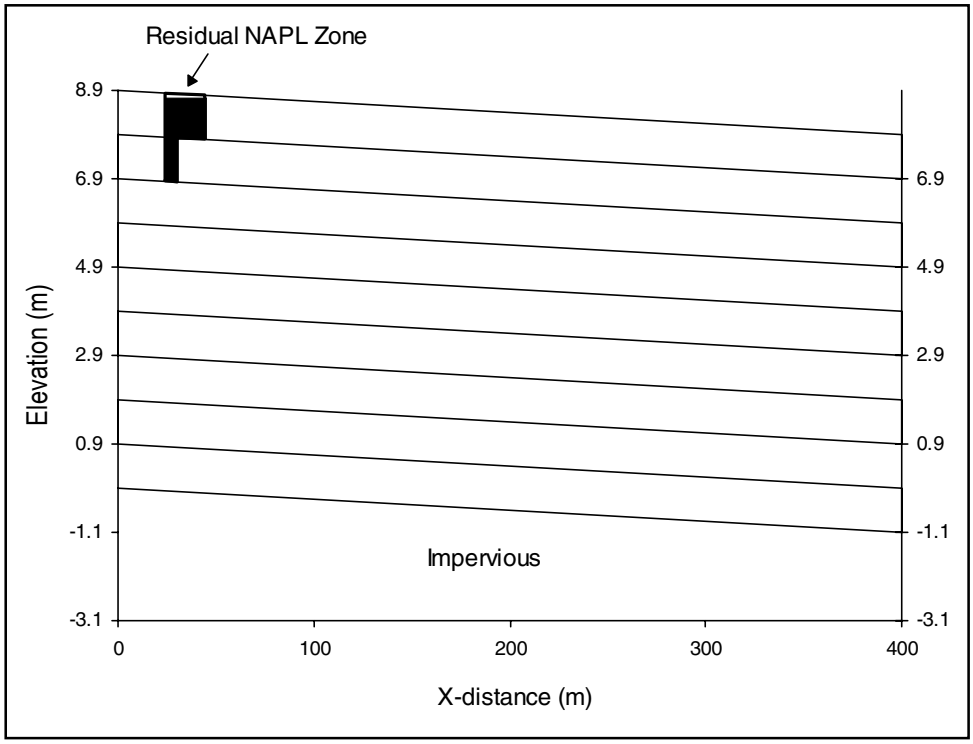

Figure 20. Vertical cross section through the SEAM3D model domain used to simulate the Laurel Bay site

Flow parameters and boundary conditions

The groundwater flow model MODFLOW (McDonald and Harbaugh 1988) was used to generate the steady-state flow field for contaminant transport. The uppermost aquifer layer was given a hydraulic conductivity of 3.383 m day^{-1}. Since the vertical thickness of each layer was 1.0 m, the transmissivity for the lower layers was also 3.383 m^2 day^{-1}. Based on the average gradient (0.005) in the measured water table, the average groundwater velocity was approximately 18 m $year^{-1}$. The vertical leakage between layers was 0.338 m day^{-1}, based on the assumption that the horizontal conductivity was ten times greater than the

vertical conductivity. This degree of anisotropy in hydraulic conductivity is not uncommon (Bouwer 1978). Boundary conditions were no flow along y = 0 and y = 98, and constant head in layer 1 equal to 8.90 m at x = 0 and 7.91 m at x = 200. Assuming a linear head drop with depth over the entire domain, the constant head values at x = 0 and x = 200 were decreased by 0.02 m for each subsequent layer to simulate the average vertical gradient measured between LB-EX-08 and LB-EX-17. Recharge at the site was not measured, so a value of 0.00042 m day^{-1} was chosen as a conservative estimate, assuming limitations due to evapotranspiration and runoff. A constant value of recharge was specified for all blocks in layer 1. The combination of the recharge flow and the vertical gradient in the constant head boundaries produced a relatively uniform horizontal gradient of 0.005 in the water table.

NAPL contamination

The gasoline leak was simulated as occurring in the 2- by 2-m block between tanks 1537 and 1538 (Figure 16). The beginning date for the simulated leak was designated as December 15, 1990, when the tanks first failed a test for tightness, and the ending date for the leak was November 15, 1991, when tank 1538 was emptied and taken out of service. Thus the duration of the leak was 330 days. NAPL was assumed to have migrated from the immediate vicinity of the tanks to produce the NAPL distribution observed by ABB-ES in 1993. The model does not simulate NAPL flow explicitly, but the effect of NAPL migration was approximated by using schedules to add NAPL to successive blocks as time progressed (Figure 21 and Table 5). Once the model added NAPL to a block, NAPL mass was diminished only by dissolution into the aqueous phase.

Time values for the NAPL schedules were determined by estimating the average velocity v_{NAPL} of the NAPL plume as (Parker, Waddill, and Johnson 1994)

$$v_{NAPL} = M_o \frac{dZ_{ao}}{dx} \tag{54}$$

where M_o is the oil mobility factor, and dZ_{ao}/dx is the gradient in the air-oil table, which can be estimated as corresponding to the water table gradient. At high volumes of hydraulically mobile or "free" NAPL per unit volume of soil, M_o reaches a constant maximum value $M_o^{\max}$, computed as

$$M_o^{\max} = \frac{\rho_{ro} K}{\eta_{ro} \theta} \tag{55}$$

where

ρ_{ro} = oil specific gravity

K = saturated hydraulic conductivity of water

η_{ro} = ratio of oil to water viscosity

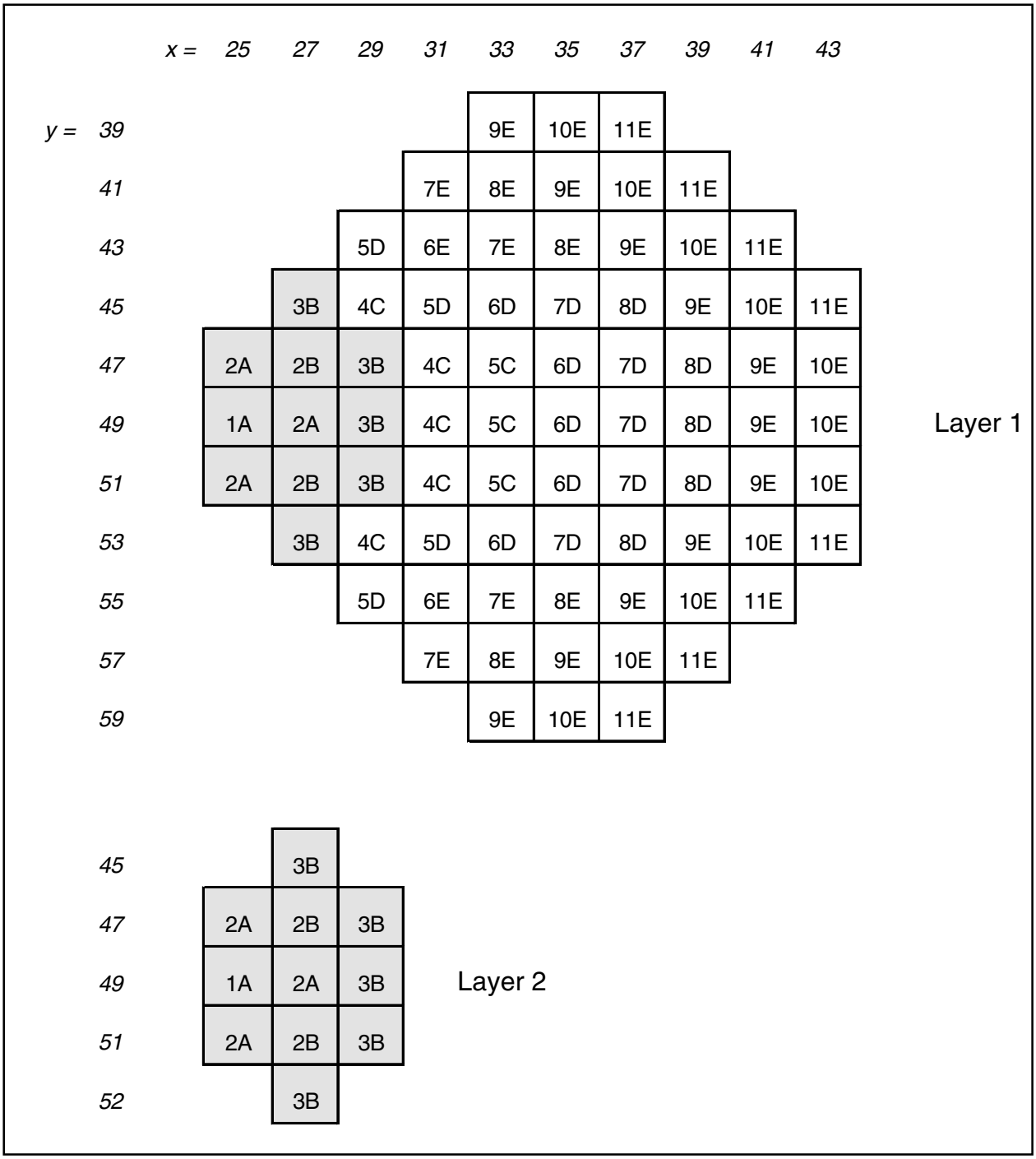

Figure 21. Location of the NAPL source within the model domain. The values of x and y indicate the distance to the center of the model blocks. Within each block, the number refers to the schedule (see Table 5) for adding NAPL to the domain, while the letter refers to the mass loading rate (Table 5). Shading indicates those blocks in which the NAPL mass was set to zero at 1,000 days to correspond to excavation of the tanks and contaminated soil

Table 5
Timing and Mass Loading Information Associated with the Schedule Numbers in Figure 21 for NAPL Mass Loading to the Model Domain

Schedule	Mass Loading Letter	NAPL Mass Loading Starting Time, day	NAPL Mass Loading Ending Time day	NAPL Mass Loading Rate, g/day	Total NAPL Mass Added To Block, kg
1	A	0	330	338	128
2	A	62	392	338	128
	B			291	96
3	B	124	454	291	96
4	C	186	516	194	64
5	C	248	578	194	64
	D			97	32
6	D	310	640	97	32
	E			48	16
7	D	372	702	97	32
	E			48	16
8	D	434	764	97	32
	E			48	16
9	D	496	826	97	32
	E			48	16
10	E	558	888	48	16
11	E	620	950	48	16

Research has shown that for gasoline, $\rho_{ro} \cong 0.8$ and $\eta_{ro} \cong 0.6$ (Parker, Waddill, and Johnson 1994), and the value $\theta = 0.35$ (Table 6) was estimated during the initial site investigation (ABB-ES 1993). Therefore, $M_o^{\max}$ was 12.9 m day^{-1}. When the free NAPL volume is large, $M_o^{\max}$ has been shown to give a reasonable estimate of v_{NAPL} (Parker, Waddill, and Johnson 1994), while for small free NAPL volumes, the value $M_o^{\max}/2$ may provide a better approximation (Parker, Waddill, and Johnson 1994). Since the observed free

Table 6
Transport Parameters

α_x, m	α_y, m	α_z, m	θ	ρ_b, g m^{-3}
8.0	1.2	0.04	0.35	1.6 x 10^6

NAPL thickness in LB-EX-1 was generally small (ABB-ES 1993), $M_o^{\max}$ /2 was used in Equation 54 to obtain v_{NAPL} = 0.032 m day^{-1}.

Each model block was 2 by 2 m, and free NAPL migrating at 0.032 m day^{-1} would take 62 days to travel 2 m to the next block. Thus, for blocks adjacent to the leak, NAPL mass loading began on day 62, following Schedule 2 (Table 5). For blocks farthest from the leak, NAPL had to travel 20 m, so mass loading began on day 620 and continued until day 950, following Schedule 11. NAPL mass loading into all blocks lasted for 330 days, under the assumption that free NAPL would continue to migrate as long as the leak persisted.

The mass loading rate for a specific block was based on an estimate of the total NAPL mass assumed to have entered that block. This total mass was derived from field measurements and theoretical worst-case NAPL saturations. Field measurements of NAPL concentrations ranged from 2.3×10^{-6} to 0.00051 g g^{-1} (ABB-ES 1993), but none of the samples were taken within 10 m of the leak, where the highest NAPL concentrations were likely to have occurred. To estimate the worst-case NAPL concentrations, it was assumed that the NAPL plume in 1993 was essentially immobile, and thus composed entirely of residual NAPL. This assumption was based on the small observed NAPL thickness (about 5 cm) in LB-EX-1 and lack of NAPL in any other monitoring wells. For sandy soils, residual NAPL saturations generally range from 0.05 to 0.20 (Wilson 1990). Thus, the worst-case NAPL saturation was taken to be 0.20. Using a soil bulk density of 1.6×10^6 g m^{-3} (Table 6) and NAPL density of 0.8×10^6 g m^{-3}, a saturation of 0.20 corresponds to a soil concentration of 0.04 $g_{NAPL}\ g_{solids}^{-1}$. Thus the total NAPL mass in the worst-case model blocks was 256 kg. In addition, it was assumed that NAPL concentrations decreased in a linear manner with distance from the leak. For the worst case, the minimum NAPL mass per block was set to 32 kg, which corresponded to a NAPL saturation of 0.025 and a soil NAPL concentration of 0.005 $g_{NAPL}\ g_{solids}^{-1}$. Since the measured soil concentrations were an order of magnitude lower than the worst-case estimates, the "best estimate" concentrations were judged to be half of the worst case.

The vertical distribution of the simulated source was based on the observed water table fluctuations of approximately 1 m. Near the leak, observed NAPL thickness ranged up to 0.9 m in LB-EX-1, so it was assumed that water table fluctuations in this area spread NAPL over the upper 2 m of the aquifer. Farther from the leak, NAPL was not observed in any of the monitoring wells, so the free NAPL thickness was assumed to be small. As a result, free NAPL would form a thin layer floating on the water table, and NAPL would not spread beyond the 1-m water table fluctuation. Thus, NAPL mass was loaded to the upper two

layers of model blocks near the leak, while the other blocks received NAPL only in the top layer (Figure 21). The shaded blocks in Figure 21 show those zones (between the source and LB-EX-01) in which the model set NAPL concentration to zero after 1,000 days to simulate the excavation of the tanks and surrounding sediments.

In gasoline, the BTEX compounds are of primary regulatory interest due to their relatively high solubility and potential toxicity. Therefore, each BTEX compound was simulated individually, while all other aromatics were treated as a single pseudo-compound. Likewise, all aliphatics were simulated as a single pseudo-compound because they are less soluble in water than BTEX, and they were assumed to degrade aerobically only. MTBE was simulated as an individual component since it was assumed to be nonbiodegradable and unretarded. Hereafter, the term substrates will refer to the BTEX, the other biodegradable aromatics, and the aliphatics; and the term tracer will refer to MTBE. The mass fractions of the model constituents in the NAPL (Table 7) were based on mass fractions of BTEX, other aromatics, aliphatics, and MTBE that are within the range observed in gasoline (Table 3). Mole fractions and solubilities of the aromatic and aliphatic pseudo-compounds were based on estimates made by Baehr and Corapcioglu (1987). No measurements were available to estimate the mass transfer coefficient k^{NAPL} describing NAPL dissolution to the aqueous phase. Therefore, k^{NAPL} was set to a high value, which allowed the aqueous phase concentration of each NAPL constituent to be equal to its equlibrium value.

Table 7
Properties and Composition of the NAPL Phase Used in the Simulations

Component	Initial Mass Fraction in NAPL, g g^{-1}	Aqueous Phase Solubility, g m^{-3}	Molecular Weight g $mole^{-1}$
Benzene	0.01	1,780	78.1
Toluene	0.08	515	92.1
Ethylbenzene	0.05	140	106.2
Xylene	0.12	180	106.2
Other aromatics	0.10	166	120.0
Aliphatics	0.55	12	97.0
Inert	0.06	0	150.0
MTBE	0.03	20,000	80.0

Transport parameters and boundary conditions

Input values for initial concentrations were based on measurements taken from uncontaminated wells at the site (ABB-ES 1993; Landmeyer, Chapelle, and Bradley 1996). At all nodes, initial concentrations were 5.0 g m^{-3} for O_2 and 100 μg g^{-1} for solid-phase Fe(III), the latter representing only the bioavailable or microbially reducible iron. For SO_4^{2-}, initial concentrations were 5.0 g m^{-3} at x = 0 and 10.0 g m^{-3} at x = 400. Initial concentrations were zero for all substrates, products, and MTBE. Threshold concentrations (below which biodegradation will not occur) were set to 10 μg g^{-1} for Fe(III) and zero for all other components. Specified concentrations in recharge water were 5.0 g m^{-3} for O_2, 15.0 g m^{-3} for SO_4^{2-}, and zero for all substrates, products, and MTBE. Boundary conditions were specified as constant concentration equal to the initial condition at x = 0 for all aqueous-phase constituents. All other blocks were allowed to be active with variable concentrations. If a solute reached the outflow boundary of the domain, solute mass was allowed to exit under a zero dispersion boundary condition.

The longitudinal dispersitivity α_x was initially chosen to be 10 m, which was 10 percent of the overall transport distance during the calibration time period. During calibration, the values for the dispersivities were refined by assuming that MTBE was recalcitrant and adjusting the dispersivities to match the measured data. Thus, α_x (Table 6) was reduced by 20 percent, and it was always assumed that the transverse dispersivity was $0.15\alpha_x$ and the vertical dispersivity was $0.005\alpha_x$. The effect of lowering the dispersivities was to produce a more conservative prediction of biodegradation, as less dispersion allowed less access to the EAs. The soil bulk density (Table 6) was chosen as typical of a sandy soil (Carsel and Parrish 1988). The model option for the linear adsorption isotherm was used in calculating retardation factors for each substrate and Fe(II). The EAs, MTBE, H_2S, and CH_4 were not retarded. To allow for maximum mobility, the distribution coefficient K_D for all substrates was chosen to be 0.057 cm g^{-1}, which was the smallest of the values measured by Landmeyer, Chapelle, and Bradley (1996) for benzene and toluene. For Fe(II), K_D was set to 0.328 cm^3 g^{-1} using trial and error adjustments to fit the measured data. Thus the retardation factor was 1.26 for all substrates and 2.5 for Fe(II).

Biodegradation parameters

Model parameters for biodegradation (Tables 8 and 9) were based on laboratory measurements, published values, and theoretical estimates. For simplicity, parameter values were not allowed to vary among the aquifer layers under the assumption that the entire 9 m of the aquifer could be considered relatively near the surface. To reflect the high rate and energy yield of aerobic metabolism, parameters controlling aerobic utilization, growth, and death were higher than those of the anaerobic processes (Tables 8 and 9). In general, parameters were identical for each substrate and for each anaerobic process unless information existed to assign distinct values to them.

Table 8
Biodegradation Parameters

Microcolony	EA	$K^{s}_{x,ls,le}$ g m^{-3}	$K^{e}_{x,le}$ g m^{-3}	$Y_{x,ls,le}$ g g^{-1}	$\gamma_{x,ls,le}$ g g^{-1}	$\kappa_{le,li}$ g m^{-3}	$\zeta_{x,li}$ g g^{-1}	M_x g m^{-3}	$k^{bk}_{d_x}$ day^{-1}
Aerobes	O_2	5.0	0.5	0.5	3.2	0.1	--	0.30	0.29
Iron reducers	Fe(III)	5.0	--	0.2	42.0	10[1]	0.2	0.01	0.0012
Sulfate reducers	SO_4	5.0	0.5	0.2	4.5	0.5	0.8	0.01	0.0012
Methanogens	CO_2	5.0	--	0.0	--	--	0.8	0.35	0.0

Note: Parameters apply to all substrates.
[1] Units are μg Fe(III) g^{-1} solids.

Table 9
Maximum Specific Rate of Substrate Utilization $\eta^{max}_{x,ls,le}$ Within Each Microbial Population

Microcolony	EA	Benzene day^{-1}	Toluene day^{-1}	Ethyl Benzene day^{-1}	Total Xylene day^{-1}	Other Aromatics day^{-1}	Aliphatics day^{-1}
Aerobes	O_2	0.640	0.640	0.640	0.640	0.640	0.640
Iron reducers	Fe(III)	0.0009	0.009	0.009	0.009	0.009	0.0
Sulfate reducers	SO_4	0.0009	0.009	0.009	0.009	0.009	0.0
Methanogens	CO_2	0.0003	0.003	0.003	0.003	0.003	0.0

For aerobic biodecay, the maximum specific rate of substrate utilization $\nu^{\max}_{x,ls,le}$ was set to 0.64 day^{-1} (Table 9), based on the laboratory estimate by Landmeyer, Chapelle, and Bradley (1996). Likewise, for anaerobic biodecay, $\nu^{\max}_{x,ls,le}$ was set initially to 0.0003 day^{-1} for benzene and 0.003 day^{-1} for all other aromatics, under the assumption that the other aromatics would degrade at a rate similar to that of toluene. During calibration, $\nu^{\max}_{x,ls,le}$ was increased by a factor of four for methanogens and three for the sulfate and iron reducers (Table 9) to match measured concentrations. This anaerobic rate is still quite low compared to the aerobic decay rate. Alkanes were assumed to be resistant to anaerobic biodecay, so $\nu^{\max}_{x,ls,le}$ of the alkanes was set to zero in each anaerobic process (Table 9). Values for half-saturation coefficients (Table 8) were based on literature values since no measurements were available.

The initial microbial biomass M_x was higher for the aerobes than for the iron or sulfate reducers (Table 8). This difference was based on the assumption that aerobic biomass would predominate when the groundwater contained significant O_2 under pristine conditions. The aerobic biomass of 0.3 g m^{-3} roughly corresponded to 1×10^6 cells cm^{-3}, assuming a cell volume of 1 μm^3 and cell density of 1.0 g cm^{-3}. This number of cells and the high $\nu^{max}_{x,ls,le}$ for O_2 allowed significant aerobic utilization of substrates to occur immediately. In contrast, anaerobic microbes under high O_2 pristine conditions were assumed to exist only in anaerobic microenvironments that develop within soil aggregates (Brock et al. 1994). Thus, the concentrations of iron and sulfate reducers were over an order of magnitude lower than those of the aerobic biomass (Table 8). As a result, the iron and sulfate reducers had to experience growth before the population exerted a significant impact on biodegradation. For the methanogens, biomass growth was not simulated. Since the model does not explicitly consider an EA for methanogens, their biomass concentration is limited only by the concentration of available substrate. When substrate is readily available, the methanogenic biomass and the rate of methanogenesis can become unrealistically high if growth is simulated. Therefore, in this case, the yield coefficient and the death rate for methanogens were set to zero, and the initial biomass concentration was set equal to the effective porosity (Table 8). Thus the rate of methanogenesis depended only on the maximum specific rate of substrate utilization $\nu^{max}_{x,ls,le}$ and the concentration of available substrate.

The yield coefficient $Y_{x,ls,le}$ for aerobes was set to 0.5 g g^{-1} (Table 8) based on measurements and past work by Arcangeli and Arvin (1992), Chen et al. (1992), and Wodzinski and Johnson (1968). For all anaerobes, $Y_{x,ls,le}$ was 0.2 g g^{-1}, corresponding to the theoretical maximum yield under sulfate reducing conditions (Edwards et al. 1992). Values for the effective death term $k^{bk}_{d_x}$ were higher for the aerobes than the anaerobes (Table 8), reflecting the dependence of $k^{bk}_{d_x}$ on $\nu^{max}_{x,ls,le}$ and $Y_{x,ls,le}$. Inhibition coefficients were relatively small, such that each EA was essentially depleted before utilization of the next EA began. Values for the inhibition coefficients were adjusted during calibration to match measured H_2S and CH_4 concentrations. EA use coefficients $\gamma_{x,ls,le}$ were estimated from the stoichiometric relationship between each EA and toluene (e.g. Borden, Gomez, and Becker 1995) and the generation term for CH_4 $\zeta_{x,ls}$ was based on the stoichiometric relationship between toluene and CH_4 (Borden, Gomez, and Becker 1995). The EA generation terms $\zeta_{x,le}$ were also based on stoichiometric relationships (Borden, Gomez, and Becker 1995; Edwards et al. 1992). During calibration, the generation term for Fe(II) was reduced from its theoretical value to match the measured concentrations of Fe(II). This reduction may be justified since Fe(II) can react chemically with compounds such as SO_4^{2-}, so only a fraction of the Fe(II) produced by the microbes will be measured in the groundwater (Lovley, Chapelle, and Woodward 1994).

SEAM3D calibration

SEAM3D predictions were compared to measured data from wells (LB-EX-1, -3, -4, -5, -7, -8, -11, -22, -RW, and MLS-1 through 5) located near a transect through the center of the plume (Figure 17). Since the wells were screened across approximately the upper 3 m of the aquifer, model predictions were averaged over the top three layers for comparison to the measured data. Likewise, measured concentrations from the multilevel samplers were generally within the upper 3 m of the aquifer (Table 4), so the measured values from the multilevel sampler ports were vertically averaged to obtain a single value for comparison. Most of the wells were sampled and analyzed for all four sampling periods (1993, 1994, 1996, and 1997), with the following exceptions. LB-EX-11 was dry in later years, so it was sampled only in 1993 and 1994. LB-EX-RW was sampled only in 1994, 1996, and 1997. Multilevel samplers 1 through 5 were sampled in 1996, and multilevel sampler 1 was sampled in 1997. Concentrations of EAs and products were not measured in 1993. SEAM3D was calibrated to the 1993, 1994, and 1996 data, and the 1997 data were used to evaluate model predictions.

As described in the sections on transport parameters and boundary conditions and biodegradation parameters, only a certain few parameters were adjusted during calibration, and the magnitude of the necessary adjustments was small. To summarize the calibration process, based on the 1993 and 1994 data, the longitudinal dispersivity α_x was reduced by 20 percent; the generation term and the retardation factor for Fe(II) were fit to observed data; the laboratory estimate for anaerobic decay rate was increased by a factor of three for the sulfate and iron reducers; and the composition of the NAPL was adjusted within ranges defined by the literature to match measured aqueous phase concentrations. Using the 1993, 1994, and 1996 data, the inhibition coefficients were adjusted to match measured H_2S and CH_4 concentrations. All other parameters were obtained from field and laboratory measurements and literature values, and adjustment in their values was not required.

Results and Discussion

Concentrations along a transect through the center of the plume

Measured and predicted concentrations were compared along a transect (Figure 17) through the center of the plume. Figure 22 shows the predicted concentrations of benzene at elapsed times of 850, 1,180, 2,020, 2,230, 4,000, and 6,000 days after the estimated start of the gasoline leak. The first four times correspond to the four sampling periods, and the available measured data are also shown. In general, measured and predicted concentrations show reasonable agreement. Measured and predicted travel distances are in general agreement, which tends to verify the estimate of groundwater velocity, retardation coefficients, and the start date for the gasoline leak.

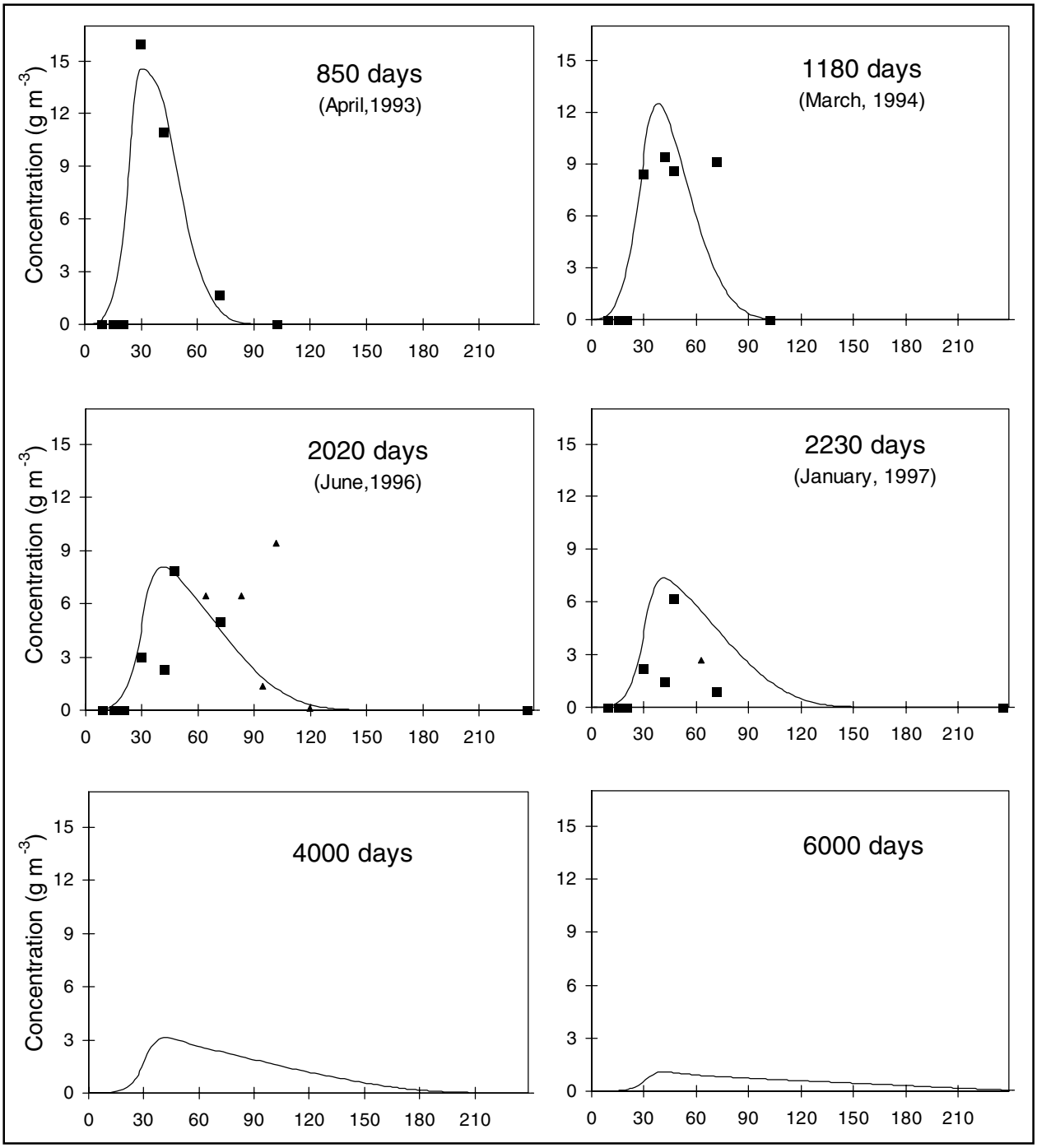

Figure 22. Comparison of measured (symbols) and predicted (lines) concentrations along a transect through the center line of the plume in the direction of flow for benzene. The x-axis is distance in units of meters. Data from the multilevel samplers are shown as triangles

Measured values of the maximum concentrations of BTEX were highest in 1993, and decreased over time (Figures 22-25), an effect which is captured by the NAPL dissolution algorithm of SEAM3D. Since BTEX and MTBE are much

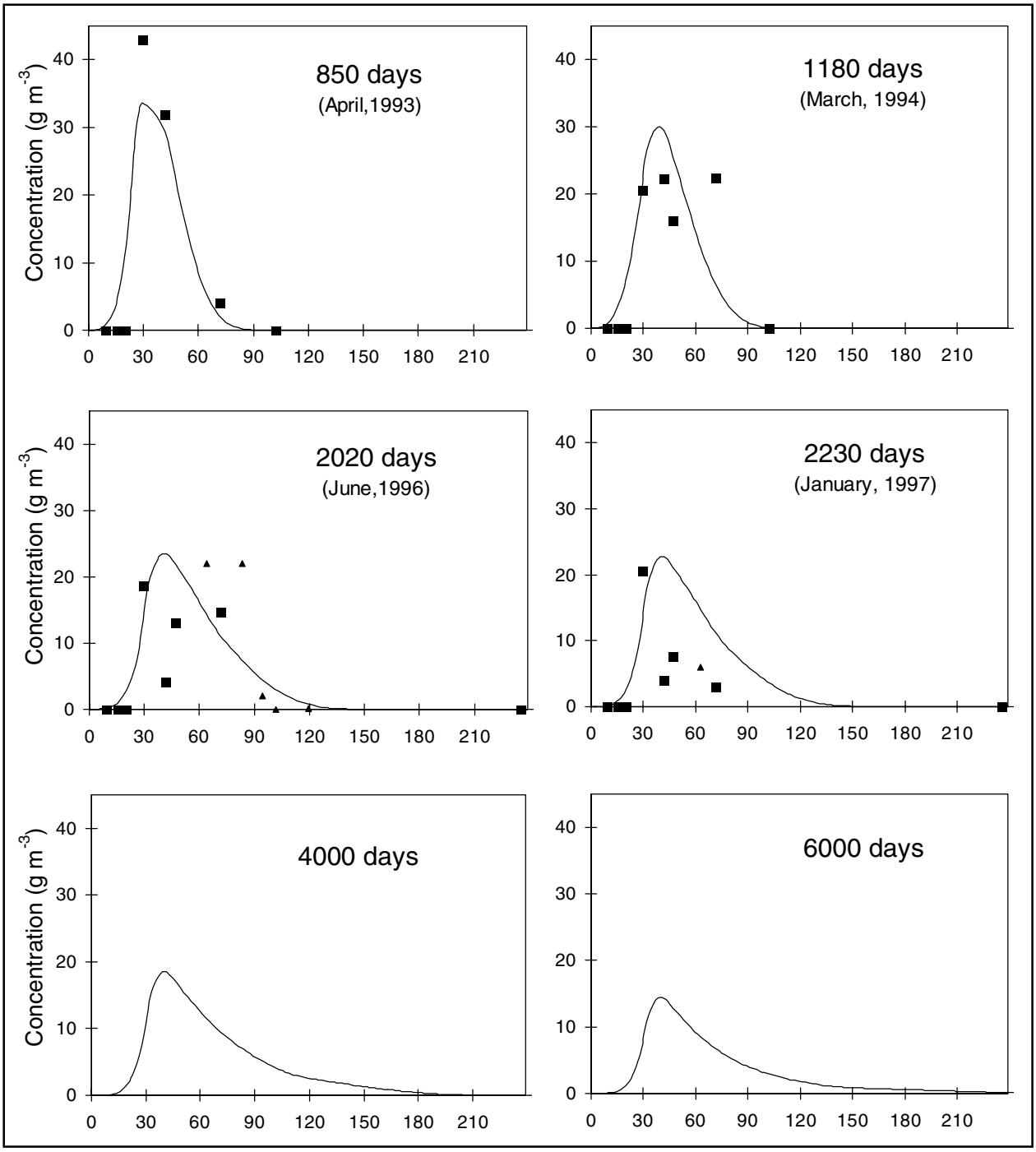

Figure 23. Comparison of measured (symbols) and predicted (lines) concentrations along a transect through the center line of the plume in the direction of flow for toluene. The x-axis is distance in units of meters. Data from the multilevel samplers are shown as triangles

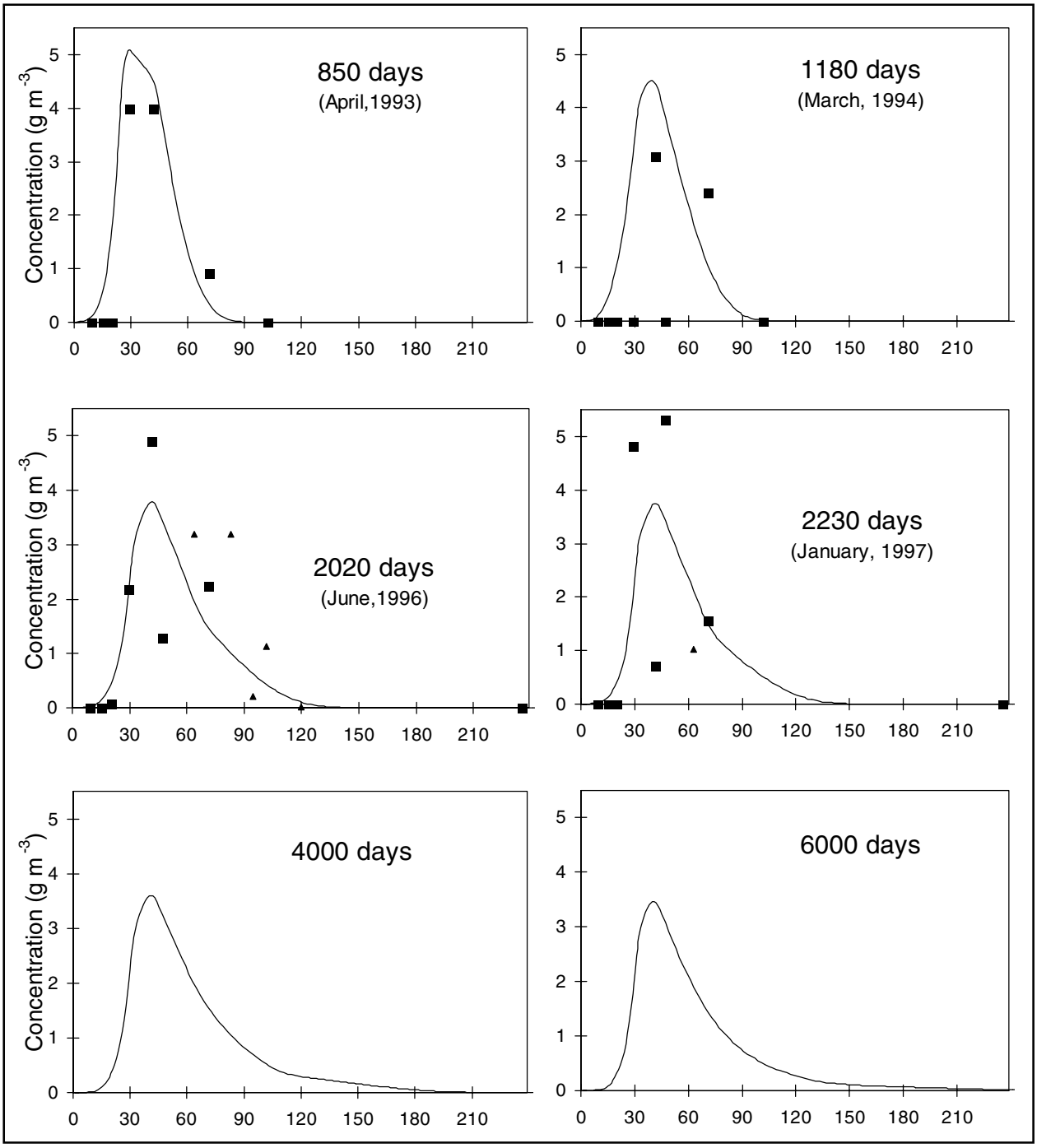

Figure 24. Comparison of measured (symbols) and predicted (lines) concentrations along a transect through the center line of the plume in the direction of flow for ethylbenzene. The x-axis is distance in units of meters. Data from the multilevel samplers are shown as triangles

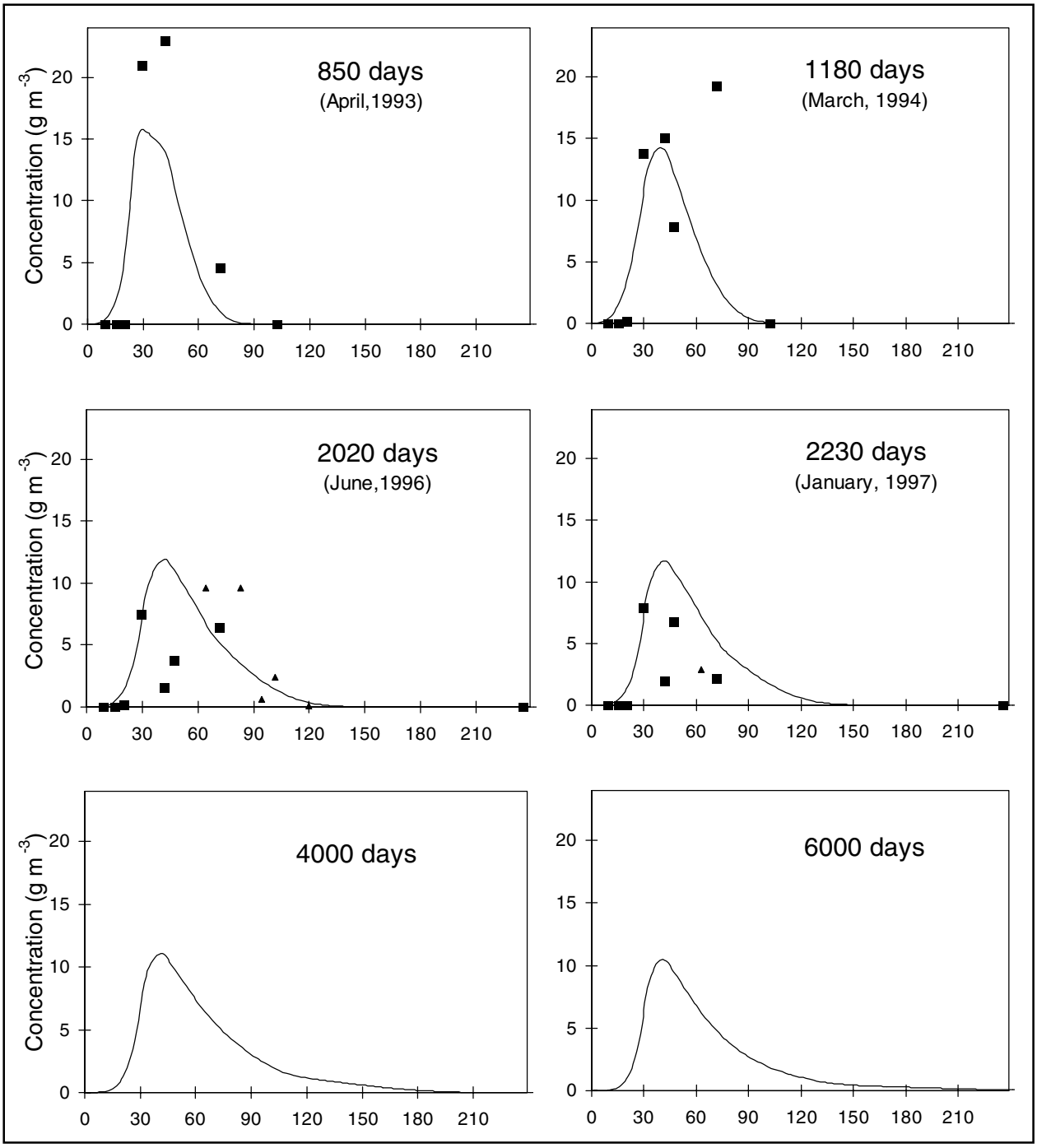

Figure 25. Comparison of measured (symbols) and predicted (lines) concentrations along a transect through the center line of the plume in the direction of flow for xylene. The x-axis is distance in units of meters. Data from the multilevel samplers are shown as triangles

more soluble in water than the aliphatics, the NAPL mass fractions of BTEX and MTBE decrease over time as mass dissolves out of the NAPL phase. Thus the equilibrium concentrations of BTEX and MTBE diminish such that their maximum aqueous concentrations also decrease. This effect is most apparent with benzene (Figure 22) and MTBE (Figure 26), which have the highest solubilities in water. For MTBE, an unusually high concentration occurred in LB-EX-7 in 1994 and MLS-4 in 1996; however, measurements at the other locations revealed low concentrations and suggested that most of the MTBE had dissolved out of the NAPL by 1996. The aliphatics showed an increase in maximum concentration (Figure 27) from 2,020 days to 6,000 days, reflecting the increase in effective concentration of aliphatics in the NAPL during this time. This occurs because the aliphatics compose a greater percentage of the remaining NAPL as the more soluble aromatics and MTBE dissolve into the aqueous phase. From 850 to 2,020 days, the decrease in aliphatic concentration is due to the effect of excavation of the contaminated soil. Since SEAM3D uses Monod kinetics, biodegradation occurs quite slowly where the BTEX concentrations are small. Therefore, small concentrations of BTEX (Figures 22-25) were transported downgradient through the zone of oxygen depletion (Figure 28) during the entire simulation. However, biodegradation does not allow significant BTEX concentrations to occur beyond x = 150 m (less than 1.0 g m^{-3} for toluene and less than 0.5 g m^{-3} for the other BTEX).

The 1994 measurements showed depletion of O_2 (Figure 28) and production of Fe(II) (Figure 29), suggesting that biodegradation of BTEX was occurring at that time, with O_2 and Fe(III) acting as EAs. Fe(II) production was observed only in locations of low concentrations of O_2, suggesting that O_2 was inhibiting Fe(III)-based biodegradation. This trend continued for 1996 and 1997, although Fe(II) adsorption caused the zone of Fe(II) depletion to lag behind the more rapidly moving O_2. For both the 1994 and 1996 sampling times, the predicted zone of O_2 depletion moved slightly ahead of the measured zone, although the measurements were sparse and the difference was not excessive (Figure 28).

At the upgradient edge of the plume, measured SO_4^{2-} concentrations were close to 5 g m^{-3}, while the value approached 15 g m^{-3} at the downgradient edge (Figure 30). Measured concentrations of H_2S were close to zero until 1996 (Figure 31), indicating that significant SO_4^{2-} reduction was not occurring in 1994. Since O_2 was already depleted, it is likely that the presence of Fe(III) was inhibiting SO_4^{2-} reduction. Furthermore, the absence of H_2S in 1994 suggests that the low SO_4^{2-} concentrations (5 g m^{-3}) measured at the upgradient boundary were not due to biological SO_4^{2-} reduction. Instead, SO_4^{2-} may have reacted chemically with species such as Fe(II) that were present at that time. This process has been reported by other researchers (e.g., Bosma et al. 1996).

Measured production of CH_4 (Figure 32) follows the same trend as that of H_2S, indicating that SO_4^{2-} reduction and methanogenesis were both inhibited through 1994. Measured values of CH_4 actually decreased between 1996 and 1997, and the data do not yet indicate whether methanogenesis will be a significant process at the site. The maximum specific rates of substrate

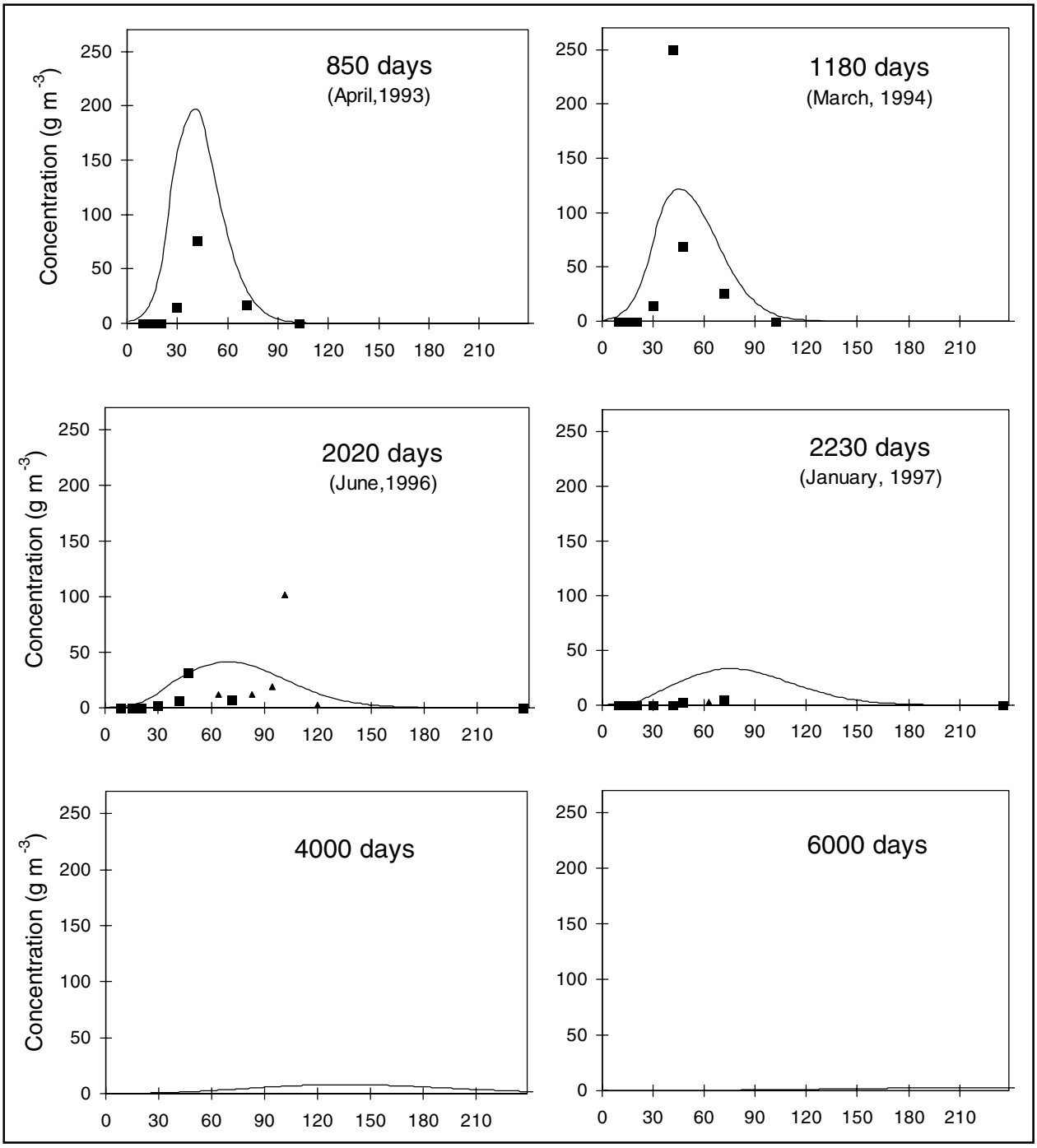

Figure 26. Comparison of measured (symbols) and predicted (lines) concentrations along a transect through the center line of the plume in the direction of flow for MTBE. The x-axis is distance in units of meters. Data from the multilevel samplers are shown as triangles

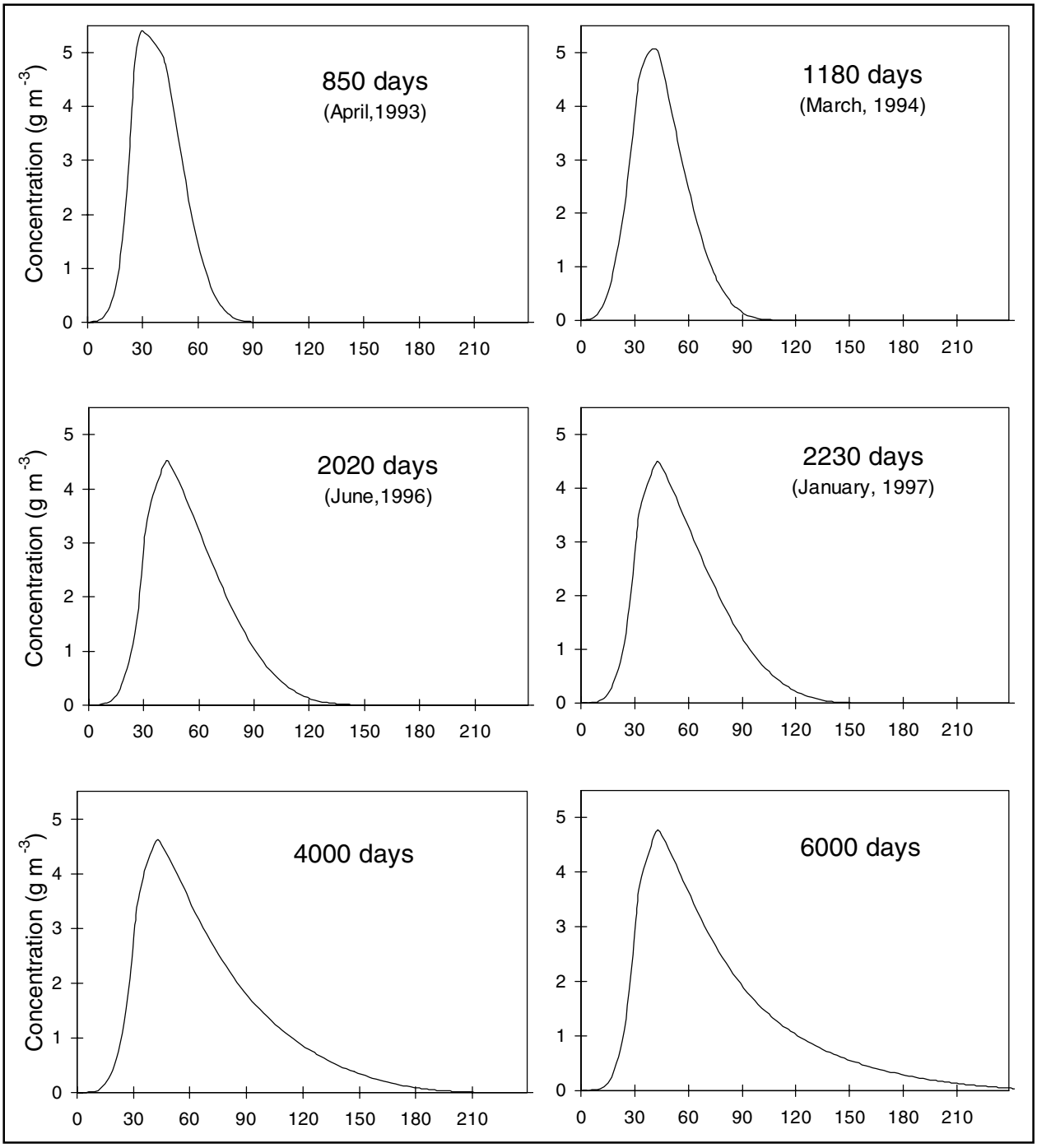

Figure 27. Predicted concentrations along a transect through the center line of the plume in the direction of flow for aliphatics. The x-axis is distance in units of meters

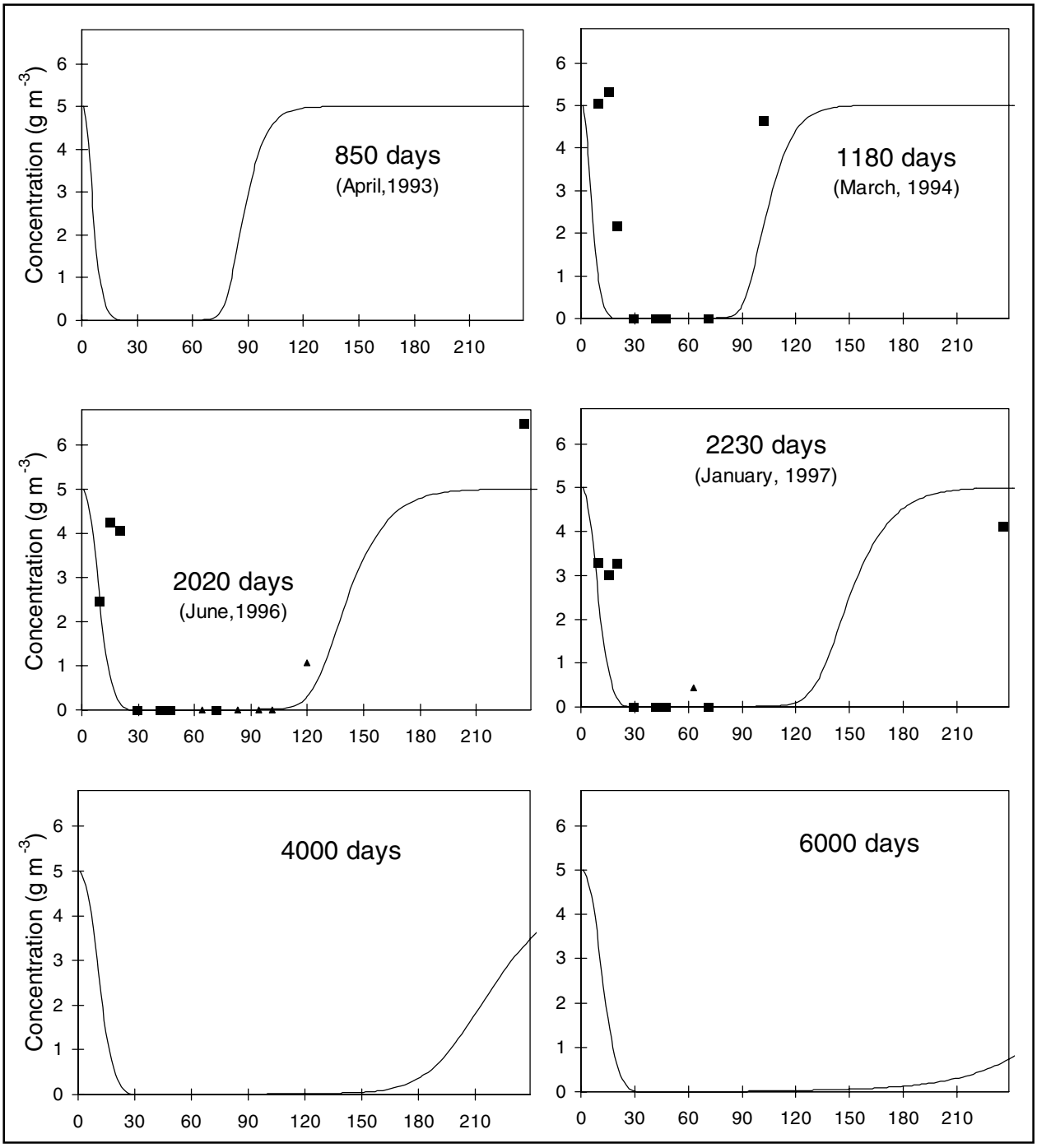

Figure 28. Comparison of measured (symbols) and predicted (lines) concentrations along a transect through the center line of the plume in the direction of flow for oxygen. The x-axis is distance in units of meters. Data from the multilevel samplers are shown as triangles

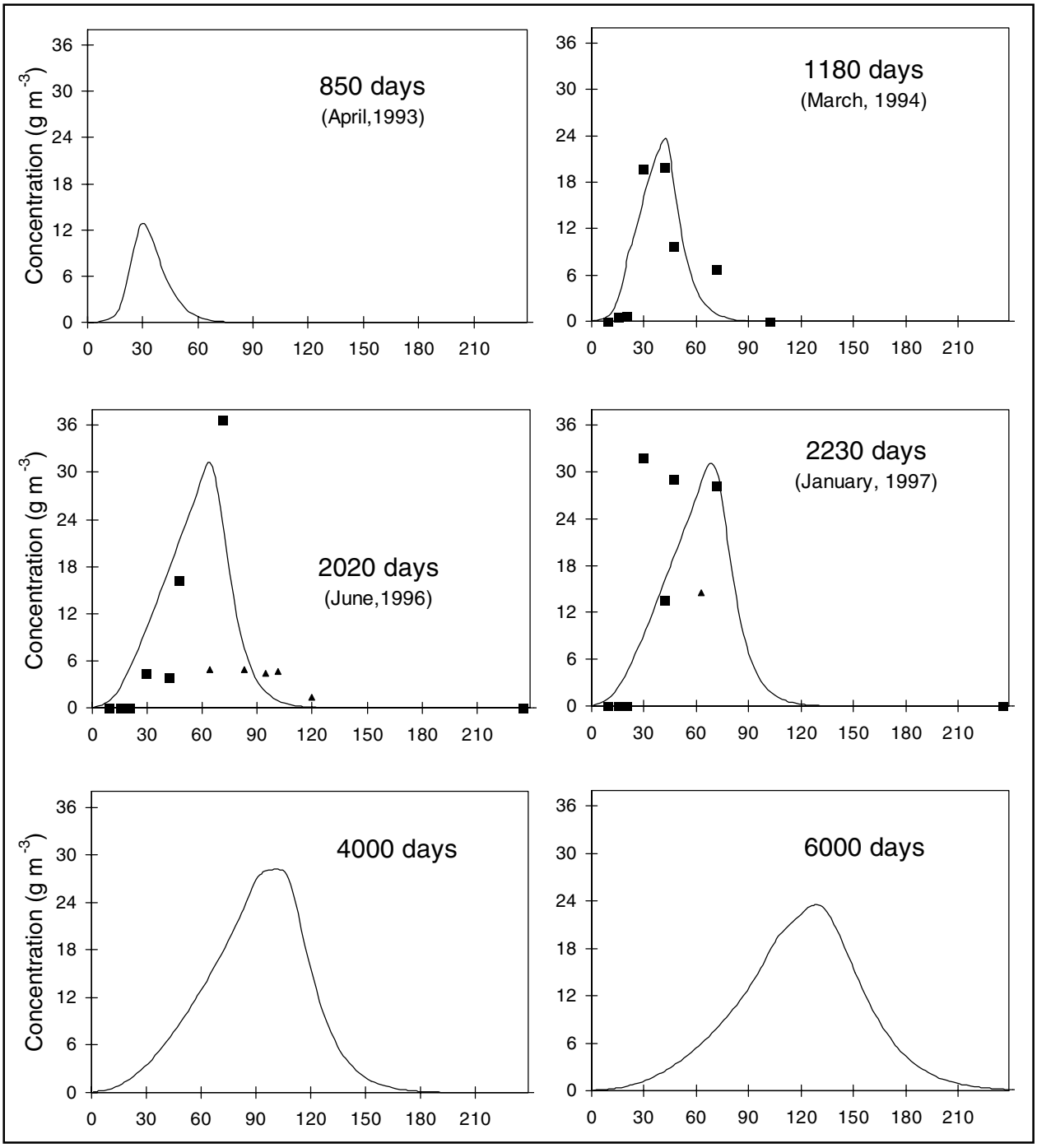

Figure 29. Comparison of measured (symbols) and predicted (lines) concentrations along a transect through the center line of the plume in the direction of flow for Fe(II). The x-axis is distance in units of meters. Data from the multilevel samplers are shown as triangles

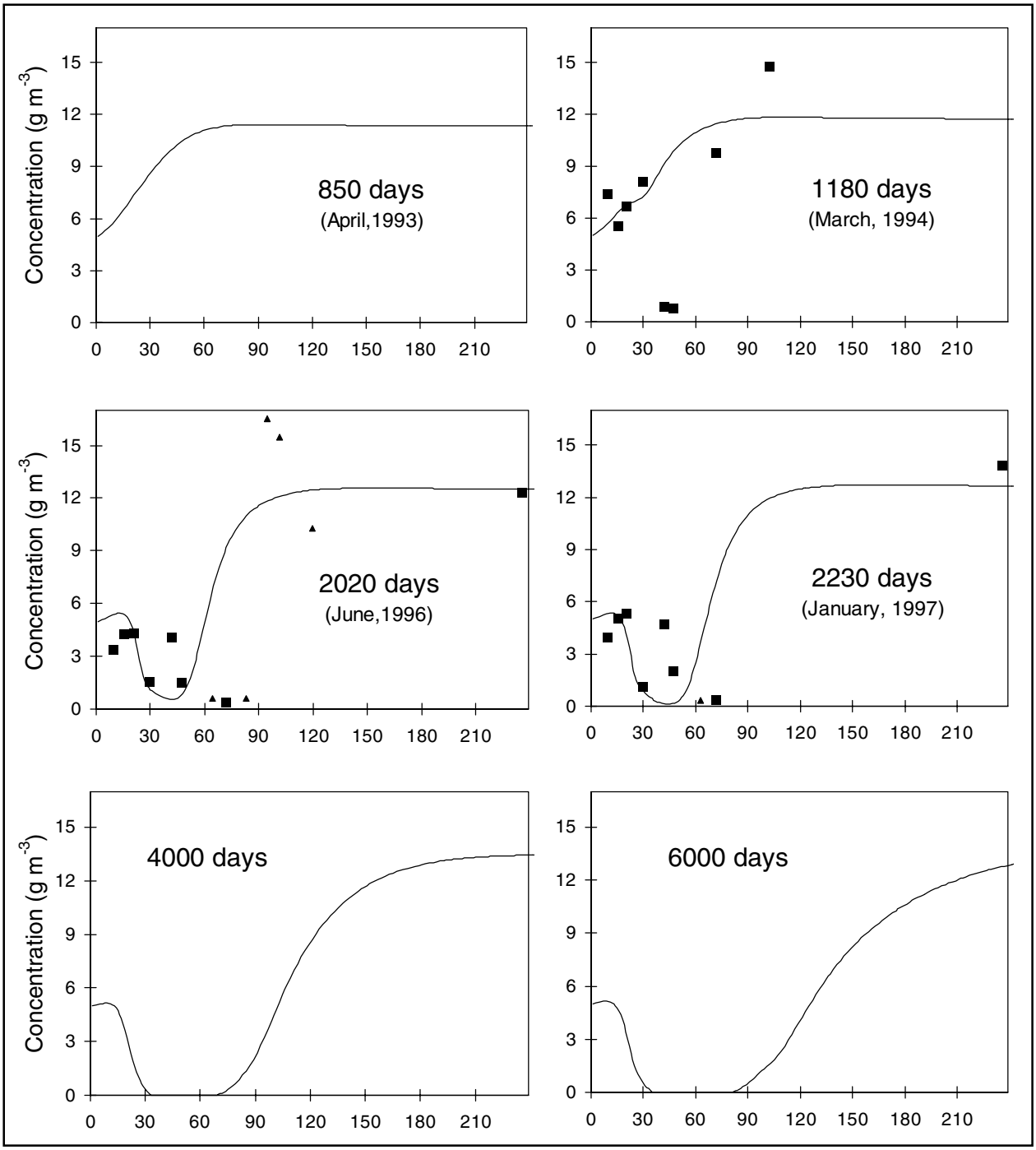

Figure 30. Comparison of measured (symbols) and predicted (lines) concentrations along a transect through the center line of the plume in the direction of flow for SO_4^{2-}. The x-axis is distance in units of meters. Data from the multilevel samplers are shown as triangles

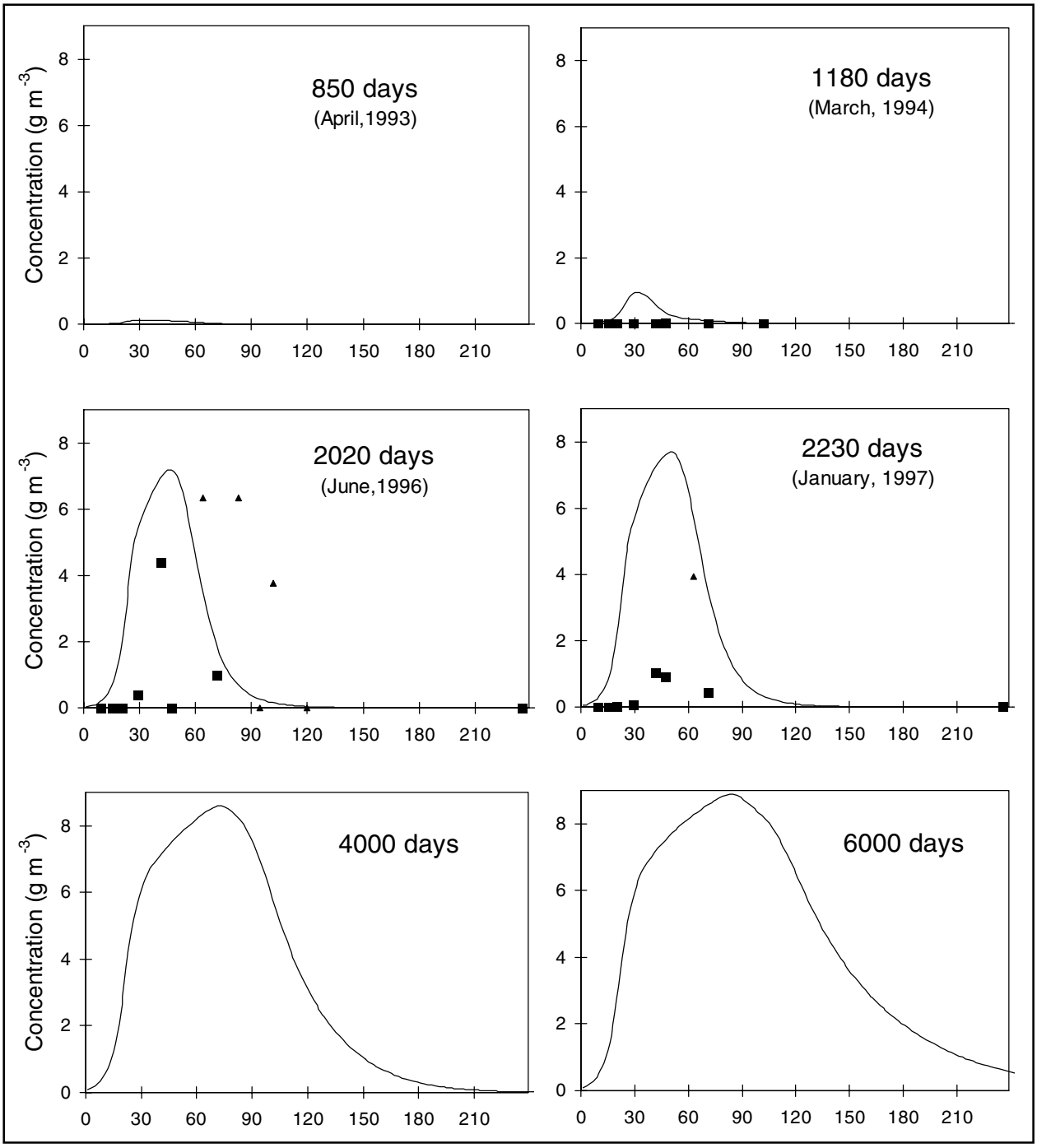

Figure 31. Comparison of measured (symbols) and predicted (lines) concentrations along a transect through the center line of the plume in the direction of flow for H_2S. The x-axis is distance in units of meters. Data from the multilevel samplers are shown as triangles

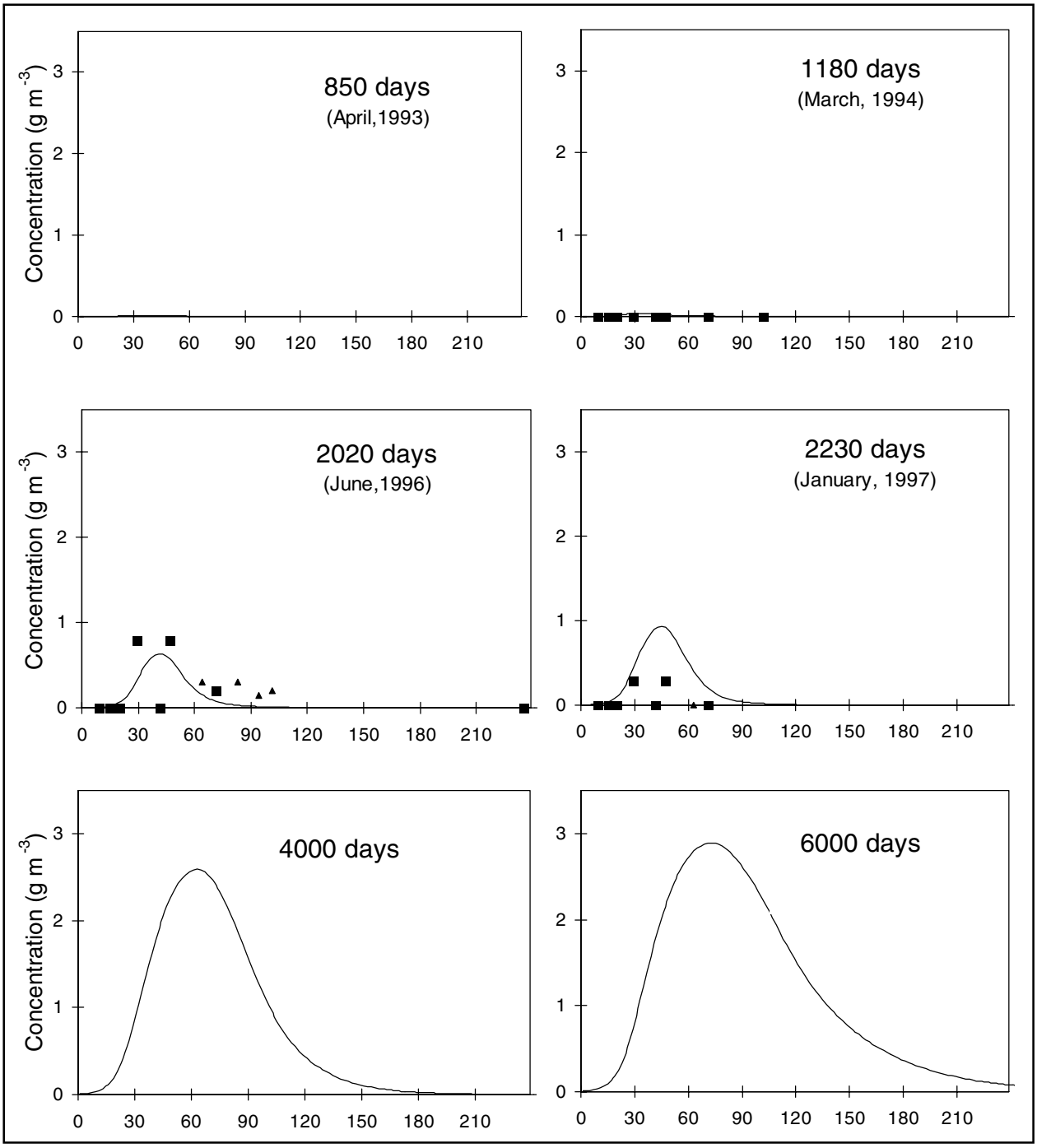

Figure 32. Comparison of measured (symbols) and predicted (lines) concentrations along a transect through the center line of the plume in the direction of flow from CH_4. The x-axis is distance in units of meters. Data from the multilevel samplers are shown as triangles

utilization $v_{x,ls,le}^{\max}$ for methanogenesis were based on the USGS estimates, which were sufficiently low (Table 9) that predicted concentrations of CH_4 do not rise above 3.0 g m^{-3} at 6,000 days (Figure 32). Possible loss mechanisms for CH_4

that are not accounted for in the model include mass transfer of CH_4 to the vadose zone and oxidation by methanotrophic bacteria. Additional field data will be required to define the role of methanogenesis more accurately at Laurel Bay.

Measured concentrations of H_2S and CH_4 indicate a lag period of at least 4 years prior to initiation of SO_4^{2-} reduction and methanogenesis. SEAM3D reproduces this lag period through the effect of the inhibition coefficients and the low initial biomass. Early in the simulation, significant concentrations of O_2 and Fe(III) inhibit SO_4^{2-} reduction and methanogenesis. After O_2 and Fe(III) have been depleted, SO_4^{2-} reduction begins to occur, but the rate is insignificant because of the small biomass of SO_4^{2-} reducers. Over time, the biomass increases to the point that significant SO_4^{2-} based biodegradation occurs. Once the SO_4^{2-} has been depleted, methanogenesis is no longer inhibited, and CH_4 production begins. If microbial growth were not part of the SEAM3D model, inhibition alone would not cause the large lag period that was observed in the field (for details, see "Alternative model scenarios"). Other researchers have shown that lag periods for hydrocarbon degradation may vary from 10 days to 3.5 months as the EA process shifts among Fe(III) reduction, SO_4^{2-} reduction, and methanogenesis (Vroblesky and Chapelle 1994).

Areal distributions

The areal distributions of benzene, toluene, and MTBE at 4,000 days are shown in Figure 33 for model layers 1, 3, 5, 7, and 9. Concentrations of benzene and toluene diminish with increasing depth, since contaminant mass must disperse from the NAPL source area to the lower layers, and significant mass remains in the NAPL. In contrast, the highest concentrations of MTBE occur in layer 5 because the majority of the MTBE has dissolved out of the NAPL phase. Thus, there is no significant source of MTBE in the upper layers, and recharge begins to dilute its concentration near the water table. BTEX spreading is limited by biodegradation and adsorption, so both hydrocarbon plumes (Figure 33) are narrower than the MTBE plume in the y-direction. In addition, the downgradient edge of the MTBE plume travels almost twice as far as the hydrocarbon plumes. Since the retardation factor for benzene and toluene is only 1.26, retardation alone does not explain the difference in travel distance, and biodegradation must contribute to the containment of the plumes.

Figure 34 shows the areal distributions of the EAs O_2, solid Fe(III), and SO_4^{2-} at 4,000 days. As expected, EA depletion decreases with depth, reflecting the distribution of the hydrocarbons. Only small amounts of Fe(III) were utilized in the bottom layers, indicating that O_2 is inhibiting Fe(III) reduction. Since O_2 and Fe(III) inhibit SO_4^{2-} use, the SO_4^{2-} depletion in the bottom layer is probably caused by dispersion from the upper layers, and not by SO_4^{2-} reduction in the bottom layer.

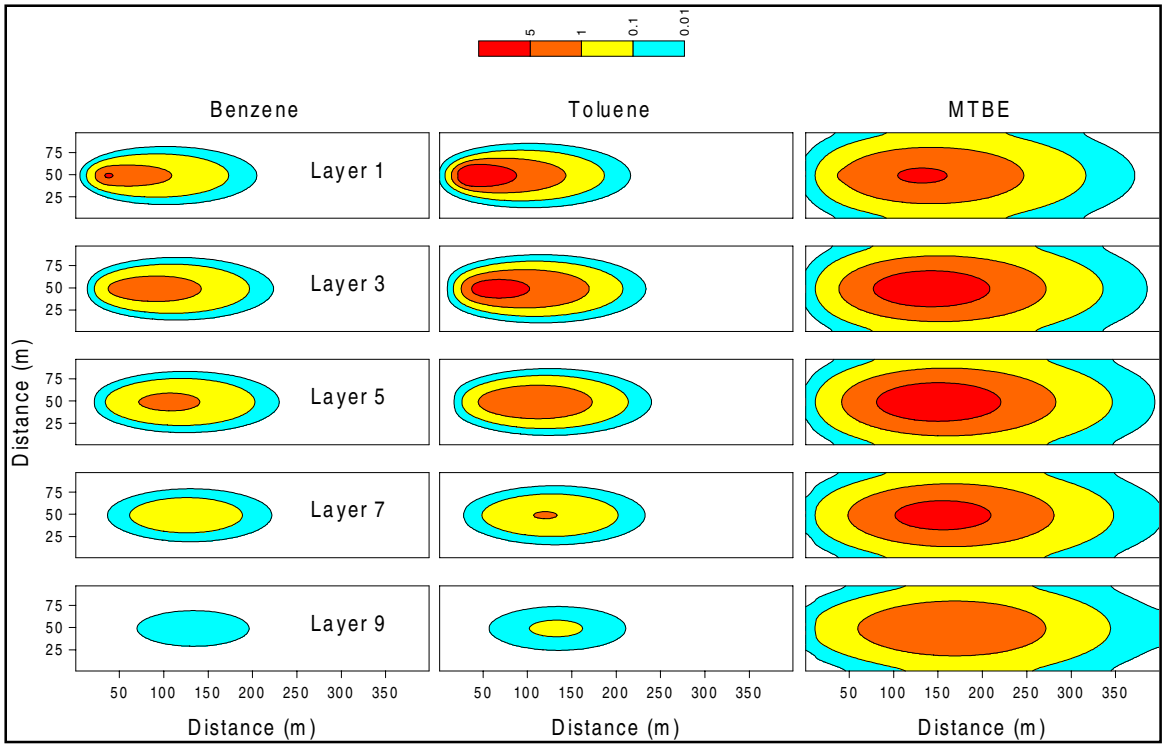

Figure 33. Areal contours of benzene, toluene, and MTBE at 4,000 days for model layers 1, 3, 5, 7, and 9. Units of the scale bar are g/m^3 for all three constituents

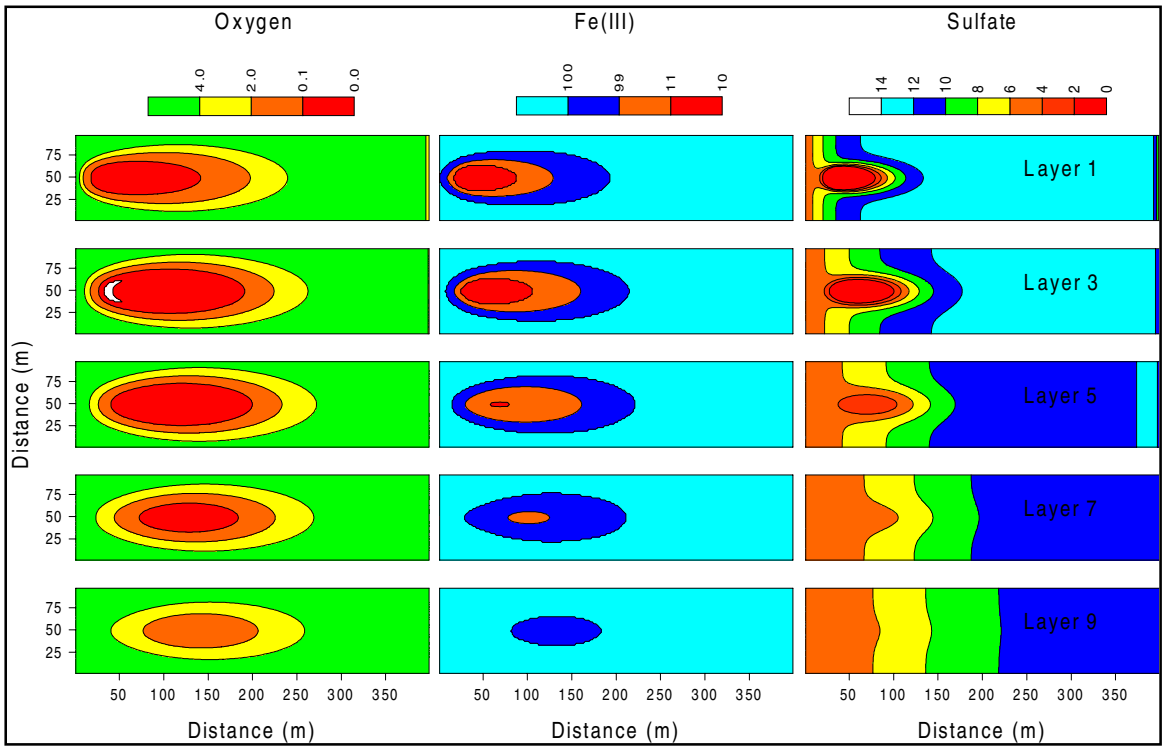

Figure 34. Areal contours of O_2, Fe(III), and SO_4^{2-} at 4,000 days for model layers 1, 3, 5, 7, and 9. Units of the scale bar are g/g for Fe(III) and g/m^3 for O_2 and SO_4^{2-}

Alternative model scenarios

Since the actual NAPL concentrations in the soil were not well characterized, a theoretical worst-case NAPL spill (see section on NAPL contamination) was simulated to show the sensitivity of model predictions to the initial amount of gasoline in the soil. For the worst case, the initial NAPL mass per block was set twice as high as the "best estimate" case. Results of the worst case and the best estimate simulations are compared for benzene in Figure 35. At early times, concentrations are only slightly sensitive to the initial amount of NAPL; however, by 4,000 days, the worst-case spill produces concentrations that are twice as high as the best-estimate spill. Thus the worst-case NAPL distribution produces aqueous contamination for longer periods of time, reflecting the concept that larger NAPL spills may require longer remediation times.

As an alternative to injecting mass of NAPL over time, an equivalent mass of NAPL was injected at time zero to simulate an instantaneous spill. This simplified approach may be warranted for sudden spills, or spills in which the leak time for NAPL is much smaller than the time for aqueous phase transport and biodegradation. In this case, the instantaneous spill places NAPL approximately 20 m downgradient of the gasoline leak at initial time. Thus the overall travel distance at 850 days is overpredicted (Figure 35) by 20 m. However, after 2,000 days, there is little difference in the instantaneous spill and the time-dependent spill, as dispersion and biodegradation have greater influence on transport than advection.

For the final alternative modeling scenario, microbial growth was eliminated from the SEAM3D simulation. The initial concentrations M_x of all microbial populations were set to 0.35 g m^{-3}, which was equal to the value of the effective porosity θ. Thus the terms M_x and θ cancel out of Equations 5 through 10, so that the R_{sink}^{bio} and the R_{source}^{bio} terms depend only on the utilization rates r_x. Without microbial growth, SO_4^{2-} reducers begin to use hydrocarbon and produce significant amounts of H_2S by 850 days (Figure 36). By 6,000 days, there is little difference in the growth and no-growth scenarios, as SO_4^{2-} depletion limits continued production of H_2S.

Conclusions

In modeling contaminant transport following a gasoline spill, SEAM3D captured the trends of BTEX biodegradation without requiring significant adjustment of parameters during calibration. Biodegradation based on multiple EAs was shown to limit BTEX concentrations and travel distance in directions transverse to average flow as well as in the flow direction. At early times, maximum concentrations of contaminant were not sensitive to the mass of NAPL spilled. However, at later times, the larger initial NAPL mass distribution produced higher contaminant concentrations. The microbial growth process allowed SEAM3D to capture the effect of time lags in biodegradation due to shifting EA processes. As the overall simulation time became much greater than the lag times, the effect of the lag became insignificant. A similar effect occurred

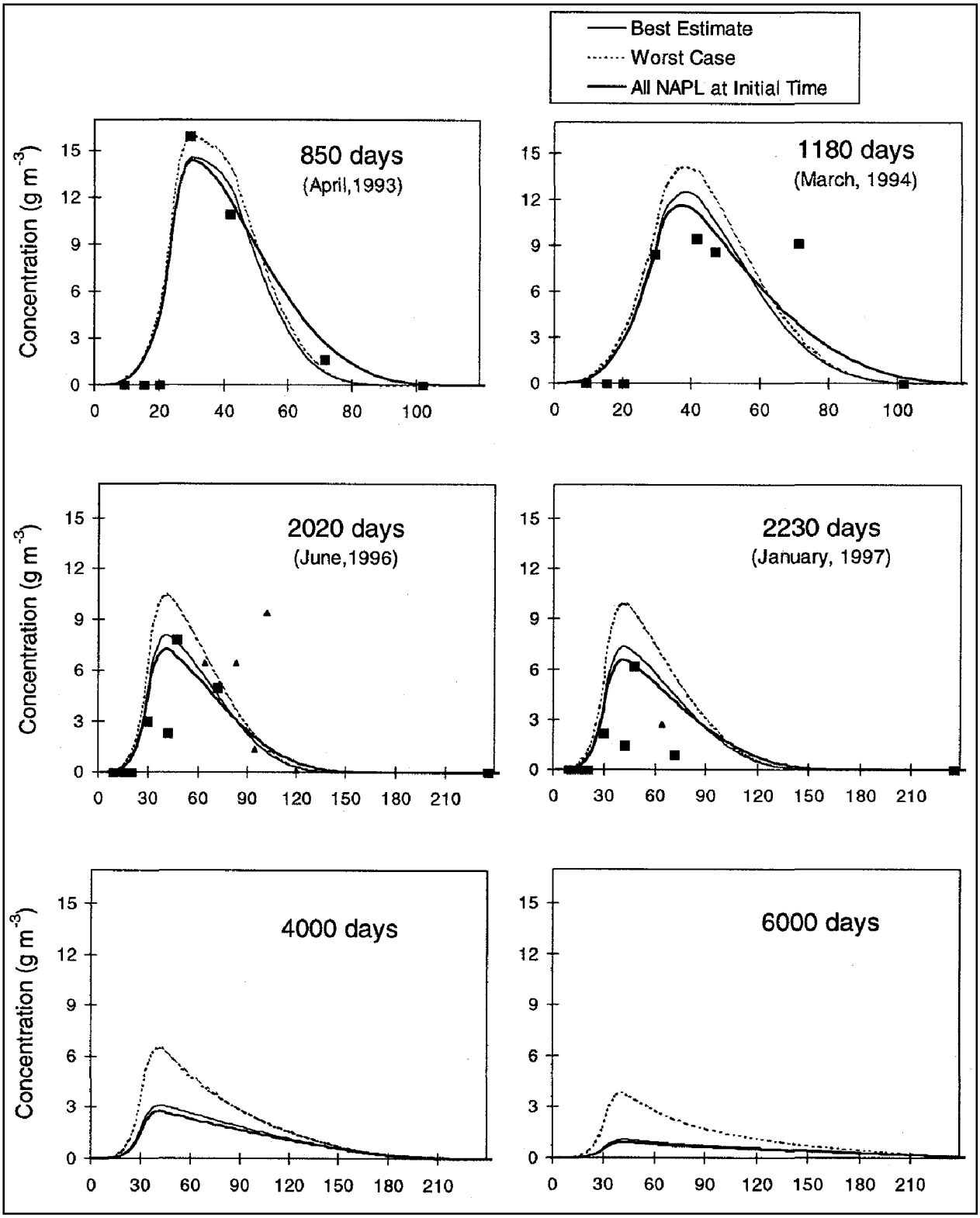

Figure 35. Comparison of benzene concentrations along a transect through the center line of the plume as predicted by SEAM3D for the best-estimate NAPL distribution, the worst-case NAPL distribution, and entire NAPL distribution applied at initial time

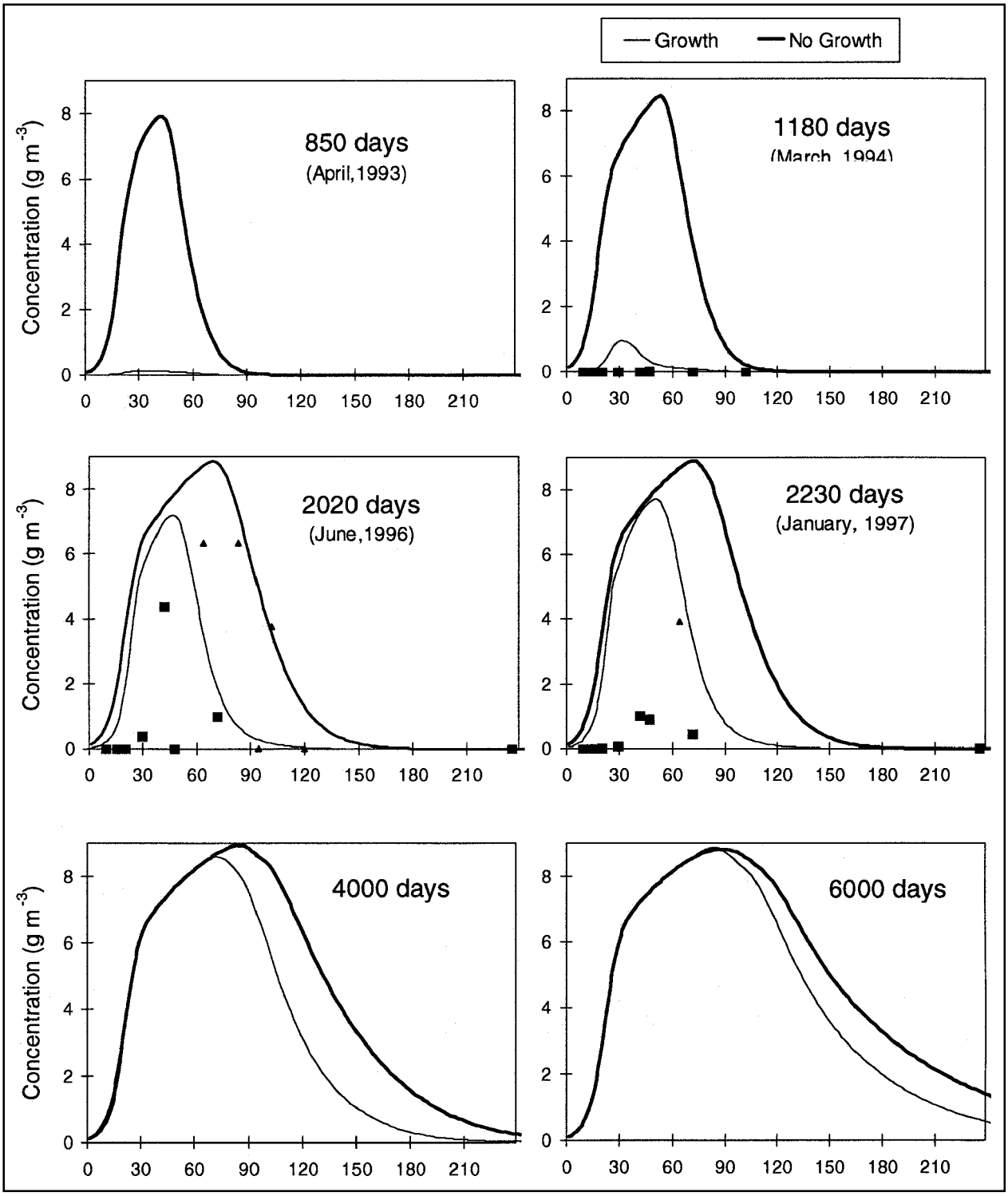

Figure 36. Comparison of H_2S concentrations along a transect through the center line of the plume as predicted by SEAM3D using microbial growth versus no microbial growth

in simulating the actual leak of NAPL into the subsurface. The timing of the NAPL leak was important early in the simulation, but the significance of the timing of the leak diminished as the simulation time became much greater than the leak duration. The results suggest that the most complex modeling approach is justified when the goal is to simulate biodegradation in close proximity to a NAPL spill or soon after a spill has occurred.

5 SEAM3D Model Input

Introduction

Since SEAM3D is based on MT3DMS (Zheng and Wang 1999), much of the input is identical for the two models, and a basic understanding of MT3DMS is the first step toward mastering SEAM3D. Users who are unfamiliar with MT3DMS will benefit from reading the MT3DMS technical documentation (Zheng and Wang 1999). The following sections summarize information from the MT3DMS technical documentation, while information relevant to the additional subroutines in SEAM3D is provided in greater detail. SEAM3D will not require detailed input or reserve computer memory for model options that are not specified by the user. For example, if dissolution of contaminants from a NAPL is not simulated, then the user does not create the NAPL dissolution input file (see section on input instructions for the NAPL dissolution package).

Estimation of model parameters for biodegradation may be based on laboratory measurements, published values, and theoretical estimates. To produce maximum flexibility, SEAM3D allows parameters to vary across the aquifer layers and among the various substrates and EAs for biodegradation. However, in the absence of detailed information, the user is advised to enter identical parameter values to describe the layers and certain biodegradation processes. Thus, parameter estimation can be simplified when available data do not support a more detailed analysis. Further information on parameter estimation is included in the detailed input instructions ("Input Instructions" section).

Types of input

Like MT3DMS, input for SEAM3D may be formatted, list-directed, or unformatted.

Formatted. Input variables may be formatted as integer, real, character, or logical. In the detailed input instructions, the format column uses *I* to specify an integer, *F* for a real number, *A* for a character variable, and *L* for a logical variable. Input conventions follow the standards of the FORTRAN 77 language.

List-directed. List-directed, or free format, input involves a sequence of values separated by blanks or commas. The list-directed record terminates when

a slash (/) is encountered, repeat counters are permitted, and each new record should begin on a new line of the input file.

Unformatted. Unformatted files contain binary characters and must be written and read by the computer. Unformatted files are smaller and can be processed more readily than formatted files.

Array readers

Most of the input data for SEAM3D is handled by the subroutines IARRAY and RARRAY in the utility module of the program. IARRAY reads one- or two-dimensional integer arrays, and RARRAY reads one- or two-dimensional real arrays. Three-dimensional arrays are handled by reading a two-dimensional areal array for each model layer. Each time an array reader is called, it initially reads an array control record, which occupies a single line of the input filed and is formatted as follows:

Record:	IREAD	CNSTNT (real) or ICONST (integer)	FMTIN	IPRN
Format:	I10	F10.0 (real) or I10 (integer)	A20	I10

If IREAD = 0, then RARRAY sets all elements of the array equal to CNSTNT, or IARRAY sets all elements equal to ICONST.

If IREAD = 100, then array values (entered on the lines following the array control record) are read in the format specified by FMTIN.

If IREAD = 101, then array values are read as blocks, which are entered on the lines following the array control record. The first line contains only the record NBLOCK, which is an integer specifying the number of blocks to follow. Each block occupies a single line, consisting of I1, I2, J1, J2, VALUE; where I1 is the index of the first row of the block, I2 is the index of the last row, J1 is the index of the first column of the block, J2 is the index of the last column, and VALUE is the value assigned to array elements within the block.

If IREAD = 102, then array values are read as zones.

If IREAD = 103, then array values are read in list-directed format.

If IREAD is equal to a nonzero value other than 100, 101, 102, or 103, then array values are read from a separate file. If IREAD is positive, then IREAD is the unit number for the separate file, which is formatted according to FMTIN. If IREAD is negative, then the separate file is unformatted, and the absolute value of IREAD is its unit number.

If IREAD $\neq$ 0 and CNSTNT or ICONST $\neq$ 0, then all elements in the array are multiplied by CNSTNT or ICONST.

The format specifier FMTIN must be enclosed in parentheses.

If IREAD ≠ 0, then IPRN acts as a flag to indicate whether the array will be printed for checking. The array will not be printed if IPRN is negative.

Units

Like MT3DMS, SEAM3D requires the user to specify units and use consistent units for all input and output variables. In addition, the time unit must be consistent with that used in the flow model. The single exception to this rule involves the concentrations of solid-phase EAs, which are entered as mass of EA per 1×10^6 mass of soil solids (e.g., micrograms per gram). Units of meters for length and grams for mass are convenient because they produce concentration units of grams per cubic meter, which is equivalent to milligrams per liter.

Input Instructions

Many of the input lines are identical in both SEAM3D and MT3DMS. In the following sections, these lines will be given the same numbering style as in the MT3DMS user guide (e.g., A1 for the first line of the Basic Transport File). Many input lines in SEAM3D are required only if certain model options are switched on. For example, if no inorganic nutrients are simulated, then nutrient parameters such as initial concentrations are not entered. In addition, six TEAPs are built into the model: oxygen, nitrate, manganese, iron, and sulfate reduction and methanogenesis. TEAPs are model options that may be switched on or off.

In the detailed input instructions, certain input lines are grouped underneath the conditional statement that indicates whether the lines should be included in the file. Often these groups are preceded by a line of descriptive text that helps the user locate the lines in the file for editing. To illustrate input structure, example input files are included with the SEAM3D source code and executable files. It is highly recommended that the user prepare input files by modifying existing files.

The terms outer loop and inner loop are used throughout the detailed input instructions to indicate the order for entering lines describing arrays of more than two dimensions. For example, in line E14 of the Biodegradation Package, the subroutine RARRAY must be called repeatedly to read the four-dimensional array XMOLD(ncol, nrow, nlay, nclny). Each time RARRAY is called, it reads a two-dimensional array XMOLD(ncol, nrow) for specified values of nlay and nclny. Thus the model must loop through values for nlay and nclny, going through the inner loop first. In other words, for the first microbial population (nclny = 1), RARRAY is called for each model layer before moving to the second microbial population (nclny = 2).

Input instructions for the Basic Transport Package

This input file contains information describing the model configuration, initial conditions, and output options. It must be created for all simulations and is read on unit 1.

Initial concentrations of hydrocarbon substrates, EAs, inorganic nutrients, products, daughters, and nonbiodegradable tracers should be based on concentrations measured in the field. If a certain process is not included in the simulation, then the corresponding parameters are not entered and need not be estimated. For example, if nitrate reduction is not simulated, then initial and minimum concentrations of nitrate are not entered in the basic transport package.

The Basic Transport Package is identical for SEAM3D and MT3DMS, with TRNOPT(6) and TRNOPT(7) defined as shown in the following tabulation. In line A3, the total number of mobile components (MCOMP) is the sum of the number of nonbiodegradable tracers, hydrocarbon substrates, aqueous-phase EAs, inorganic nutrients, products, and daughters. The number of solid-phase EAs is not included in this total since they will be entered in the Biodegradation Package. In SEAM3D, MCOMP should be set equal to NCOMP. The initial concentrations of components must be entered in the following order:

1. Nonbiodegradable tracers
2. Hydrocarbon substrates
3. Aqueous-phase EAs
4. Inorganic nutrients
5. Products
6. Daughters

Line	Variable	Format	Description
A3	NLAY	I10	Total number of layers
	NROW	I10	Total number of rows
	NCOL	I10	Total number of columns
	NPER	I10	Total number of stress periods
	NCOMP	I10	Total number of components
	MCOMP	I10	Total number of mobile components
A5	TRNOPT(10) TRNOPT(6) for biodegradation TRNOPT(7) for NAPL dissolution	10L2	Flags for major transport options: advection, dispersion, source/sink mixing, chemical reactions, solver technique, biodegradation, and NAPL dissolution. Enter *T* to include the option in the simulation; enter *F* to omit the option.

Input instructions for the Advection Package

This input file must be created only if the Advection Package is specified in the Basic Transport Package; i.e., TRNOPT(1) is set to *T*. Input for advection is read on unit 2, and advection is normally included in all simulations. SEAM3D supports only either the standard finite difference solution or the third-order total variation diminishing (TVD) solution for advection. Because SEAM3D does not support other advection solution methods, parameters for particle tracking are not required.

Line	Variable	Format	Description
B1	MIXELM	I10	Flag indicating advection solution method MIXELM = 0 for upstream finite difference method MIXELM = -1 for third-order TVD
	PERCEL	F10.0	Courant number (generally, PERCEL ≤ 0.2)
	MXPART	I10	Not used by SEAM3D, so any integer may be entered

Input instructions for the Dispersion Package

This input file must be created only if the Dispersion Package is specified in the Basic Transport Package; i.e., TRNOPT(2) is set to *T*. Input for dispersion is read on unit 3, and dispersion is normally included in all simulations. The Dispersion Package is identical for SEAM3D and MT3DMS.

Input instructions for the Source/Sink Mixing Package

This input file must be created if source/sink options (including constant head or general-head-dependent boundary conditions) are specified in the flow model. It is also necessary to specify the Source/Sink Mixing Package in the Basic Transport Package; i.e., TRNOPT(3) is set to *T*. Input for source/sink mixing is read on unit 4. The location and rates for the fluxes (due to wells, drains, recharge, evapotranspiration, rivers, and general-head-dependent boundary conditions) are obtained from the flow solution through the unformatted head and flow file. If a flux is positive, then it acts as a source, and concentrations must be specified. If a flux is negative, then it acts as a sink, and concentrations are set equal to the current concentrations within the block. The Source/Sink Mixing Package is identical for SEAM3D and MT3DMS.

Input instructions for the Reaction Package

This input file must be created only if the Reaction Package is specified in the Basic Transport Package; i.e., TRNOPT(4) is set to *T*. Input is read on unit 9, and the Reaction Package is identical for SEAM3D and MT3DMS.

Input instructions for the Biodegradation Package

This input file must be created only if the Biodegradation Package is specified in the Basic Transport Package; i.e., TRNOPT(6) is set to *T*. Input is read on unit 11.

Due to the difficulty in quantifying aquifer microbes, data on the initial microbial biomass M_x may not be available, and only a rough estimate of M_x may be obtained. Under pristine conditions, when the groundwater contains significant O_2, it can be assumed that aerobic biomass predominates. Anaerobic microbes would exist only in anaerobic microsites that develop within soil aggregates. Thus, the value of M_x for each anaerobic biomass can be estimated as an order of magnitude lower than for the aerobic biomass. In general, if M_x for the anaerobes is on the order of 0.01 g m^{-3}, then the anaerobic biomass must

undergo significant growth before the population exerts a significant impact on biodegradation. For the aerobes, M_x equal to 0.3 g m^{-3} corresponds to 1×10^6 cells cm^{-3}, assuming a cell volume of 1 μm^3, cell density of 1.0 g cm^{-3}, and aquifer porosity of 0.3. This number of cells usually allows significant aerobic utilization of substrates to occur without additional microbial growth. The minimum concentrations of substrates, EAs, and nutrients may be set to zero unless measured data indicate otherwise.

To reflect the high rate and energy yield of aerobic metabolism, parameters controlling aerobic utilization, growth, and death should generally be much higher than those of the anaerobic processes. The maximum specific rate of substrate utilization $\nu^{\max}_{x,ls,le}$ may be based on laboratory or field estimates. Certain substrates, such as those in the alkane group, are resistant to anaerobic biodecay, so $\nu^{\max}_{x,ls,le}$ for alkanes may be set to zero for each anaerobic process. Alkanes would still biodegrade using oxygen. For aerobic biodegradation of hydrocarbons, laboratory estimates of $\nu^{\max}_{x,ls,le}$ have been reported as 1.0 day^{-1} (Kindred and Celia 1989), 1.7 day^{-1} (Borden and Bedient 1986), 3.5 to 8.0 day^{-1} (Arcangeli and Arvin 1992), and 8.3 to 9.9 day^{-1} (Chen et al. 1992). Biodegradation rates in the field may be much lower than observed in the laboratory. A field study by MacIntyre et al. (1993) found that aerobic biodecay of benzene could be approximated by a pseudo-first-order rate constant of 0.0070 day^{-1}. Chapelle and Lovley (1990) reported that microbial metabolic rates based on laboratory incubations may overpredict in situ rates by two orders of magnitude.

Values of the half-saturation coefficients for substrates $K^s_{x,ls,le}$ and EAs $K^e_{x,le}$ may be based on literature values if no measurements are available. For hydrocarbons, $K^s_{x,ls,le}$ has been reported in the range of 0.1 g m^{-3} (Kindred and Celia 1989), 0.13 g m^{-3} (Borden and Bedient 1986), 0.6 g m^{-3} (Arcangeli and Arvin 1992), 1.88 to 4.55 g m^{-3} (Chang, Voice, and Criddle 1993), 12.2 to 17.4 g m^{-3} (Chen et al. 1992). For oxygen, $K^e_{x,le}$ has been reported as 0.10 g m^{-3} (Borden and Bedient 1986; Kindred and Celia 1989; Chen et al. 1992). For nitrate, $K^e_{x,le}$ has been reported as 0.1 g m^{-3} (Kindred and Celia 1989), and 2.6 g m^{-3} (Chen et al. 1992). With the exception of oxygen, values for half-saturation coefficients are reported over a wide range, but SEAM3D model results are generally much more sensitive to biomass concentration and $\nu^{\max}_{x,ls,le}$ than to the half-saturation coefficients.

The yield coefficient $Y_{x,ls,le}$ for aerobes is often estimated as 0.5 g g^{-1} (Arcangeli and Arvin 1992; Borden and Bedient 1986; Chen et al. 1992; Wodzinski and Johnson 1968), although values as low as 0.25 have been used (Kindred and Celia 1989). For anaerobes, $Y_{x,ls,le}$ is usually lower than for aerobes, with 0.2 g g^{-1} being the theoretical maximum yield under sulfate reducing conditions (Edwards et al. 1992). It is recommended that the user

allow SEAM3D to calculate values for the effective death terms $k_{d_x}^{bk}$ internally, using the method described in the section "Microbial growth equations" in Chapter 2.

When an inhibition coefficient $\kappa_{le,li}$ is assigned a small value relative to its corresponding EA, the EA must be essentially depleted before utilization of the next EA begins. In contrast, the inhibition process becomes insignificant if $\kappa_{le,li}$ is assigned a large value. Numerous values for inhibition coefficients have been reported. For inhibition by oxygen, $\kappa_{le,li}$ values vary between 0.01 and 0.1 g m^{-3} (Kindred and Celia 1989; Chen et al. 1992). Research has shown that methanogenesis may predominate over SO_4^{2-} reduction when the SO_4^{2-} concentration falls between 0.6 to 1.4 g m^{-3} (Vroblesky, Bradley, and Chapelle 1996). Thus the value of $\kappa_{le,li}$ for SO_4^{2-} inhibition of methanogenesis should be within a similar range. In general, values of $\kappa_{le,li}$ for a particular inhibitor need not vary among the EA processes that are inhibited. For example, a value of $\kappa_{le,li}$ = 0.1 g m^{-3} could be used to describe oxygen inhibition of all of the anaerobic processes. Values of $\kappa_{le,li}$ may be adjusted during calibration to match measured concentrations of products.

EA use coefficients $\gamma_{x,ls,le}$ can be estimated from the stoichiometric relationship between each EA and the corresponding substrate. For aromatic hydrocarbons, there is little variation in the stoichiometry, and toluene may be used as a representative compound. Thus values for $\gamma_{x,ls,le}$ should be approximately equal to 3.1 g g^{-1} for O_2, 4.8 g g^{-1} for NO_3^-, 42.0 g g^{-1} for Fe(III), 4.5 g g^{-1} for SO_4^{2-} (Borden, Gomez, and Becker 1995), and 18.0 g g^{-1} for Mn(IV) (Baedecker et al. 1993). The actual value of $\gamma_{x,ls,le}$ will depend somewhat on the specific hydrocarbon and the amount of microbial assimilation of substrate into cell material. The generation term for CH_4 $\zeta_{x,ls}$ can be estimated as 0.8 g g^{-1}, based on the stoichiometric relationship between toluene and methane (Borden, Gomez, and Becker 1995). The EA generation terms $\zeta_{x,le}$ can also be based on stoichiometric relationships. If N_2 is the final product of NO_3^- reduction, then $\zeta_{x,le}$ should be close to 0.5 g g^{-1}. For H_2S production, $\zeta_{x,le}$ should be close to 1.0 g g^{-1} (Edwards et al. 1992). During calibration, the generation term for Fe(II) will often need to be reduced from its theoretical value to match the measured concentrations of Fe(II). This reduction is necessary because Fe(II) can react chemically with compounds such as SO_4^{2-}; thus, only a fraction of the Fe(II) produced by microbes may be measured in the groundwater (Lovley, Chapelle, and Woodward 1994).

Line	Variable	Format	Description
E1	NTRAC	I10	Total number of nonbiodegradable tracers $0 \le NTRAC \le 5$
	NHCAR	I10	Total number of biodegradable substrates $1 \le NHCAR \le 8$
	NNUTR	I10	Total number of inorganic nutrients $0 \le NNUTR \le 5$
	NDAUT	I10	Total number of daughter products $0 \le NDAUT \le NHCAR$
E2	STOCHOPT	L2	Flag for spatial variability option for maximum specific rate of substrate utilization. Enter *T* to allow the parameter to vary in space; enter *F* for constant value.
E3	CLNOPT(6)	6L2	Flags for TEAP options: aerobes, NO_3 reducers, Mn(IV) reducers, Fe(III) reducers, SO_4^{2-} reducers, methanogens. Enter *T* to include the TEAP in the simulation; enter *F* to omit.
E4	ENDOPT(4)	4L2	Flags for product options: N_xO_y, Mn(II), Fe(II), H_2S. Enter *T* to include the product in the simulation; enter *F* to omit. Note that ENDOPT(5) for CH_4 is automatically set from CLNOPT(6) for methanogens.
E5	Descriptive text	None	"Hydrocarbon Minimum Concentrations"
E6	AHMIN(nhcar)	F10.0	Minimum concentrations: Enter AHMIN for each hydrocarbon
E7	Descriptive text	None	"Electron Acceptor Starting Concentrations"
E8	SEOLD(ncol, nrow, nlay, nslid)	RARRAY	Starting concentrations: Enter SEOLD(ncol, nrow) for each layer (inner loop) and for each solid-phase EA (outer loop). The solid-phase EAs are read in the following order: Fe(III), Mn(IV). NSLID is the total number of solid-phase EAs (calculated automatically from the TEAP options)
E9	SEMIN(nslid)	F10.0	Minimum concentrations: Enter SEMIN after SEOLD(ncol, nrow) for each solid-phase EA
E10	AEMIN(nelec)	F10.0	Minimum concentrations: Enter AEMIN for each EA
E11	Descriptive text	None	"Nutrient Minimum Concentrations"
E12	ANMIN(nnutr)	F10.0	Minimum concentrations: Enter ANMIN for each nutrient
E13	Descriptive text	None	"Biomass Starting Concentrations"
E14	XMOLD(ncol, nrow, nlay, nclny)	RARRAY	Starting concentrations: Enter XMOLD(ncol, nrow) for each layer (inner loop) and for each microbial population (outer loop). NCLNY is the total number of microcolonies in the simulation
E15	XMMIN	RARRAY	Minimum concentration for all microcolonies: Enter XMMIN after the last entry of XMOLD(ncol, nrow)
E16	NITER	I5	Number of biodegradation time-steps per transport time-step

E17	KSCR, ISCR,JSCR	3I10	Layer, row, and column indices for screen output
E18	Descriptive text	None	"Electron Acceptor Inhibition Terms"

(Enter lines E19 and E20 if the total number of EA processes (including methanogenesis) > 1)

E19	Descriptive text	None	"Inhibition of [inhibitee]" Enter this line prior to each inhibitor process.
E20	AKINH(ninh, ninh)	F10.0	EA inhibition coefficient: Enter AKINH(lj, lk) for each inhibitor *lk* (inner loop) of EA process *lj* (outer loop) Note that EA process *lj* will require entry of (*lj* - 1) inhibitors NINH = the total number of EA processes minus one

Example 1: Simulate aerobes and NO_3^- reducers (NINH = 1)

Line 1:
Line 2: "Inhibition of NO_3^-"

AKINH(1,1) -- coefficient of O_2 inhibition of NO_3^-

Example 2: Simulate aerobes, Fe(III), SO_4^{2-} reducers, and methanogens (NINH = 3)

Line 1: "Inhibition of Fe(III)"
Line 2: AKINH(1,1) -- coefficient of O_2 inhibition of Fe(III)

Line 3: "Inhibition of SO_4^{2-}"
Line 4:
Line 5: AKINH(2,1) -- coefficient of O_2 inhibition of SO_4^{2-}

AKINH(2,2) -- coefficient of Fe(III) inhibition of SO_4^{2-}

Line 6:
Line 7: "Inhibition of methanogenesis"
Line 8: AKINH(3,1) -- coefficient of O_2 inhibition of methanogenesis
Line 9: AKINH(3,2) -- coefficient of Fe(III) inhibition of methanogenesis

AKINH(3,3) -- coefficient of SO_4^{2-} inhibition of methanogenesis

E21	Descriptive text	None	"Elec. Acc. Product Generation Coefs."

(Enter line E22 if NENDE > 0)

E22	ENDE(nende)	F10.0	EA product generation coefficient: Enter line E22 NENDE times NENDE is the number of products from the EAs (specified in ENDOPT of the Basic Transport Package).
E23	Descriptive text	None	"Methane Generation Coefficients"

(Enter line E24 if methanogenesis is simulated)

E24	ENDH(nhcar)	F10.0	Methane generation coefficients: Enter line E24 NHCAR times
E25	Descriptive text	None	"Daughter Generation Coefficients"

(Enter line E26 if NDAUT >0)

E26	ENDD(ndaut)	F10.0	Daughter generation coefficients: Enter line E26 NDAUT times
E27	Descriptive text	None	"Electron Acceptor Use Coefficients"
E28	AGAM(nhcar, neatot)	F10.0	Use coefficients: Enter line E28 for each hydrocarbon (inner loop) and for EA (outer loop) EA loop is read in the following order: O_2, NO_3^-, Fe(III), Mn(IV), SO_4^{2-} (i.e., from highest to lowest energy). NEATOT is the total number of EAs simulated. Lines are not read for EAs that are not included in the simulation
E29	Descriptive text	None	"Nutrient Use Coefficients"

(Enter line E30 if NNUTR > 0)

E30	APSI(nhcar, nnutr)	F10.0	Nutrient use coefficients: Enter line E30 for each hydrocarbon (inner loop) and for each nutrient (outer loop)

(Enter lines E31 through E39 NCLNY times:
microbial populations will be read in the order of highest to lowest energy)

E31	Descriptive text	None	Microbial Population Name, e.g. "Aerobes"
E32	Descriptive text	None	"Death Rate"
E33	XKD	F10.0	First-order decay rate for the microbial population XKD < 0 death rate calculated by model (recommended) XKD = 0 no microbial death XKD > 0 death rate is constant at the specified value
E34	AKHALFH(nhcar, nli, nclny)	F10.0	Hydrocarbon half-saturation constant: Enter line E34 for each EA utilized by the microbes (inner loop) and for each hydrocarbon (outer loop) NLI is the number of EAs utilized by the microbes: NLI = 2 for NO_3^- reducers NLI = 1 for all other populations

(Do not enter line E35 for Fe(III) or Mn(IV) reducers)

E35	AKHALFE(nli, nclny)	F10.0	EA half-saturation constant: Enter line E35 for each EA utilized by the microbes

(Enter line E36 if NNUTR > 0)

E36	AKHALFN(nnutr, nli, nclny)	F10.0	Nutrient half-saturation constant: Enter line E36 for each EA utilized by the microbes (inner loop) and for each nutrient (outer loop)

(Enter line E37 if STOCHOPT(1) is".true." -- see line E2)

E37	VSPMAX(ncol, nrow, nlay, nhcar, nli, nclny)	RARRAY	Maximum specific rate of substrate utilization: Enter VSPMAX(ncol, nrow) for each layer (inner loop), each EA utilized by the microbes (middle loop), and for each hydrocarbon (outer loop)

(Enter line E38 if STOCHOPT(1) is".false." -- see line E2)

E38	VSPMAX(nhcar, nli, nclny)	F10.0	Maximum specific rate of substrate utilization: Enter line E38 for each EA utilized by the microbes (inner loop) and for each hydrocarbon (outer loop)
E39	YIELD(nhcar, nli, nclny)	F10.0	Yield coefficients: Enter line E39 for each EA utilized by the microbes (inner loop) and for each hydrocarbon (outer loop)

Input instructions for the NAPL Dissolution Package

This input file must be created only if the NAPL Dissolution Package is specified in the Basic Transport Package; i.e., TRNOPT(7) is set to *T*. Input is read on unit 22.

Normally, the number of hydrocarbon substrates in the NAPL (NHDIS) will correspond to the number in the overall simulation (NHCAR). However, it is possible to have NHCAR > NHDIS, since contaminants may derive from sources

other than the NAPL. Estimates of the initial mass fractions within the NAPL may be obtained from laboratory analysis or from the literature. For example, if the NAPL is gasoline, mass fractions of benzene, toluene, ethylbenzene, and xylenes have been reported (e.g., Sigsby et al. 1987). Values for solubility and molecular weight are readily available from chemical handbooks.

Line	Variable	Format	Description
FS1	MXDIS	I10	Number of nodes where NAPL concentration is specified
	IMLOAD	I10	Flag for mass loading to NAPL: = 0 No time-dependent mass loading is simulated = 1 Time-dependent mass loading is simulated
	NHDIS	I10	Number of hydrocarbons in the NAPL (0 ≤ NHDIS ≤ NHCAR)
	NTDIS	I10	Number of tracers in the NAPL (0 ≤ NTDIS ≤ NTRAC)
(Enter the following line only if IMLOAD =1)			
FS2	NSCH	I10	Number of schedules for simulation of mass loading
	MAXSUB	I10	Maximum number of subschedules per schedule
FS3	Descriptive text	None	"Initial Mass Fractions of Hydrocarbons"
FS4	FRAH(nhdis)	F10.0	Initial mass fraction in NAPL: Enter line F4 NHDIS times
FS5	Descriptive text	None	"Initial Mass Fractions of Tracers in NAPL"
FS6	FRAT(ntdis)	F10.0	Initial mass fraction in NAPL: Enter line F6 NTDIS times
FS7	Descriptive text	None	"Hydrocarbon Solubility"
FS8	FRAH(nhdis)	F10.0	Solubility: Enter line F8 NHDIS times
FS9	Descriptive text	None	"Tracer Solubility"
FS10	FRAT(ntdis)	F10.0	Solubility: Enter line F10 NTDIS times
FS11	Descriptive text	None	"Hydrocarbon Molecular Weight"
FS12	WTMOLH(nhdis)	F10.0	Molecular weight: Enter line F12 NHDIS times
FS13	Descriptive text	None	"Tracer Molecular Weight"
FS14	WTMOLT(ntdis)	F10.0	Molecular weight: Enter line F14 NTDIS times
FS15	Descriptive text	None	"Inert Fraction Molecular Weight"
FS16	WTMOLI	F10.0	Molecular weight
FS17	Descriptive text	None	"NAPL Parameters"
(Enter line F18 MXDIS times)			
FS18	KK	I10	Layer number of block containing NAPL mass
	II	I10	Row number of block containing NAPL mass
	JJ	I10	Column number of block containing NAPL mass
	ISCH	I10	Schedule number for mass loading: Enter any value if IMLOAD = 0
	SINERT	F10.0	Initial concentration of NAPL ($M\,M^{-1}$)
	DIFALP	F10.0	Dissolution rate (T^{-1})
	TIMEEX	F10.0	Time when NAPL mass is removed from the block (i.e., excavation). Enter a number larger than the total simulation time to prevent excavation

(Enter the remaining lines only if IMLOAD =1)

FS19	Descriptive text	None	"NAPL Mass Loading"
(Enter lines 20 and 21 NSCH times; i.e., for isch = 1 to NSCH)			
FS20	NSUB(isch)	I10	Number of subschedules in schedule ISCH: $1 \leq NSUB(isch) \leq MAXSUB$
	SCHTIME(isch, 1)	F10.0	Starting time for NAPL loading according to subschedule 1
	SCHVAL(isch, 1)	F10.0	Mass rate of NAPL loading according to subschedule 1 ($M\ T^{-1}$).

(Enter line 21 for isub = 2 to NSUB(isch)

FS21	SCHTIME(isch, isub)	F10.0	Starting time for NAPL loading according to subschedule ISUB SCHTIME(isch, nsub(isch)) must be greater than the total simulation time
	SCHVAL(isch, isub)	F10.0	Mass rate of NAPL loading according to subschedule ISUB ($M\ T^{-1}$).

6 SEAM3D Model Output and Postprocessing

Introduction

The basic output structure for SEAM3D is similar to that of MT3DMS (Zheng and Wang 1999), and SEAM3D writes output information for all hydrocarbon substrates, EAs, and other constituents in the simulation. The following sections summarize information from the MT3DMS technical documentation (Zheng and Wang 1999), while information relevant to the additional output of SEAM3D is provided in greater detail.

Output Files

Each time SEAM3D is run, the program generates a standard output file, plus optional output files as requested by the user in the Basic Transport Package (see "Input instructions for the Basic Transport Package" in Chapter 5). Options within the Basic Transport Package allow the user to control the frequency and type of information written to the output files. The output files are described in the following paragraphs.

Standard output file

This file echoes the input data to allow the user to verify the accuracy of the specified parameters, flags, and options. The standard output filename (for example SEAM3D.OUT) is specified by the user at the beginning of the simulation. Each line of input is written to the standard output file immediately after being read. If an input error causes the program to stop, the user can find the location of the error by examining the standard output file with any text editor. The input error will almost always involve the line that follows the last line successfully written to the standard output file. For the times selected by the user, the standard output file will contain mass balance information and concentrations of hydrocarbon substrates, EAs, nutrients, products, daughters, and tracers specified in the simulation.

Unformatted concentration files

For each user-specified time, these files contain concentrations that can be read by the postprocessing programs or used for continuation of a run. Each aqueous-phase constituent will have an unformatted concentration file named MT3D*nnn*.UCN, where *nnn* is the constituent index number. The naming system in the following tabulation is used:

Model Constituent	File Name		Notes
Tracers	MT3D*nnn*.UCN	*nnn* = 001, NT	NT = no. of tracers
Hydrocarbon substrates	MT3D*nnn*.UCN	*nnn* = NT+1, NH	NH = NT+ no. of hydrocarbons
Aqueous-phase EAs	MT3D*nnn*.UCN	*nnn* = NH+1, NE	NE = NH+ no. of aqueous EAs
Nutrients	MT3D*nnn*.UCN	*nnn* = NE+1, NN	NN = NE + no. of nutrients
End products	MT3D*nnn*.UCN	*nnn* = NN+1, NP	NP = NN + no. of products
Daughters	MT3D*nnn*.UCN	*nnn* = NP+1, ND	ND = NP + no. of daughters
Solid-phase EAs	SMSEA*nn*.UCN	*nn* = 01, nslid	nslid = no. of solid-phase EAs
Microbial population	SMXM*nn*.UCN	*nn* = 01, nclny	nclny = no. of microbial populations

For example, if one tracer, one hydrocarbon substrate, and one aqueous-phase EA were simulated, then concentrations of the tracer would be written to MT3D001.UCN, concentrations of the hydrocarbon would be written to MT3D002.UCN, concentrations of the aqueous-phase EA would be written to MT3D003.UCN, and concentrations of the microbial population would be written to SMXM01.UCN.

Observation point files

For each user-specified observation point, these files contain concentrations versus time in a format that can be read by any text editor. Each aqueous-phase constituent will have an observation file named MT3D*nnn*.OBS, where *nnn* is the constituent index number. In addition, each solid-phase EA will have an observation file named SMSEA*nn*.OBS, where *nn* is the index number for the solid-phase EA. Finally, each microbial population will have an observation file named SMXM*nn*.OBS, where *nn* is the index number for the microbial population.

Total mass file

This file, named SMMASS.DAT, contains a time series of the total mass of each constituent in the aqueous, sorbed, and NAPL phases. Total mass is calculated for the entire model domain by summing the mass within each block over the total number of blocks. For the aqueous phase, the mass within each

block is the aqueous concentration divided by porosity times the block volume. For the sorbed phase, the mass within each block is the solid-phase concentration times bulk density times the block volume. For the NAPL, the mass within each block is the NAPL concentration times bulk density times the block volume. The first line of SMMASS.DAT contains a descriptive header that uses the following naming convention:

HC*i*	*i*th hydrocarbon substrate
aEA*i*	*i*th aqueous-phase EA
sEA*i*	*i*th solid-phase EA
Nu*i*	*i*th nutrient
Pr*i*	*i*th product
Tr*i*	*i*th tracer
Mic*i*	*i*th microbial population

In addition, suffixes are used on the header terms, with "Aqu" indicating aqueous-phase mass, "Ads" indicating adsorbed mass, "NAPL" indicating NAPL mass, and "Tot" indicating the total of the aqueous, adsorbed, and NAPL masses.

Mass balance summary file

Each aqueous-phase constituent will have a mass balance summary file named MT3D*nnn*.MAS, where *nnn* is the constituent index number. This file contains a summary of the mass budget for each constituent simulated.

Model grid configuration file

This file, named MT3D.CNF, contains information on the spatial discretization to be used by the postprocessing program.

Postprocessing

The postprocessing programs included with SEAM3D are identical to those of MT3DMS. The program PM.EXE uses the unformatted concentrations files (*.UCN) and the model grid configuration file (MT3D.CNF) to produce data files for plotting. To run PM.EXE, type the name of the executable file (i.e., "PM") at the command prompt, and follow the instructions. Note that PM transforms the SEAM3D coordinate system from the upper, top, left corner of block (1, 1, 1) to the lower, bottom, right corner of block (1, NROW, NLAY). Thus the x-axis remains the same, while the y- and z-axes are reversed to correspond to the coordinate system of most graphical programs.

The program SAVELAST.EXE extracts the last concentrations saved in the *.UCN files for use as the starting concentrations for a continuation run (Appendix A). To run SAVELAST.EXE, type the name of the executable file (i.e., "SAVELAST") at the command prompt. The program will prompt for the

name of the unformatted concentration file to be read as input and the name of the output file for output.

Since the structure of unformatted files is compiler specific, the user will need to compile PM.EXE and SAVELAST.EXE with the same compiler that was used for SEAM3D and MODFLOW. Thus it may be necessary to recompile the source codes PM.FOR and SAVELAST.FOR. Additional information on the postprocessing programs may be found in the MT3DMS technical documentation.

References

ABB Environmental Services, Inc. (1993). "Contaminant assessment report: Marine Corps Exchange Service Station, Laurel Bay," GWPD#A-07-AA-13575, Knoxville, TN.

Arcangeli, J. P., and Arvin, E. (1992). "Modeling of toluene biodegradation and biofilm growth in a fixed biofilm reactor," Water Sci. Tech. 26(3-4), 617-626.

Arcangeli, J. P., and Arvin, E. (1994). "Biodegradation of BTEX compounds in a biofilm system under nitrate reducing conditions." *Hydrocarbon bioremediation.* R. E. Hinchee, B. C. Alleman, R. E. Hoeppel, and R. N. Miller, ed., Lewis Publishers, Boca Raton, FL, 374-382.

Atlas, R. M., and Cerniglia, C. E. (1995). "Bioremediation of petroleum pollutants: Diversity and environmental aspects of hydrocarbon biodegradation," *BioScience* 45, 332-338.

Baehr, A. L., and Corapcioglu, M. Y. (1987). "A compositional multiphase model for groundwater contamination by petroleum products. II: Numerical solution," *Water Resour. Res.* 23(1), 201-213.

Baedecker, M. J., Cozzarelli, I. M., Eganhouse, R. P., Siegel, D. I., and Bedient, P. C. (1993). "Crude oil in a shallow sand and gravel aquifer. III: Biogeochemical reactions and mass balance modeling in anoxic groundwater," *Applied Geochemistry* 8, 569-586.

Bailey, J. E., and Ollis, D. F. (1977). *Biochemical engineering fundamentals.* McGraw-Hill, New York.

Borden, R. C., and Bedient, P. B. (1986). "Transport of dissolved hydrocarbons influenced by oxygen limited biodegradation. I: Theoretical development," *Water Resour. Res.* 22, 1973-1982.

Borden, R. C., Gomez, C. A., and Becker, M. T. (1995). "Geochemical indicators of intrinsic bioremediation," *Ground Water* 33, 180-189.

Bosma, T. N. P., Ballemans, E. M. W., Hoekstra, N. K., te Welscher, R. A. G., Smeenk, J. G. M. M., Schraa, G., and Zehnder, A. J. B. (1996). "Biotransformation of organics in soil columns and an infiltration area," *Ground Water* 34, 49-56.

Bouwer, H. (1978). *Groundwater hydrology.* McGraw-Hill, New York, 56.

Brauner, J. S., and Widdowson, M. A. (1997). "Sequential electron acceptor model for evaluation of *in situ* bioremediation of petroleum hydrocarbon contaminants in groundwater," *Annals of the New York Academy of Sciences* 829, 399-419, Engineering Foundation, New York.

Brock, T. D., Madigan, M. T., Martinko, J. M., and Parker, J. (1994). *Biology of microorganisms.* 7th ed., Prentice-Hall, Englewood Cliffs, NJ.

Button, D. K. (1985). "Kinetics of nutrient-limited transport and microbial growth," *Microbiol. Rev* 49, 270-297.

Carsel, R. F., and Parrish, R. S. (1988). "Developing joint probability distributions of soil water retention characteristics," *Water Resour. Res.* 24, 755-769.

Chang, M.-K., Voice, T. C., and Criddle, C. S. (1993). "Kinetics of competitive inhibition and cometabolism in the biodegradation of benzene, toluene, and p-xylene by two *Pseudomonas* isolates," *Biotech. and Bioeng.* 41(11), 1057-1065.

Chapelle, F. H. (1993). *Ground-water microbiology and geochemistry.* Wiley & Sons, New York.

Chapelle, F. H., and Bradley, P. M. (1998). "Selecting remediation goals by assessing the natural attenuation capacity of groundwater systems," *Bioremed. J.* 2(3 & 4), 227-238.

Chapelle, F. H., and Lovley, D. R. (1990). "Rates of microbial metabolism in deep coastal plain aquifers," *Appl. Environ. Microbiol.* 56(6), 1865-1874.

Chen, Y. M., Abriola, L. M., Alvarez, P. J. J., Anid, P. J., and Vogel, T. M. (1992). "Modeling transport and biodegradation of benzene and toluene in sandy aquifer material: Comparisons with experimental measurements," *Water Resour. Res.* 28, 1833-1847.

Corapcioglu, M. Y., and Baehr, A. L. (1987). "A compositional multiphase model for groundwater contamination by petroleum products. I: Theoretical considerations," *Water Resour. Res.* 23(1), 191-200.

de Blanc, P. C., McKinney, D. C., and Speitel, G. E. (1995). "Modeling subsurface biodegradation of non-aqueous phase liquids: A literature review," CRWR 257, Center for Research in Water Studies, University of Texas, Austin.

Edwards, E. A., Wills, L. E., Reinhard, M., and Grbic-Galic, D. (1992). "Anaerobic degradation of toluene and xylene by aquifer microorganisms under sulfate-reducing conditions," *Appl. Environ. Microbiol.* 58(3), 794-800.

Grbic-Galic, D., and Vogel, T. M. (1987). "Transformation of toluene and benzene by mixed methanogenic cultures," *Appl. Environ. Microbiol.* 53, 254-260.

Imhoff, P. Y., Jaffe, P. R., and Pinder, G. F. (1993). "An experimental study of complete dissolution of a nonaqueous phase liquid in saturated porous media," *Water Resour. Res.* 30(2), 307-320.

Jørgensen, B. B. (1989). "Biochemistry of chemoautotrophic bacteria." *Autotrophic bacteria.* H. G. Schegel and B. Bowien, ed., Science Tech. Publishers, Madison, WI, 117-146.

Kim, S., and Corapcioglu, M. Y. (1996). "A kinetic approach to modeling mobile bacteria-facilitated groundwater contaminant transport," *Water Resour. Res.* 32, 321-331.

Kindred, J. S., and Celia, M. A. (1989). "Contaminant transport and biodegradation. II: Conceptual model and test simulations," *Water Resour. Res.* 25(6), 1149-1159.

Landmeyer, J. E., Chapelle, F. H., and Bradley, P. M. (1996). "Evaluation of intrinsic bioremediation as an option to contain gasoline contamination, Laurel Bay Exchange, Marine Corps Air Station, Beaufort, South Carolina," Water Resources Investigation Report No. 96-4026, U.S. Geological Survey, Denver, CO.

Lovley, D. R. (1991). "Dissimilatory Fe(III) and Mn(IV) reduction," *Microbiol. Rev.* 55, 259-287.

Lovley, D. R., and Lonergan, D. J. (1990). "Anaerobic oxidation of toluene, phenol and p-cresol by the dissimilatory iron-reducing organism GS-15," *Appl. Environ. Microbiol.* 56, 858-864.

Lovley, D. R., Chapelle, F. H., and Woodward, J. C. (1994). "Use of dissolved H_2 concentrations to determine distribution of microbially catalyzed redox reactions in anoxic groundwater," *Environ. Sci. Technol.* 28(7), 1205-1210.

Ludvigsen, L., Heron, G., Albrechtsen, H., and Christensen, T. H. (1995). "Geomicrobial and geochemical redox processes in a landfill-polluted aquifer." *Intrinsic bioremediation.* R. E. Hinchee, J. T. Wilson, and D. C. Downey, ed., Battelle Press, Columbus, OH, 135-142.

MacIntyre, W. G., Boggs, M., Antworth, C. P., and Stauffer, T. B. (1993). "Degradation kinetics of aromatic organic solutes introduced into a heterogeneous aquifer," *Water Resour. Res.* 29(12), 4045-4051.

Mayer, A. S., and Miller, C. T. (1996). "The influence of mass transfer characteristics and porous media heterogeneity on nonaqueous phase dissolution," *Water Resour. Res.* 32(6), 1551-1567.

McDonald, J. M., and Harbaugh, A. W. (1988). "A modular three-dimensional finite-difference ground-water flow model," *Tech. of Water Resources Investigation of the USGS, Book 6,* Scientific Software Group, Washington, DC.

Parker, J. C., Waddill, D. W., and Johnson, J. A. (1994). *UST corrective action technologies: Engineering design of free product recovery systems,* U.S. Environmental Protection Agency, Risk Reduction Engineering Laboratory, Edison, NJ.

Parker, J. C., Katyal, A. K., Kaluarachchi, J. J., Lenhard, R. J., Johnson, T. J., Jayaraman, K., Ünlü, K., and Zhu, J. L. (1991). "Modeling multiphase organic chemical transport in soils and ground water," EPA/600/2-91/042, U.S. Environmental Protection Agency, Washington, DC.

Parr, J. L., Walters, G., and Hoffman, M. (1991). "Sampling and analysis of soils for gasoline range organics." *Hydrocarbon contaminated soils and groundwater: Analysis, fate, environmental and public health effects, and remediation.* P. T. Kostecki and E. J. Calabrese, ed., Lewis Publishers, Chelsea, MI, 120-132.

Pfannkuch, H. O. (1984). "Determination of the contaminant source strength from mass exchange processes at the petroleum-ground-water interface in shallow aquifer systems." *Proceedings, NWWA/API Conference on Petroleum Hydrocarbons and Organic Chemicals in Groundwater – Prevention, Detection, and Restoration,* Worthington, OH, 5-7 November. National Water Well Association.

Powers, S. E., Abriola, L. M., and Weber, W. J. (1994). "An experimental investigation of nonaqueous phase liquid dissolution in saturated subsurface systems: Transient mass transfer rates," *Water Resour. Res.* 30(2), 321-332.

Reuter, P., Rabus, R., Wilkes, H., Aeckersberg, F., Rainey, F. A., Jannasch, H. W., and Widdel, F. (1994). "Anaerobic oxidation of hydrocarbons in crude oil by new types of sulphate-reducing bacteria," *Nature* 372, 455-458.

Rixey, W. G., and Dortch, I. J. (1992). "Effects of oxygenated fuels on groundwater contamination: Equilibria and transport considerations." *Hydrocarbon contaminated soils and groundwater.* E. J. Calabrese and P. T. Kostecki, ed., Lewis Publishers, Chelsea, MI, Vol 2, 115-136.

Rixey, W. G., Johnson, P. C., Deeley, G. M., Byers, D. L., Dortch, I. J. (1991). "Mechanisms for the removal of residual hydrocarbons from soils by water, solvent, and surfactant flushing." *Hydrocarbon contaminated soils.* E. J. Calabrese and P. T. Kostecki, ed., Lewis Publishers, Chelsea, MI, Vol 1, 387-409.

Simkins, S., and Alexander, M. (1984). "Models for mineralization kinetics with the variables of substrate concentration and population density," *Appl. Environ. Microbiol.* 47, 1299-1306.

Sigsby, J. E., Silvestre, T., Ray, W., Lang, J. M., and Duncan, J. W. (1987). "Volatile organic compound emissions from 46 in-use passenger cars," *Environ. Sci. Technol.* 21(5), 466-475.

Voss, C. I. (1984). "A finite-element simulation model for saturated-unsaturated, fluid-density-dependent ground-water flow with energy transport or chemically-reactive single-species solute transport," Water Resources Investigation Report No. 84-4369, U.S. Geological Survey, Denver, CO.

Vroblesky, D. A., and Chapelle, F. H. (1994). "Temporal and spatial changes of terminal electron-accepting processes in a petroleum hydrocarbon-contaminated aquifer and significance for contaminant biodegradation," *Water Resour. Res.* 30, 1561-1570.

Vroblesky, D. A., Bradley, P. M., and Chapelle, F. H. (1996). "Influence of electron donor on the minimum sulfate concentration required for sulfate reduction in a petroleum hydrocarbon-contaminated aquifer," *Environ. Sci. Technol.* 30(4), 1377-1381.

Waddill, D. W., and Widdowson, M. A. (1997). "SEAM3D: A numerical model for three-dimensional solute transport and sequential electron acceptor-based biodegradation in groundwater," Prepared for the U.S. Army Engineer Research and Development Center, Environmental Laboratory, Vicksburg, MS, by Virginia Polytechnic Institute and State University, Blacksburg, Va.

Widdowson, M. W., Molz, F. J., and Benefield, L. D. (1988). "A numerical transport model for oxygen- and nitrate-based respiration linked to substrate and nutrient availability in porous media," *Water Resour. Res.* 24, 1553-1565.

Wilson, J. L., Conrad, S. H., Mason, W. R., Peplinski, W., and Hagan, E. (1990). "Laboratory investigation of residual liquid organics from spills, leaks, and the disposal of hazardous wastes in groundwater," EPA/600/6-90/004, U.S. Environmental Protection Agency, Washington, DC.

Wodzinski, R. S., and Johnson, M. J. (1968). "Yields of bacterial cells from hydrocarbons," *Appl. Microbiol.* 16, 1886-1891.

Zheng, C. (1990). "MT3D: A modular three-dimensional transport model for simulation of advection, dispersion, and chemical reactions of contaminants in groundwater systems," Reference Manual, Prepared for the U.S. Environmental Protection Agency, Robert S. Kerr Environmental Research Laboratory, Ada, OK.

Zheng, C. (1993). "Extension of the method of characteristics for simulation of solute transport in three dimensions," *Ground Water* 31, 456-465.

Zheng, C., and Bennett, G. D. (1995). *Applied contaminant transport modeling: Theory and practice.* Van Nostrand Reinhold, New York.

Zheng, C., and Wang, P. P. (1999). “MT3DMS: A modular three-dimensional multispecies transport model for simulation of advection, dispersion, and chemical reactions of contaminants in groundwater systems, Documentation and user’s guide,” Contract Report SERDP-99-1, U.S. Army Engineer Research and Development Center, Vicksburg, MS.

Appendix A
Instructions for Executing a SEAM3D Simulation

Execution of SEAM3D is essentially identical to MT3DMS (Zheng and Wang 1999), with the exception that the user does not specify the name of the standard output file, and additional input files may need to be specified. It is recommended that SEAM3D be run from the directory that contains the input files. At the operating system command line, the user enters the path to the directory containing the SEAM3D executable file and the name of the executable.

For example, if input files have been created in the **`c:\seam3d\test`** directory, and the executable file **`SEAM3D.EXE`** is located in the **`c:\seam3d`** directory, then the following steps should be taken:

a. Change directories so that **`c:\seam3d\test`** is the current directory. The command prompt should appear as **`c:\seam3d\test>`**

b. Type **`SEAM3D`** (the directory **`c:\seam3d`** must be included in the operating system path). The program prompts for the required input files, and pauses while the user enters the corresponding file names. If the test problem includes all of the available packages in SEAM3D, then the screen prompts will appear as follows (with user input shown to the right in bold):

```
Enter name for Basic Transport Input File:  BTN.INP
Enter name for Advection Input File:  ADV.INP
Enter name for Dispersion Input File:  DSP.INP
Enter name for Sink & Source Input File:  SSM.INP
Enter name for Chemical Reaction Input File:  RCT.INP
Enter name for Biodegradation Input File:  BIO.INP
Enter name for NAPL Dissolution Input File:  DIS.INP
Enter name for Unformatted Head & Flow File:  FLO.INP
Print out Heads and Flow Terms for Checking? (Y/N)  N
```

As an alternative to entering the file names from the keyboard, the user may create a response file that contains the required file names in the proper order. For this example, a response file named **RUN.FIL** would contain the following:

```
BTN.INP
ADV.INP
DSP.INP
SSM.INP
RCT.INP
BIO.INP
DIS.INP
FLO.INP
N
```

At the command prompt, the user enters **SEAM3D < RUN.FIL**, and the program reads the input file names from the response file instead of the screen. Note that if an input package is not included in the simulation, then SEAM3D will not prompt for its filename, and the corresponding line should not be included in **RUN.FIL**. In this example, if NAPL dissolution had not been simulated, then the line containing **DIS.INP** would be omitted.

Continuation of a Previous Simulation

The continuation of a previous simulation in SEAM3D follows the same method used by MT3DMS and MODFLOW. The user must save the concentrations from the previous run in the **SM*.UCN** files by setting the logical flag SAVUCN to "true" in line A15 of the Basic Transport File. If concentrations have been saved at more than one time, then the program SAVELAST should be run to extract the concentrations at the final time of the previous run. The files **SM*.UCN** must be renamed, and then they can be specified as the starting concentration files in the continuation simulation (see "Input Instructions," Chapter 5, for details).

Note that the mass budget terms are set to zero at the start of each simulation, so the mass budget for the continuation run will not reflect information from the previous simulation. Also, the total simulation time is reset to zero at the start of each run, so the user must add the final time of the previous run to the total time for the continuation.

Appendix B
Notation

Symbols

C	Concentration of a limiting factor
D_{ij}	Tensor for the hydrodynamic dispersion coefficient (L^2T^{-1})
dZ_{ao}/dx	Gradient in the air-oil table
E_{le}	EA concentration ($M_{le}L^{-3}$) for le = 1, 2, and 5
E_{li}	Concentration of the inhibiting EA
$\overline{E}_{le}$	Effective concentration of EA le ($M_{le}L^{-3}$)
$\overline{E}_{li}$	Effective concentration of inhibiting EA le by EA li
E^*_{le}	EA point source concentration ($M_{le}L^{-3}$)
E^t_{le}	Threshold EA concentration
EA	Electron acceptor
f_{ls}	Mole fraction of substrate ls in the NAPL ($mol_{ls} \cdot mol_{NAPL}^{-1}$)
$G_x^{bk,0}$	Growth rate at time zero
$G_{x,ls,le}$	Growth rate due to hydrocarbon substrates
I^{NAPL}	NAPL concentration of inert (i.e., relatively insoluble) constituents ($M_I M_{solid}^{-1}$)
$I_{le,li}$	Inhibition function
j,i,k	Indices for columns, rows, and layers, respectively, of the model domain

k^{NAPL}	Mass transfer rate coefficient
k_1	First-order decay
k_{d_x}	"Effective" death rate (T^{-1})
$k_{d_x}^{bk}$	Background death rate
K	Saturated hydraulic conductivity of water
K^c	Half-saturation constant for concentration of a limiting factor
K_D	Distribution coefficient
$K_{x,le}^{e}$	EA half-saturation coefficient
$K_{x,ln}^{n}$	Half-saturation constant for nutrient *ln* ($M_{ln}L^{-3}$)
$K_{x,ls,le}^{s}$	Half-saturation constant for substrate *ls* utilizing EA *le* ($M_{ls}L^{-3}$)
$\overline{K}_{x,le}^{e}$	Effective half-saturation constant for EA *le* ($M_{le}L^{-3}$)
$\overline{K}_{x,ln}^{n}$	Effective half-saturation constant for nutrient *ln* ($M_{ln}L^{-3}$)
$\overline{K}_{x,ls,le}^{s}$	Effective half-saturation constant for substrate *ls* utilizing EA *le* ($M_{ls}L^{-3}$)
M_b	Microbial biomass
M_{ls}	Total mass of the aqueous phase
M_o	Oil mobility factor
M_s	Substrate mass
M_x	Microbial biomass concentration ($M_b L_{pm}^{-3}$) for x = 1,2,...,NM (number of microcolonies)
$M_o^{\max}$	Constant maximum value of oil mobility factor
M_{ls}^{NAPL}	Total mass of substrate
$M_{ls}^{NAPL,0}$	Initial NAPL mass of substrate *ls*
M_{ls}^{o}	Initial aqueous phase mass of substrate

N_{ln} Aqueous phase nutrient concentration ($M_{ln}L^{-3}$) for ln = 1,2,...,NN (number of nutrients)

$\overline{N}_{ln}$ Effective concentration of nutrient ln ($M_{ln}L^{-3}$)

N^{*}_{ln} Nutrient point source concentration ($M_{ln}L^{-3}$)

N^{t}_{ln} Threshold aqueous phase nutrient concentration

N_x Monod function describing nutrient limitations

$NAPL$ Nonaqueous phase liquid

NS Number of substrates

P_{lp} Aqueous phase product concentration ($M_{lp}L^{-3}$) for lp = 1,2,...,NP (number of products)

P^{*}_{lp} Product point source concentration ($M_{lp}L^{-3}$)

q_s Volumetric flux of water per unit volume of aquifer (T^{-1}) with $q_s > 0$ for sources and $q_s < 0$ for sinks

$r_{x,le}$ Utilization rate of EA le in microcolony x ($M_{le}M_b^{-1}T^{-1}$)

$r_{x,ln}$ Utilization rate of nutrient ln in microcolony x ($M_{ln}M_b^{-1}T^{-1}$)

$r_{x,ls}$ Utilization rate of substrate ls in microcolony x ($M_{ls}M_b^{-1}T^{-1}$)

R_{ln} Retardation factor for nutrient ln (L^o)

R_{lp} Retardation factor for product lp (L^o)

R_{ls} Retardation factor for substrate ls (L^o)

$R^{bio}_{sink,le}$ EA biodegradation sink term ($M_{le}L^{-3}T^{-1}$)

$R^{bio}_{sink,\mathrm{ln}}$ Nutrient biodegradation sink term ($M_{ln}L^{-3}T^{-1}$)

$R^{bio}_{sink,ls}$ Substrate biodegradation sink term ($M_{ls}L^{-3}T^{-1}$)

R^{bio}_{source} Biodegradation source term ($M_{lp}L^{-3}T^{-1}$)

$R^{NAPL}_{source,ls}$ Substrate source term due to nonaqueous phase liquid (NAPL) dissolution ($M_{ls}\,L^{-3}T^{-1}$)

S_{ls}	Aqueous phase substrate concentration ($M_{ls}L^{-3}$) for ls = 1,2,…,NS (number of substrates)
$\overline{S}_{ls}$	Effective concentration of substrate ls ($M_{ls}L^{-3}$)
S_{ls}^{*}	Substrate point source concentration ($M_{ls}L^{-3}$)
S_{ls}^{eq}	Equilibrium concentration
S_{ls}^{NAPL}	NAPL mass of substrate ls per unit mass dry soil ($M_{ls}M_{solid}^{-1}$)
$S_{ls}^{NAPL,0}$	Initial NAPL concentration of substrate
S_{ls}^{sol}	Solubility of pure substrate ls in water
S_{ls}^{t}	Threshold concentration of substrate ls
t	Time (T)
T_{lt}^{NAPL}	NAPL concentration of nonbiodegradable tracer lt ($M_{ls}M_{solid}^{-1}$)
$T_{lt}^{NAPL,0}$	Initial NAPL concentration of tracer
$TEAP$	Terminal electron-accepting process
$\overline{v}_i$	Average pore-water velocity (LT^{-1})
x_i	Distance (L)
x_j	Distance (L)
$Y_{x,ls,le}$	Biomass yield coefficient ($M_bM_{ls}^{-1}$), representing the mass of microcolony x produced per unit mass of substrate ls while utilizing EA le
$\alpha_x, \alpha_y, \alpha_z$	Longitudinal, transverse, and vertical dispersivity, respectively
$\gamma_{x,ls,le}$	EA use coefficient ($M_{le}M_{ls}^{-1}$), representing the mass of EA le used per unit mass of substrate ls
$\zeta_{x,le}$	EA product generation coefficient
$\zeta_{x,li}$	Generation coefficient
$\zeta_{x,ls}$	Product generation coefficient ($M_{lp}M_{ls}^{-1}$)
$\zeta_{x,ls}^{dau}$	Daughter product generation coefficient ($M_{ld}M_{ls}^{-1}$)

η_{ro} Ratio of oil to water viscosity

θ Effective transport porosity (L^o)

κ Inhibition coefficent

$\kappa_{le,li}$ EA inhibition coefficient ($M_{le}L^{-3}$) representing inhibition of the use of EA *le* by EA *li*

λ_{lp} Product first-order decay coefficient (T^{-1})

μ^{max} Maximum specific growth rate

ν Utilization rate

ν^{max} Maximum specific rate of substrate utilization

v_{NAPL} Average velocity of the NAPL plume

$\nu_{x,ls,le}$ Specific rate of substrate utilization for microcolony *x* growing on substrate *ls* and EA *le* ($M_{ls}M_b^{-1}T^{-1}$)

$\nu^{\max}_{x,ls,le}$ Maximum specific rate of substrate utilization

ρ_b Bulk density of the porous medium ($M_{solid}L_{pm}^{-3}$)

ρ_{ro} Oil specific gravity

$\psi_{x,ln}$ Nutrient utilization term

$\psi_{x,ls,le}$ Nutrient use coefficient ($M_{ln}M_{ls}^{-1}$) representing the mass of nutrient *ln* used per unit mass of substrate *ls*

ω_j Molecular weight of NAPL constituent *j*

Electron Acceptors

CO_2 Carbon dioxide

FE(III) Ferric iron

Mn(IV) Oxidized manganese

NO_3^- Nitrate

O_2 Oxygen

SO_4^{2-}	Sulfate

Products of Biodegradation

CH_4	Methane
Fe(II)	Ferrous iron
H_2S	Hydrogen sulfide
Mn(II)	Reduced manganese
N_{user}	User-specified nitrogenous compound

REPORT DOCUMENTATION PAGE

Form Approved
OMB No. 0704-0188

1. AGENCY USE ONLY *(Leave blank)*	2. REPORT DATE	3. REPORT TYPE AND DATES COVERED
	November 2000	Final report

4. TITLE AND SUBTITLE
SEAM3D: A Numerical Model for Three-Dimensional Solute Transport and Sequential Electron Acceptor-Based Bioremediation in Groundwater

5. FUNDING NUMBERS
WU CU-1062

6. AUTHOR(S)
Dan W. Waddill, Mark A. Widdowson

7. PERFORMING ORGANIZATION NAME(S) AND ADDRESS(ES)
Virginia Polytechnic Institute and State University
The Charles E. Via, Jr., Department of Civil and Environmental Engineering
Blacksburg, VA 24061-0105

8. PERFORMING ORGANIZATION REPORT NUMBER
ERDC/EL TR-00-18

9. SPONSORING/MONITORING AGENCY NAME(S) AND ADDRESS(ES)
See reverse.

10. SPONSORING/MONITORING AGENCY REPORT NUMBER

11. SUPPLEMENTARY NOTES

12a. DISTRIBUTION/AVAILABILITY STATEMENT
Approved for public release; distribution is unlimited

12b. DISTRIBUTION CODE

13. ABSTRACT ***(Maximum 200 words)***

This report describes the development, verification, and field application of SEAM3D (Sequential Electron Acceptor Model, 3 Dimensional), a numerical model for subsurface solute transport with aerobic and sequential anaerobic biodegradation. The model can depict multiple constituents in a three-dimensional, anisotropic, heterogeneous domain. Hydrocarbon contaminants are simulated as electron donors (i.e., substrates) for microbial growth, with available electron acceptors utilized sequentially. SEAM3D can account for products of biodegradation as well as a daughter product for each substrate. Biodegradation follows Monod kinetics, modified to include the effects of electron acceptability and nutrient availability through inhibition functions. Microbial biomass is simulated as scattered microcolonies attached to the porous medium with negligible interphase diffusional limitations to microbial growth. This report also includes instructions for model application.

14. SUBJECT TERMS

Biodegradation	In situ bioremediation	Sequential electron acceptors
Groundwater	Modeling	
Hydrocarbon contaminants	SEAM3D	

15. NUMBER OF PAGES
108

16. PRICE CODE

17. SECURITY CLASSIFICATION OF REPORT	18. SECURITY CLASSIFICATION OF THIS PAGE	19. SECURITY CLASSIFICATION OF ABSTRACT	20. LIMITATION OF ABSTRACT
UNCLASSIFIED	UNCLASSIFIED		

9. (Concluded).

Strategic Environmental Research and Development Program
Arlington, VA 22203;
U.S. Army Engineer Research and Development Center
Environmental Laboratory
3909 Halls Ferry Road, Vicksburg, MS 39180-6199